# Computational Homogenization based on Statistically Similar Representative Volume Elements


## Daniel Balzani


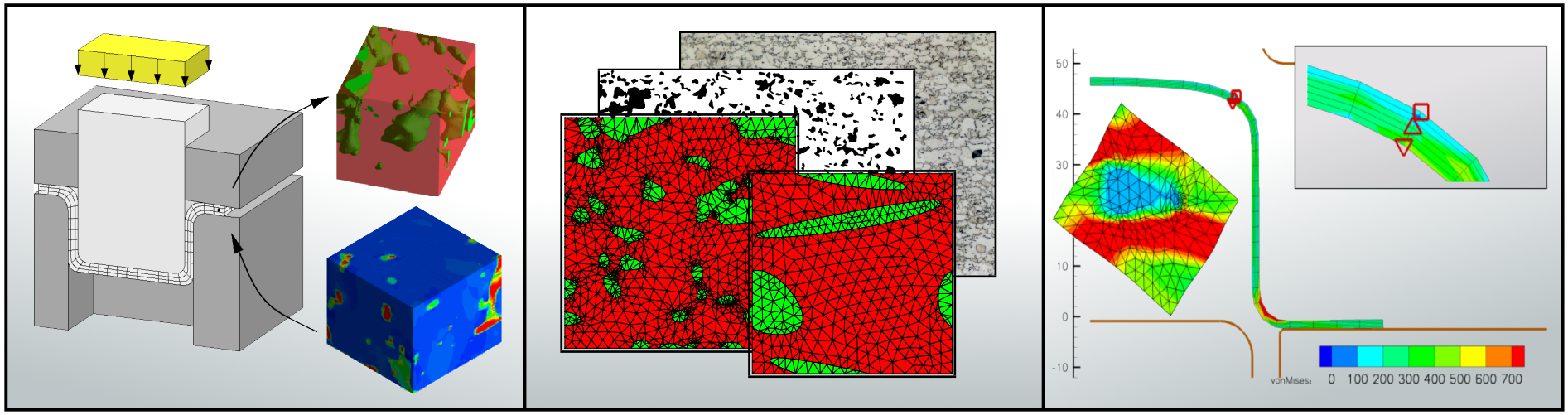


- Introduction/motivation
- Micro-heterogeneous materials
- Direct micro-macro-transition approach
- Construction of Statistically similar RVEs (SSRVEs)


**Acknowledgement:**
- Jörg Schröder, Dominik Brands, Lisa Scheunemann
- DFG for financial support (FOR 797) MICROPLAST




# Simulation of Engineering Problems based on the FE-Method

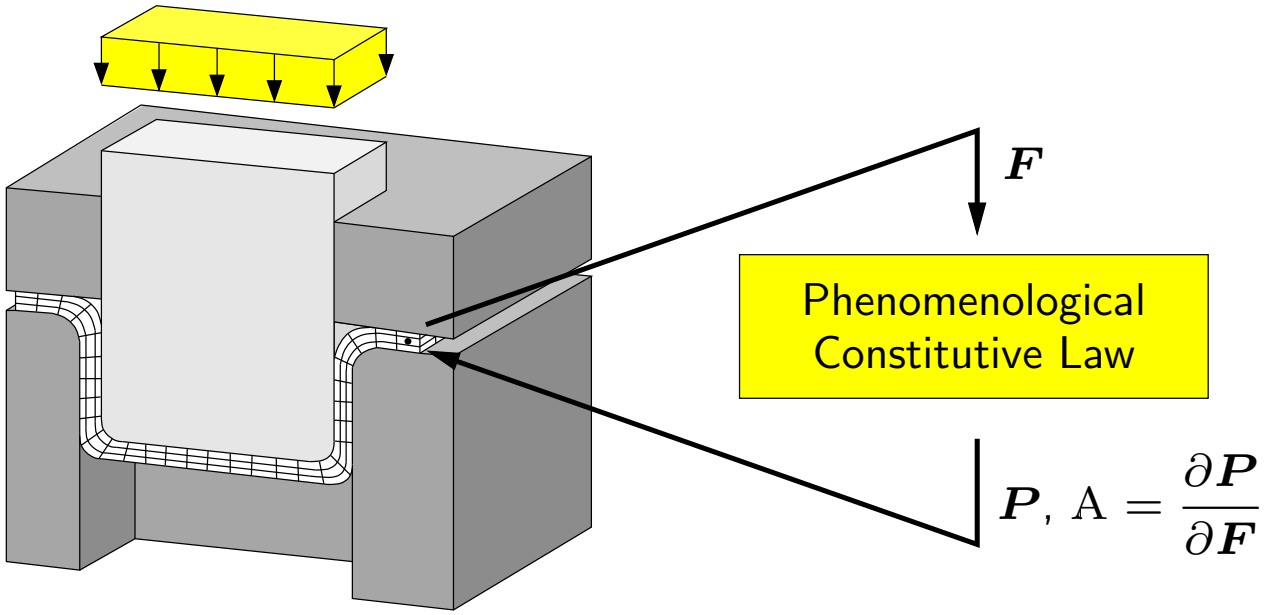


**Task:** Compute the deformation field $\boldsymbol{x}$ in a deformable solid as a result of a given loading situation under consideration of boundary conditions

Discretization of physical body in terms of finite elements:

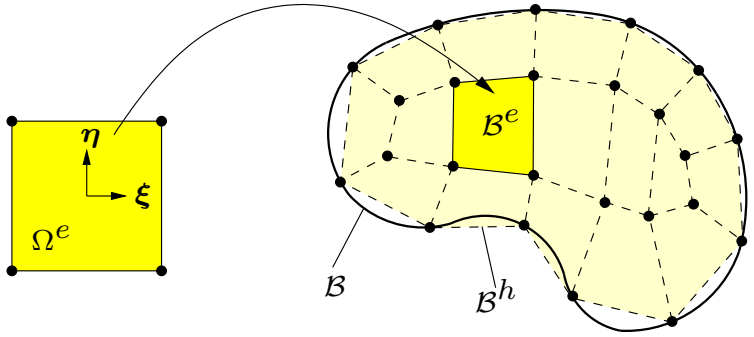


$$\mathcal{B} = \bigcup_e \mathcal{B}^e$$



# Phenomenological Constitutive Law?

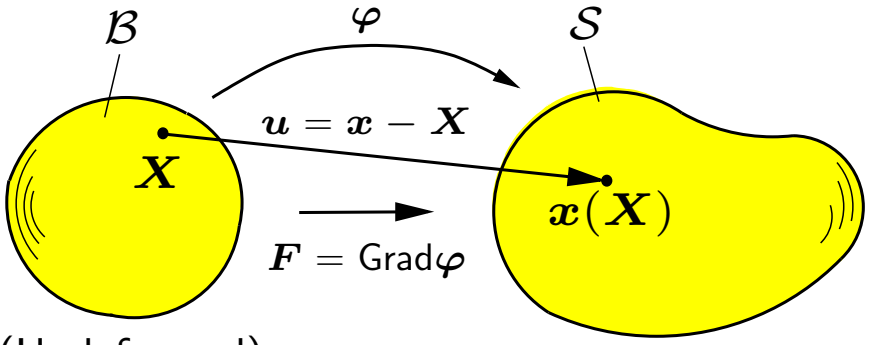


Material-dependent constitutive equations describing the relation between

- Deformation measure: e.g. Finger tensor $\boldsymbol{b} = \boldsymbol{F}\boldsymbol{F}^T$
- Stress measure: e.g. Kirchhoff stress tensor $\boldsymbol{\tau}$

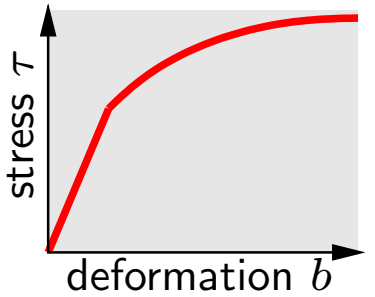


$\Rightarrow$ Reasonable results for approximately homogeneous materials!

$\Rightarrow$ Construction of phenomenological constitutive laws difficult for micro-heterogeneous materials due to complex macroscopic material behavior



# Example: Fiber-Reinforced Materials

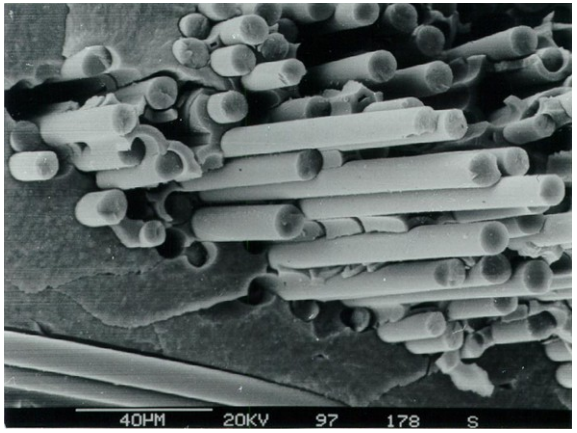


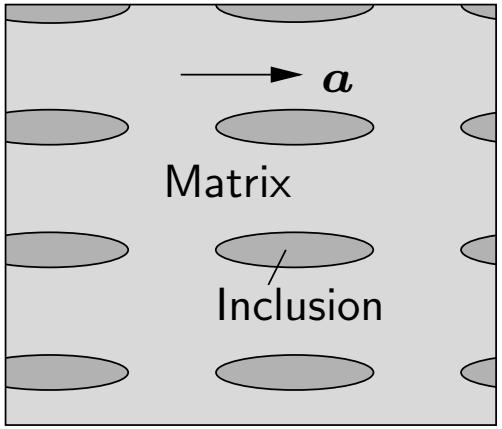


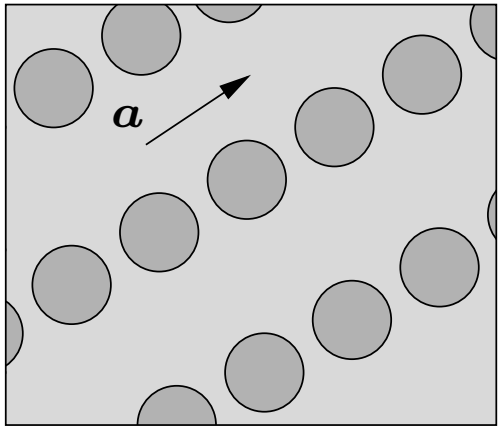


⇒ Morphology and arrangement of inclusions governs anisotropic properties

**Macroscopic example:** quadratic disc with a hole

Stiffer direction is characterized by an arrow ($\boldsymbol{a}$), no resistence of fibers under compression

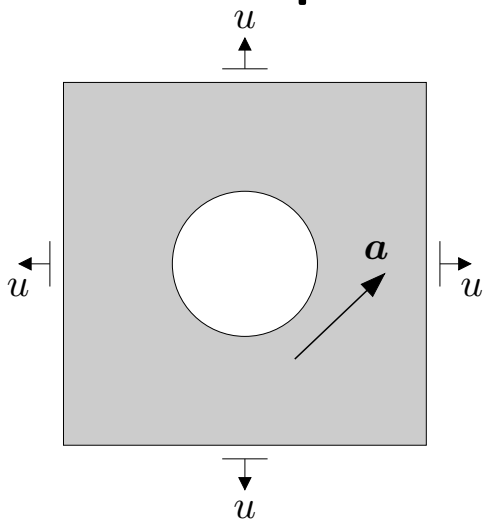


How does the hole deform?

movie

⇒ Appropriate models for anisotropic elasticity exist



# Example: Multiphase Steel

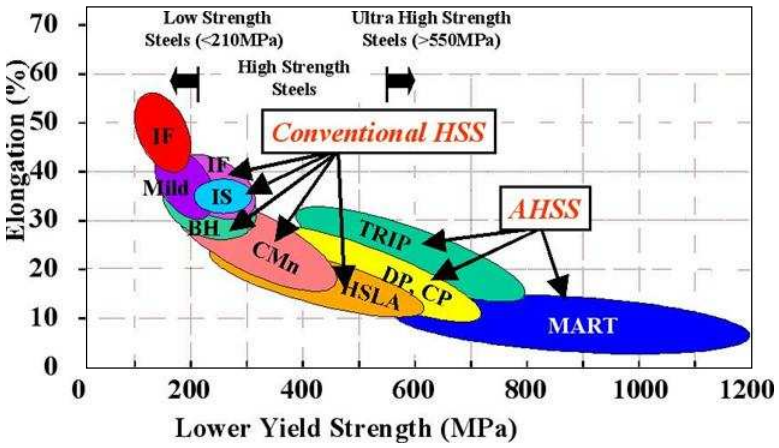


Advanced High Strength Steels (AHSS):

- light-weight construction
- enhancement of crash-safety

Material properties:

- lower weight of engineering constructions due to higher strength and formability

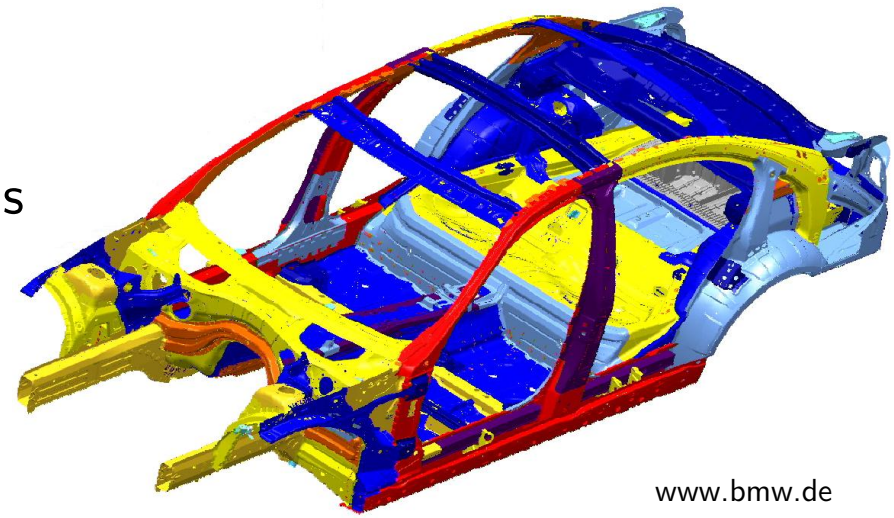

www.bmw.de

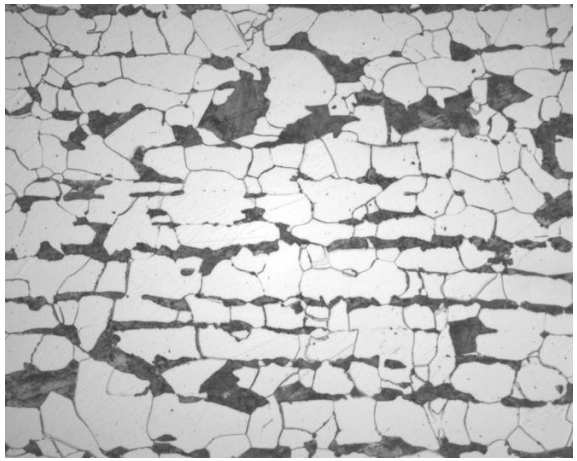

Complex microstructure leads to kinematic hardening at macroscale due to interaction of phases

→ Appropriate phenomenological model is difficult



# Identification of Macroscopic Material Behavior

- In general based on experiments $\rightarrow$ elaborate and expensive
- Alternative: FE-calculation of a representative volume element (RVE) of the micro-heterogeneous material

**FE-calculation of microscopic boundary value problems**

1. Discretization of a suitable RVE (e.g. periodic unitcell of periodic microstructure)
2. Application of suitable boundary conditions (e.g. displacement-driven bcs, based on macroscopic deformation gradient $\overline{\boldsymbol{F}}$)
3. Solution of microscopic boundary value problem
   $\rightarrow$ Distribution of microscopic fields $\boldsymbol{F}$, $\boldsymbol{\tau}$
4. Calculation of macroscopic stresses, e.g. as a volume average $\overline{\boldsymbol{P}} = \frac{1}{V} \int_{\mathcal{B}} \boldsymbol{P}\, dV, \;\; \boldsymbol{P} = \boldsymbol{\tau} \boldsymbol{F}^{-T}$

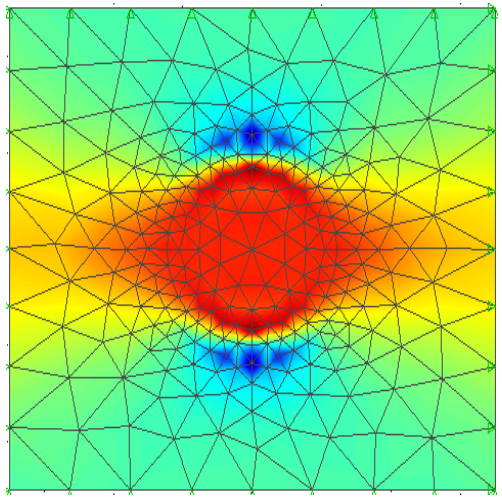



# Direct Incorporation of Microstructure

## Microscopic FE-discretization of dual phase steel:

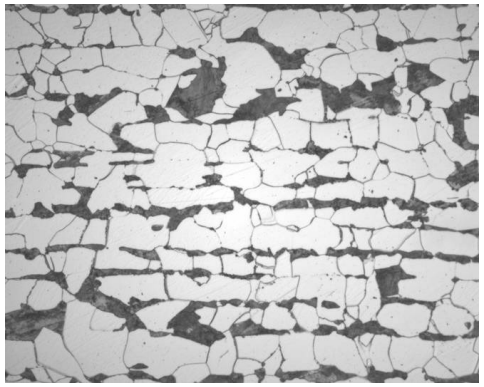

Real microstructure

$\Rightarrow$


Binary image

$\Rightarrow$

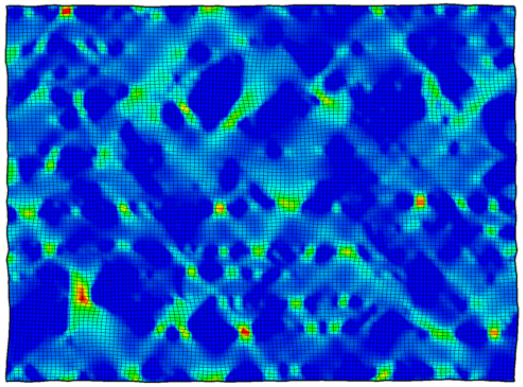

FE-calculation movie

## Direct micro-macro approach:

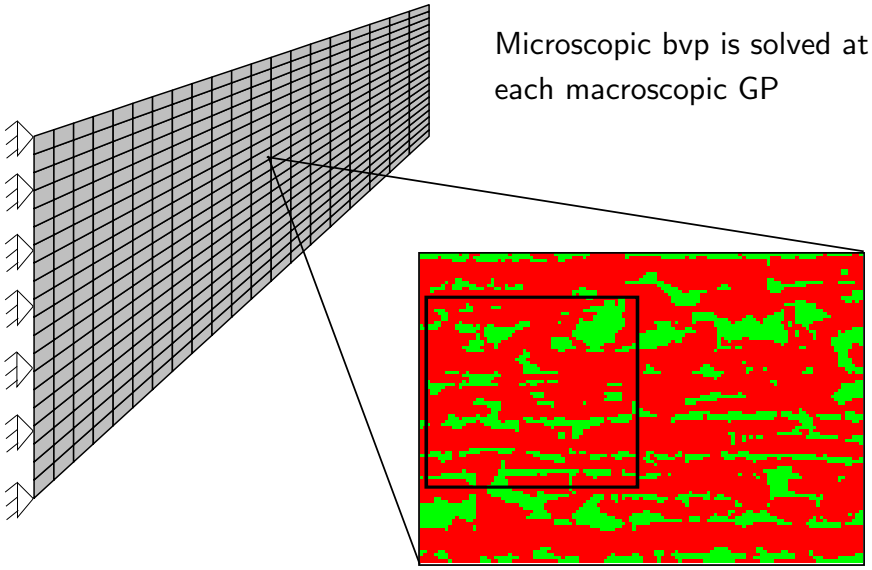

Microscopic bvp is solved at each macroscopic GP

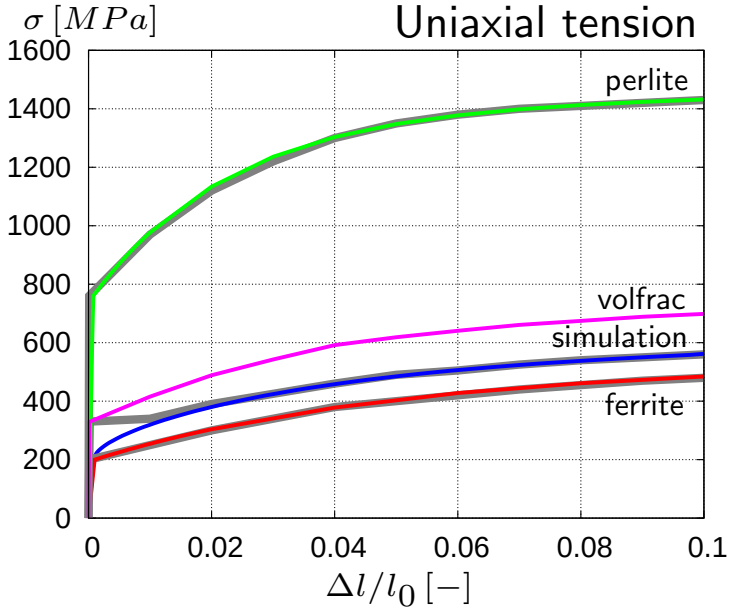


**Goal:** Setup of an algorithmically consistent FE$^2$-homogenization scheme!



# Selected References


- Ghosh S., Lee K., Moorthy S.; Multiple scale analysis of heterogeneous elastic structures using homogenisation theory and voronoi cell finite element method. *International Journal of Solids and Structures* 1995; **32**:27-62
- Smit R.J.M., Brekelmans W.A.M., Meijer H.E.H.; Prediction of the mechanical behaviour of non-linear heterogeneous systems by multilevel finite element modeling. *Computer Methods in Applied Mechanics and Engineering* 1998; **155**:181-192
- Moulinec H., Suquet P.; A numerical method for computing the overall response of nonlinear composites with complex microstructure. *Computer Methods in Applied Mechanics and Engineering* 1998; **157**:69-94
- Miehe C, Schröder J, Schotte J.; Computational homogenization analysis in finite plasticity. Simulation of texture development in polycrystalline materials. *Computer Methods in Applied Mechanics and Engineering* 1999; **171**:387-418
- Miehe C, Schotte J, Schröder J.; Computational micro-macro transitions and overall moduli in the analysis of polycrystals at large strains. *Computational Materials Science* 1999; **16**:372-382
- Feyel F, Chaboche JL.; $FE^2$ multiscale approach for modelling the elastovisco-plastic behavior of long fiber SiC/Ti composite materials. *Computer Methods in Applied Mechanics and Engineering* 2000; **183**:309-330




# **Selected References** (cont'd)


- Terada K., Kikuchi N.; A class of general algorithms for multi-scale analysis of heterogeneous media. *Computer Methods in Applied Mechanics and Engineering* 2001; **190**:5427-5464
- Kouznetsova V.G., Brekelmans W.A.M., Baaijens F.T.P.; An approach to micro-macro modeling of heterogeneous materials. *Computational Mechanics* 2001; **27**:37-48
- Kouznetsova V.G, Geers M.G.D., Brekelmans W.A.M.; Multi-scale constitutive modelling of heterogeneous materials with gradient-enhanced computational homogenisation scheme. *International Journal for Numerical Methods in Engineering* 2002; **54**:1235-1260
- Kouznetsova V.G., Geers M.G.D., Brekelmans W.A.M. ; Multi-scale second order computational homogenization of multi-phase materials: A nested finite element solution strategy. *Computer Methods in Applied Mechanics and Engineering* 2004; **193**:5525-5550
- Ozdemir I., Brekelmans W.A.M., Geers M.G.D.; Computational homogenization for heat conduction in heterogeneous solids. *International Journal for Numerical Methods in Engineering* 2008; **73**:185-204




# **Selected References** (cont'd)


- Verhoosel C.V., Remmers J.J.C., Gutiérrez M.A., de Borst R.; Computational homogenization for adhesive and cohesive failure in quasi-brittle solids. *International Journal for Numerical Methods in Engineering* 2010; **83**:1155-1179
- Temizer I., Wriggers P.; Inelastic analysis of granular interfaces via computational contact homogenization. *International Journal for Numerical Methods in Engineering* 2010; **84**:883-915
- Geers M.G.D., Kouznetsova V.G., Brekelmans W.A.M.; Multi-scale computational homogenization: Trends and challenges. *Journal of Computational and Applied Mathematics* 2010; **234**:2175-2182


.

.

.



# Direct Micro-Macro Transition Approach ($FE^2$)

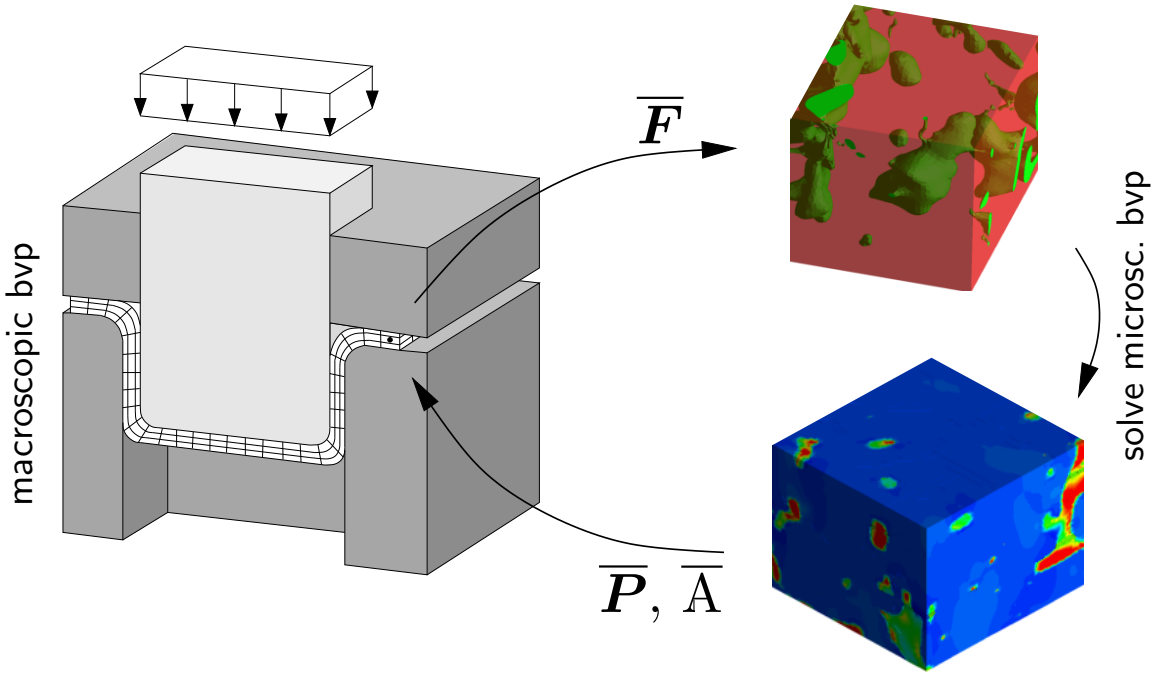


**Microscale:**

1. FE-Discretization of a representative volume element (RVE) and application of e.g. displacement boundary conditions $\boldsymbol{x} = \overline{\boldsymbol{F}}\boldsymbol{X}$ on $\partial\mathcal{B}$

2. Solution of non-linear microscopic boundary value problem

3. Calculation of macroscopic stresses $\overline{\boldsymbol{P}}$ and tangent moduli $\overline{\mathbb{A}} = \dfrac{\partial\overline{\boldsymbol{P}}}{\partial\overline{\boldsymbol{F}}}$

Suquet [1987], Miehe et al. [...], JS [...], Geers et al. [...], Bertram et al. [...], Wriggers et al. [...], ...



# Benefits of $FE^2$

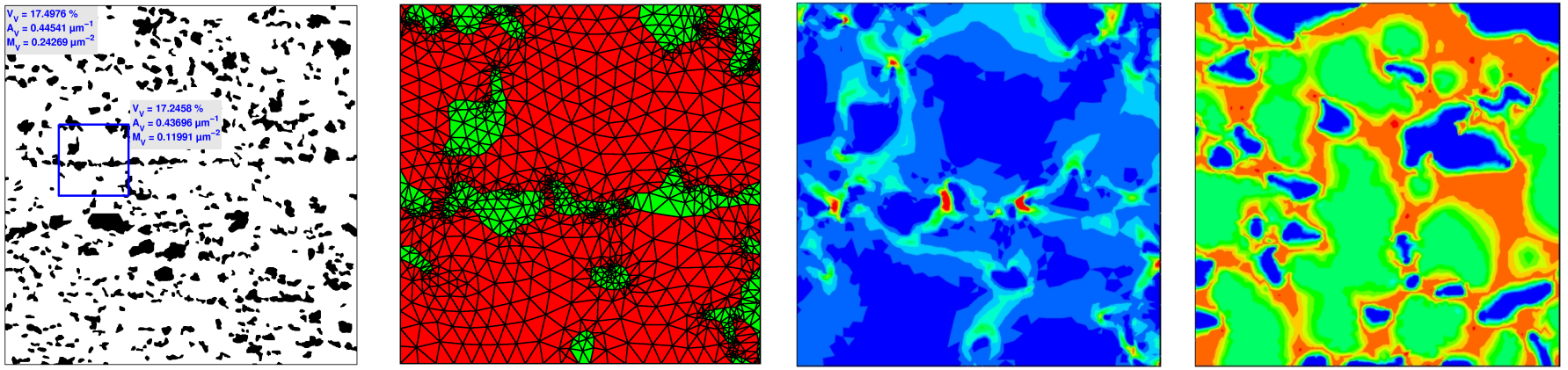


- A priori micromechanically motivated model
- No phenomenological constitutive law at the macroscale required
- Anisotropic finite plasticity with kinematic hardening at macroscale representable due to interaction of individual phases at the microscale
- Incorporation of mechanical phenomena observed at the microscale such as:
  - ⋆ Eigenstresses due to microscopic phase transformations or thermal loading
  - ⋆ Graded microscopic material properties or grain boundary effects
- ...



# Drawback of FE$^2$: Computationally Expensive Method

**Macroscale**

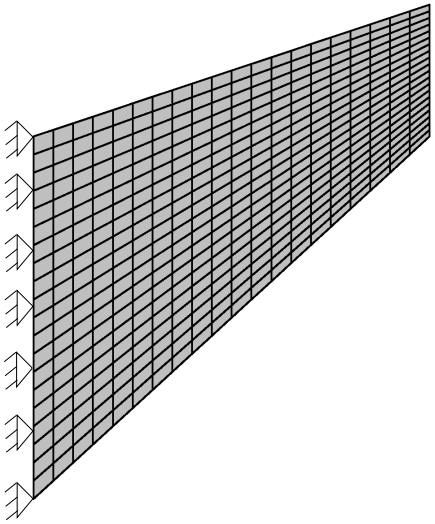

**Microscale**

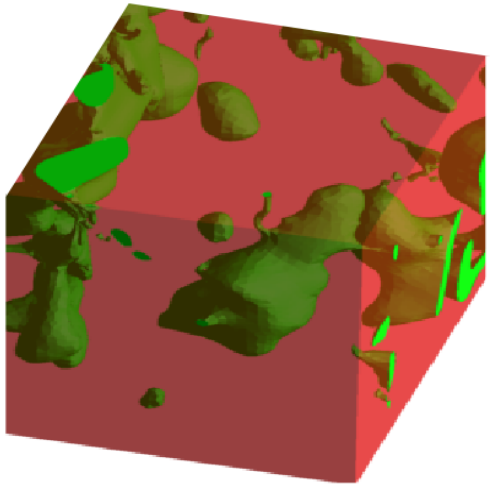

Macroscopic BVP: $20 \times 20$ quadrilateral elements with 4 Gauss-points (GPs) each
$\rightarrow$ 1 600 GPs = microscopic bvps (to be solved at each macroscopic iteration)

Microscopic BVP: approx. 100 000 tetrahedral elements with 5 GPs each
$\rightarrow 1 \cdot 10^6$ dofs, $100\,000 \times 5 \times 10 = 5 \cdot 10^6$ history variables (for plasticity)

**History memory requirements:**

$1600 \times (5\,000\,000 + 1\,000\,000) \times 8$ byte $\approx$ 76 Gbyte

**Computing time:** (assume 1 hour for solution of one microscopic bvp)

$1600 \times 1 = 1600$ h $\approx$ 67 days per macroscopic iteration step



# Drawback of FE$^2$: Computationally Expensive Method

**Macroscale**

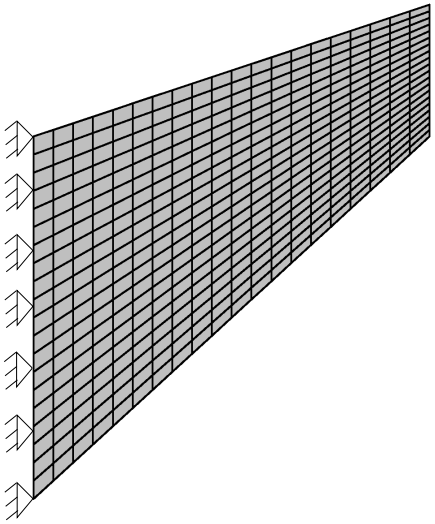

**Microscale**

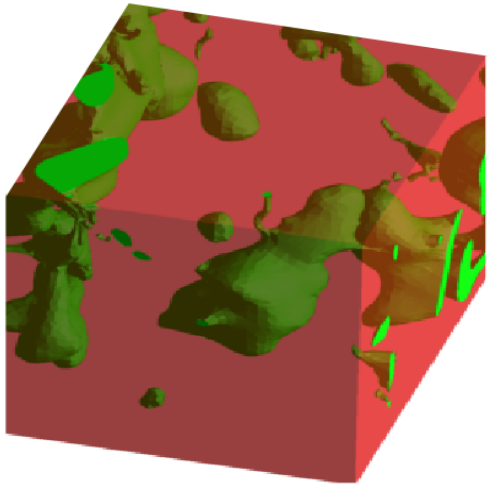

Macroscopic BVP: 20 $\times$ 20 quadrilateral elements with 4 Gauss-points (GPs) each
$\rightarrow$ 1 600 GPs = microscopic bvps (to be solved at each macroscopic iteration)

Microscopic BVP: approx. 100 000 tetrahedral elements with 5 GPs each
$\rightarrow 1 \cdot 10^6$ dofs, $100\,000 \times 5 \times 10 = 5 \cdot 10^6$ history variables (for plasticity)

**Possible outcome:**

- Strong parallelization of microscopic boundary value problems (BVPs)
- Adaptive method: Only consider FE$^2$ at points of interest
- Reduction of memory and computing time of microscopic BVP
  $\rightarrow$ utilization of simplified RVEs



# Macroscopic Boundary Value Problem

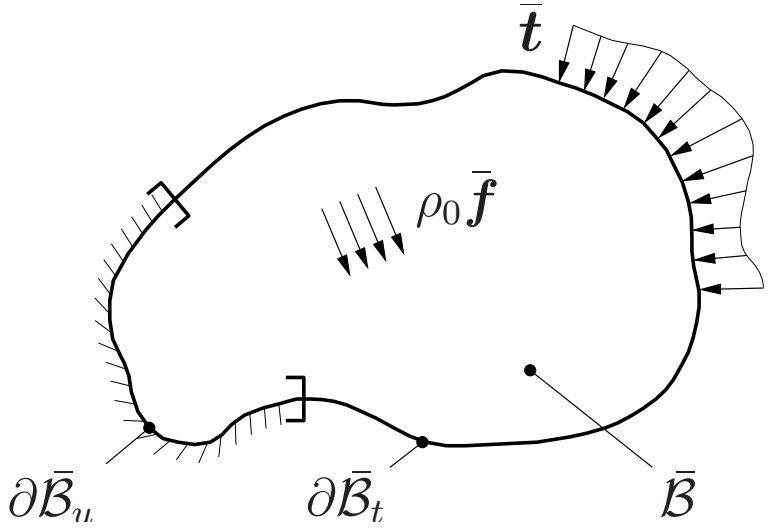


balance equation:

$$\mathrm{Div}_{\overline{X}}[\overline{\boldsymbol{P}}] + \rho_0\ \overline{\boldsymbol{f}} = \boldsymbol{0} \quad \text{in} \quad \overline{\mathcal{B}}$$

boundary conditions

$$\overline{\boldsymbol{u}} = \overline{\boldsymbol{u}}_0 \text{ on } \partial\overline{\mathcal{B}}_u \quad \text{and} \quad \bar{\boldsymbol{t}}_0 = \overline{\boldsymbol{P}}\ \overline{\boldsymbol{N}} \text{ on } \partial\overline{\mathcal{B}}_t$$

The principle of virtual work $\overline{G} := \int_{\overline{\mathcal{B}}} (\mathrm{Div}_{\overline{X}}\overline{\boldsymbol{P}} + \rho_0\ \overline{\boldsymbol{f}}) \cdot \delta\overline{\boldsymbol{u}}\ dV = 0$ leads to

$$\overline{G} := \int_{\overline{\mathcal{B}}} (\delta\overline{\boldsymbol{F}} : \overline{\boldsymbol{P}} - \delta\overline{\boldsymbol{x}} \cdot \rho_0\overline{\boldsymbol{f}})\, dV - \int_{\partial\overline{\mathcal{B}}_t} \delta\overline{\boldsymbol{x}} \cdot \bar{\boldsymbol{t}}_0\, dA = 0\,, \text{ with } \delta\overline{\boldsymbol{F}} = \mathrm{Grad}_{\overline{X}}\delta\overline{\boldsymbol{x}}$$

and the linearization (neglecting unconservative loads) is given by

$$\mathrm{Lin}\overline{G} = \overline{G}|_{\overline{\boldsymbol{x}}^\star} + \Delta\overline{G} \quad \text{with} \quad \Delta\overline{G} = \int_{\overline{\mathcal{B}}} \delta\overline{\boldsymbol{F}} : \overline{\mathbb{A}} : \Delta\overline{\boldsymbol{F}}\, dV$$

Note: At the macroscale the consistent moduli $\overline{\mathbb{A}} = \partial_{\overline{\boldsymbol{F}}}\overline{\boldsymbol{P}}$ have to be derived!



# Microscopic Boundary Value Problem

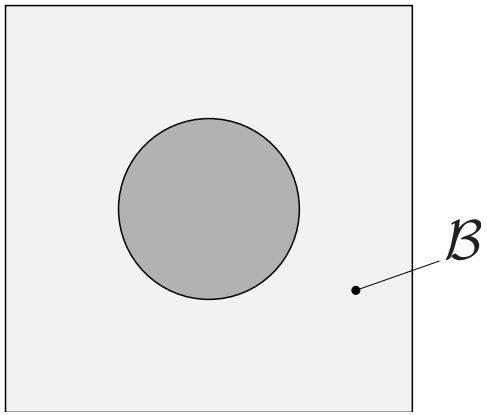


macroscopic stress condition

$$\overline{\boldsymbol{P}} = \frac{1}{V}\int_{\mathcal{B}} \boldsymbol{P}\, dV = \frac{1}{V}\int_{\partial\mathcal{B}} \boldsymbol{t}\otimes\boldsymbol{X}\, dA$$

macroscopic deformation condition

$$\overline{\boldsymbol{F}} = \frac{1}{V}\int_{\mathcal{B}} \boldsymbol{F}\, dV = \frac{1}{V}\int_{\partial\mathcal{B}} \boldsymbol{x}\otimes\boldsymbol{N}\, dA$$

balance of linear momentum: $\mathrm{Div}[\boldsymbol{P}] = \boldsymbol{0}$ in $\mathcal{B}$

weak form of balance of linear momentum $G := \int_{\mathcal{B}} \mathrm{Div}\boldsymbol{P}\cdot\delta\boldsymbol{x}\, dV = 0$ , leads to

$$\boxed{G := \int_{\mathcal{B}} \delta\boldsymbol{F} : \boldsymbol{P}\, dV - \int_{\partial\mathcal{B}_t} \delta\boldsymbol{x}\cdot\boldsymbol{t}_0\, dA = 0\,,\ \text{with}\ \delta\boldsymbol{F} = \mathrm{Grad}_X\delta\boldsymbol{x}}$$

and the linearization

$$\mathrm{Lin}G = G|_{\boldsymbol{x}^\star} + \Delta G \quad \text{with} \quad \Delta G = \int_{\mathcal{B}} \delta\boldsymbol{F} : \mathrm{A} : \Delta\boldsymbol{F}\, dV, \quad \mathrm{A} = \partial_{\boldsymbol{F}}\boldsymbol{P}$$

Note: At the microscale suitable boundary conditions have to be defined!



# Macro-Homogeneity-Condition

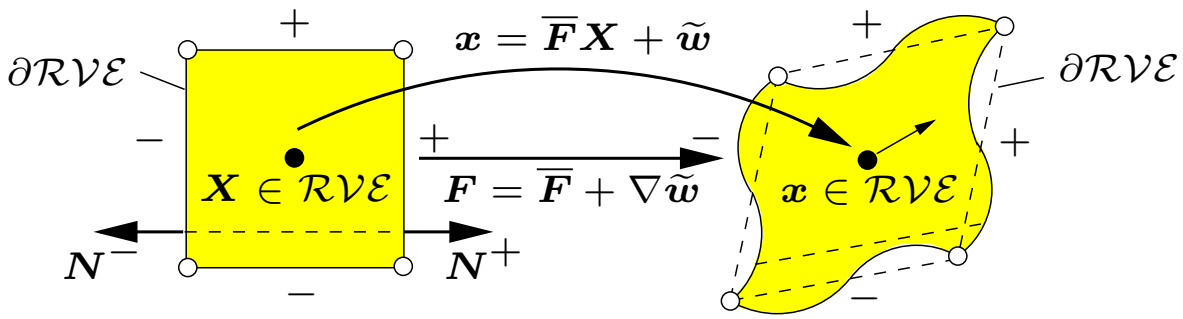


The Macro-Homogeneity condition (Hill criterion)

$$\overline{\boldsymbol{P}} : \dot{\overline{\boldsymbol{F}}} = \frac{1}{V}\int_{\mathcal{B}} \boldsymbol{P} : \dot{\boldsymbol{F}}\, dV$$

is fulfilled by applying the three types of boundary conditions:

| | | | | |
|---|---|---|---|---|
| (i) | Stress bc's | $\boldsymbol{t}_0$ | $= \overline{\boldsymbol{P}}\boldsymbol{N}$ | on $\partial\mathcal{B}$ |
| (ii) | Displacements bc's | $\boldsymbol{x}$ | $= \overline{\boldsymbol{F}}\boldsymbol{X}$ | on $\partial\mathcal{B}$ |
| (iii) | Periodic bc's | $\left\{ \begin{array}{l} \boldsymbol{x} \\ \widetilde{\boldsymbol{w}}^+ \end{array} \right.$ | $\left. \begin{array}{l} = \overline{\boldsymbol{F}}\boldsymbol{X} + \widetilde{\boldsymbol{w}} \\ = \widetilde{\boldsymbol{w}}^-,\ \boldsymbol{t}_0^+ = -\boldsymbol{t}_0^- \end{array} \right\}$ | on $\partial\mathcal{B}$ |

for the microscopic BVP, $\mathrm{Div}[\boldsymbol{P}] = \boldsymbol{0}$ in $\mathcal{B}$; the weak form of equilibrium reads

$$G := \int_{\mathcal{B}} \delta\widetilde{\boldsymbol{F}} : \boldsymbol{P}\, dV = 0, \quad \Delta G = \int_{\mathcal{B}} \delta\widetilde{\boldsymbol{F}} : \mathrm{A} : \Delta\boldsymbol{F}\, dV, \quad \text{with} \quad \delta\widetilde{\boldsymbol{F}} = \mathrm{Grad}\,\delta\widetilde{\boldsymbol{w}}$$



# Influence of Different Boundary Conditions

periodic microstructure

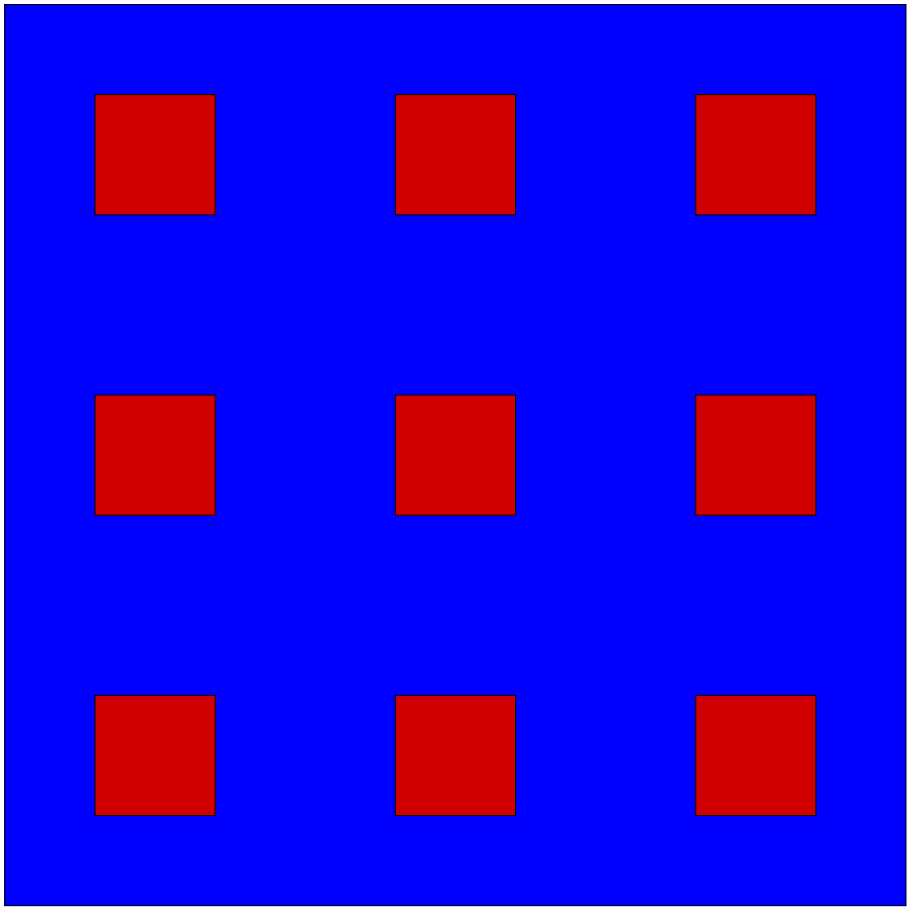

2 possible RVEs

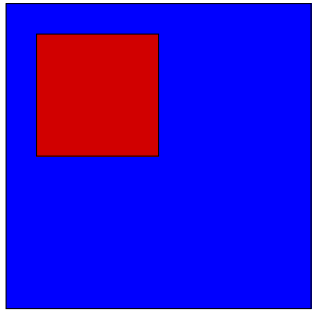

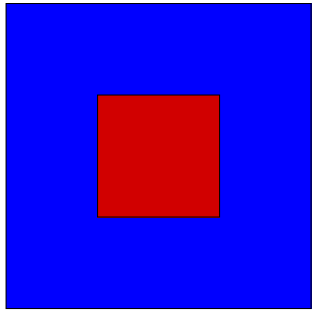

(taken from SCHRÖDER [2000], habilitation thesis, report no. I-7, Institut für Mechanik, Lehrstuhl I, Prof. Dr.-Ing. C. Miehe, Stuttgart)



# Influence of Different Boundary Conditions

**Distribution of stress $\sigma_{11}$**

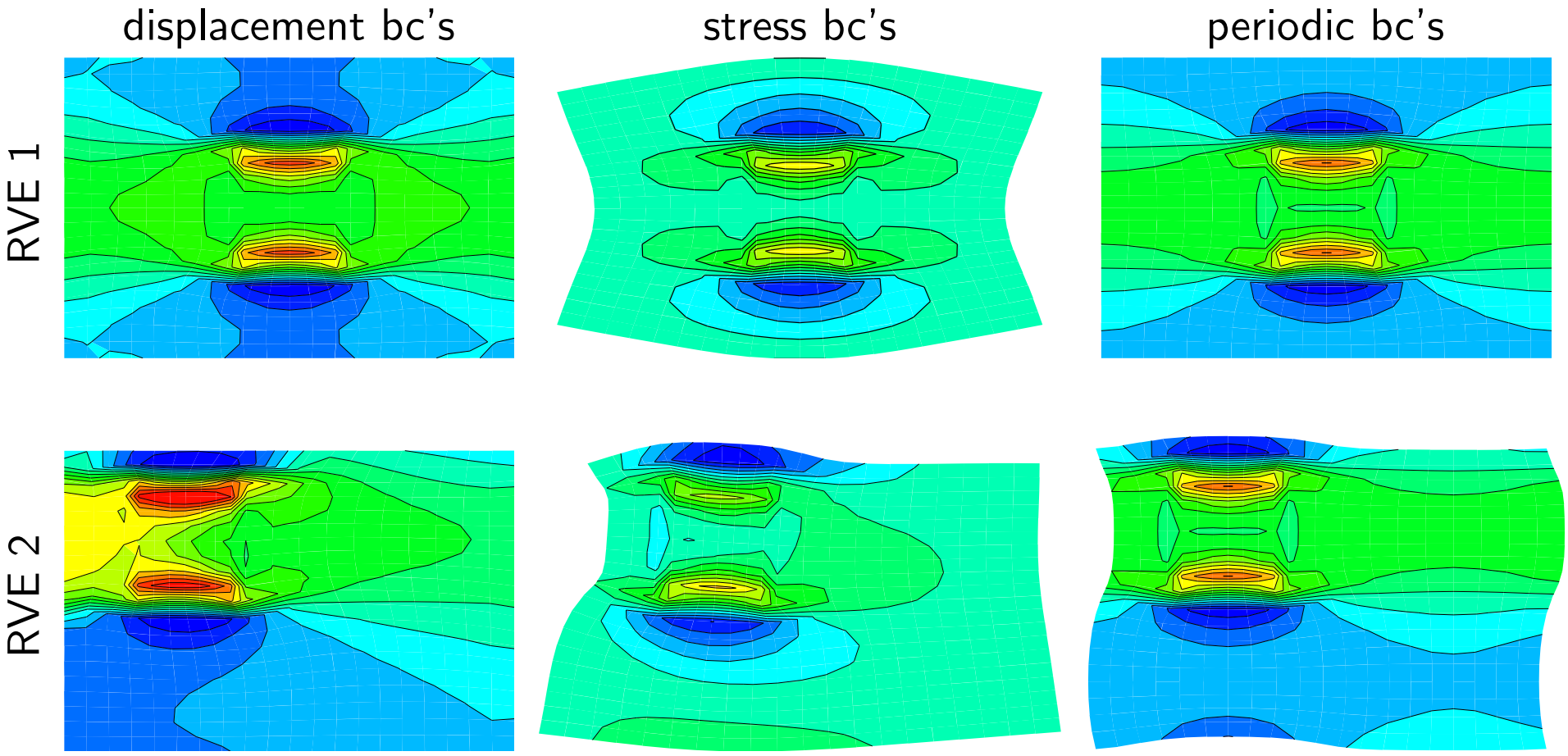


$\rightarrow$ Only the application of periodic boundary conditions results in a stress distribution, which is nearly independent from the relative location of the inclusion.

(taken from SCHRÖDER [2000], habilitation thesis, report no. I-7, Institut für Mechanik, Lehrstuhl I, Prof. Dr.-Ing. C. Miehe, Stuttgart)



# Computation of Algorithmic Consistent Overall Moduli

The incremental constitutive relation at the macroscale reads

$$\Delta\overline{\boldsymbol{P}} = \overline{\mathbb{A}} : \Delta\overline{\boldsymbol{F}} = \left\{ \frac{1}{V} \frac{\partial}{\partial \overline{\boldsymbol{F}}} \int_{\mathcal{B}} \boldsymbol{P}(\boldsymbol{F})\, dV \right\} : \Delta\overline{\boldsymbol{F}}$$

with the overall (effective) moduli

$$\overline{\mathbb{A}} = \frac{1}{V} \int_{\mathcal{B}} \frac{\partial}{\partial \overline{\boldsymbol{F}}} \boldsymbol{P}(\boldsymbol{F})\, dV = \frac{1}{V} \int_{\mathcal{B}} \frac{\partial \boldsymbol{P}(\boldsymbol{F})}{\partial \boldsymbol{F}} : \frac{\partial \boldsymbol{F}}{\partial \overline{\boldsymbol{F}}}\, dV$$

exploiting the decomposition of $\boldsymbol{F}$ $(\boldsymbol{x} = \overline{\boldsymbol{F}}\boldsymbol{X} + \tilde{\boldsymbol{w}} \;\rightarrow\; \nabla\boldsymbol{x} = \nabla\overline{\boldsymbol{F}}\boldsymbol{X} + \nabla\tilde{\boldsymbol{w}})$

$$\boldsymbol{F} = \overline{\boldsymbol{F}} + \widetilde{\boldsymbol{F}}$$

leads with the abbreviation $\mathbb{A} := \partial_F \boldsymbol{P}(\boldsymbol{F})$ to

$$\overline{\mathbb{A}} = \frac{1}{V} \int_{\mathcal{B}} \mathbb{A}\, dV + \frac{1}{V} \int_{\mathcal{B}} \mathbb{A} : \frac{\partial \widetilde{\boldsymbol{F}}}{\partial \overline{\boldsymbol{F}}}\, dV \qquad (*)$$

Sensitivity of $\widetilde{\boldsymbol{F}}$ with respect to $\overline{\boldsymbol{F}}$ ?



# Computation of Algorithmic Consistent Overall Moduli (cont'd)

Consideration of weak form of balance of linear momentum at the microscale

$$G = -\int_{\mathcal{B}} \mathrm{Div}\boldsymbol{P} \cdot \delta\widetilde{\boldsymbol{w}}\, dV = \int_{\mathcal{B}} \delta\widetilde{\boldsymbol{F}} : \boldsymbol{P}\, dV - \int_{\partial\mathcal{B}} \delta\widetilde{\boldsymbol{w}} \cdot \boldsymbol{t}\, dA$$

Linearization of $G$ at an equilibrium state $G = 0 \;\rightarrow\; \Delta G = 0$

$$\int_{\mathcal{B}} \delta\widetilde{\boldsymbol{F}} : \mathbb{A} : \Delta\boldsymbol{F}\, dV = 0 \;\rightarrow\; \int_{\mathcal{B}} \delta\widetilde{\boldsymbol{F}} : \mathbb{A} : \Delta\overline{\boldsymbol{F}}\, dV + \int_{\mathcal{B}} \delta\widetilde{\boldsymbol{F}} : \mathbb{A} : \Delta\widetilde{\boldsymbol{F}}\, dV = 0$$

Ansatz in a typical finite element

$$\begin{aligned} \widetilde{\boldsymbol{w}} &= \mathbb{N}^e\widetilde{\boldsymbol{d}}, \quad & \delta\widetilde{\boldsymbol{w}} &= \mathbb{N}^e\delta\widetilde{\boldsymbol{d}}, \quad & \Delta\widetilde{\boldsymbol{w}} &= \mathbb{N}^e\Delta\widetilde{\boldsymbol{d}}, \\ \widetilde{\boldsymbol{F}} &= \mathbb{B}^e\widetilde{\boldsymbol{d}}, \quad & \delta\widetilde{\boldsymbol{F}} &= \mathbb{B}^e\delta\widetilde{\boldsymbol{d}}, \quad & \Delta\widetilde{\boldsymbol{F}} &= \mathbb{B}^e\Delta\widetilde{\boldsymbol{d}} \end{aligned}$$

$$\sum_{e=1}^{nele} \left\{ \delta\widetilde{\boldsymbol{d}}^T \left( \boldsymbol{l}^e\, \Delta\overline{\boldsymbol{F}} + \boldsymbol{k}^e \Delta\widetilde{\boldsymbol{d}} \right) \right\} = 0$$

with the abbreviations

$$\boldsymbol{k}^e = \int_{\mathcal{B}} \mathbb{B}^{eT} \mathbb{A}\, \mathbb{B}^e\, dV\,, \quad \boldsymbol{l}^e = \int_{\mathcal{B}} \mathbb{B}^{eT} \mathbb{A}\, dV$$



# Computation of Algorithmic Consistent Overall Moduli (cont'd)

Application of standard assembling procedure yields

$$\delta \boldsymbol{D}^T \left( \mathbb{K} \Delta \widetilde{\boldsymbol{D}} + \mathbb{L} \Delta \overline{\boldsymbol{F}} \right) = 0$$

with global stiffness matrix and generalized right hand sides (micro continuum)

$$\mathbb{K} = \mathop{\mathbf{A}}_{e=1}^{nele} \boldsymbol{k}^e \,, \quad \mathbb{L} = \mathop{\mathbf{A}}_{e=1}^{nele} \boldsymbol{l}^e$$

solution for incremental fluctuation field

$$\Delta \widetilde{\boldsymbol{D}} = -\mathbb{K}^{-1} \mathbb{L} \, \Delta \overline{\boldsymbol{F}}$$

Inserting in equation (*) and exploiting $\widetilde{\boldsymbol{F}} = \mathbb{B} \widetilde{\boldsymbol{d}}$ yields

$$\overline{\mathbb{A}} = \frac{1}{V} \int_{\mathcal{B}} \mathbb{A} \, dV + \frac{1}{V} \mathbb{L}^T \frac{\partial}{\partial \overline{\boldsymbol{F}}} \Delta \widetilde{\boldsymbol{D}}$$

$$\boxed{\overline{\mathbb{A}} = \frac{1}{V} \int_{\mathcal{B}} \mathbb{A} \, dV - \frac{1}{V} \mathbb{L}^T \mathbb{K}^{-1} \mathbb{L}}$$



# Isotropic Finite $J_2$-Plasticity

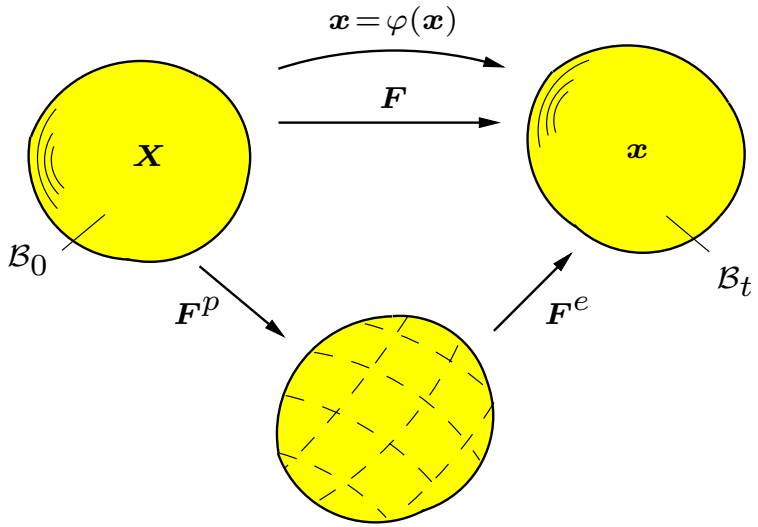


Multiplicative decomposition (Flory [1961], Lee & Liu [1967])

$$\boldsymbol{F} = \boldsymbol{F}^e \boldsymbol{F}^p \quad \text{with} \quad \boldsymbol{F} = \text{Grad}\boldsymbol{x}$$

Right and left Cauchy-Green tensors

$$\boldsymbol{C} = \boldsymbol{F}^T \boldsymbol{F}; \quad \boldsymbol{C}^p = \boldsymbol{F}^{pT} \boldsymbol{F}^p; \quad \boldsymbol{C}^e = \boldsymbol{F}^{eT} \boldsymbol{F}^e$$

$$\boldsymbol{b} = \boldsymbol{F} \boldsymbol{F}^T; \quad \boldsymbol{b}^p = \boldsymbol{F}^p \boldsymbol{F}^{pT}; \quad \boldsymbol{b}^e = \boldsymbol{F}^e \boldsymbol{F}^{eT}$$

**References:** Simo & Ortiz [85], Simo [85,92,...], Simo & Miehe [92], Miehe [92,...], Miehe & Stein [92], Klinkel [2000], de Souza Neto, Peric & Owen [2007], ...



# Constitutive Model and Parameters

## Finite $J_2$-Plasticity:

Simo & Ortiz [85], Simo [85,92,...], Simo & Miehe [92],...

$$\boldsymbol{F} = \boldsymbol{F}^e \boldsymbol{F}^p, \quad \boldsymbol{b}^e = \boldsymbol{F}^e \boldsymbol{F}^{eT} = \sum_{A=1}^{3} (\lambda_A^e)^2 \boldsymbol{n}_A \otimes \boldsymbol{n}_A$$

$$\psi = \psi^e(\boldsymbol{b}^e) + \psi^p(\alpha)$$

$$\psi^e = \frac{\lambda}{2}[\epsilon_1^e + \epsilon_2^e + \epsilon_3^e]^2 + \mu[(\epsilon_1^e)^2 + (\epsilon_2^e)^2 + (\epsilon_3^e)^2]$$

$$\text{with} \quad \epsilon_A^e = \log(\lambda_A^e)$$

$$\psi^p = y_\infty \alpha - \frac{1}{\eta}(y_0 - y_\infty)\exp(-\eta\alpha) + \tfrac{1}{2}\, h\, \alpha^2$$

$$\boldsymbol{\tau} = \kappa\, \mathrm{tr}\boldsymbol{\epsilon}^e \mathbf{1} + 2\,\mu\, \mathrm{dev}\boldsymbol{\epsilon}^e$$

$$\beta = y_\infty + (y_0 - y_\infty)\exp(-\eta\alpha) + h\, \alpha$$

$$\phi = ||\mathrm{dev}\boldsymbol{\sigma}|| - \sqrt{\tfrac{2}{3}}\beta, \quad \tfrac{1}{2}\mathcal{L}(\boldsymbol{b}^e)\boldsymbol{b}^{e-1} = -\lambda \partial_\tau \Phi$$

$$\dot{\alpha} = \sqrt{\tfrac{2}{3}}\lambda$$

$$\lambda \geq 0; \quad \Phi \leq 0; \quad \lambda\Phi = 0$$

Numerical implementation: Klinkel [2000]

## Parameters:

| | | matrix |
|---|---|---|
| $E$ | [MPa] | 206,000.0 |
| $\nu$ | [-] | 0.3 |
| $y_0$ | [MPa] | 200.0 |
| $y_\infty$ | [MPa] | 200.0 |
| $\eta$ | [-] | 0.0 |
| $h$ | [MPa] | 10000.0 |

| | | inclusion |
|---|---|---|
| $E$ | [MPa] | 206,000.0 |
| $\nu$ | [-] | 0.3 |



# Example: Cyclic Tension Test

homogeneous

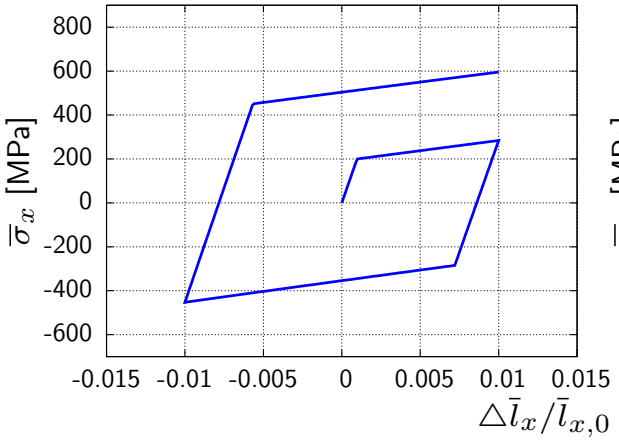


$$f_B = \frac{450-450}{450} = 0.0$$

volume fraction $10\%$

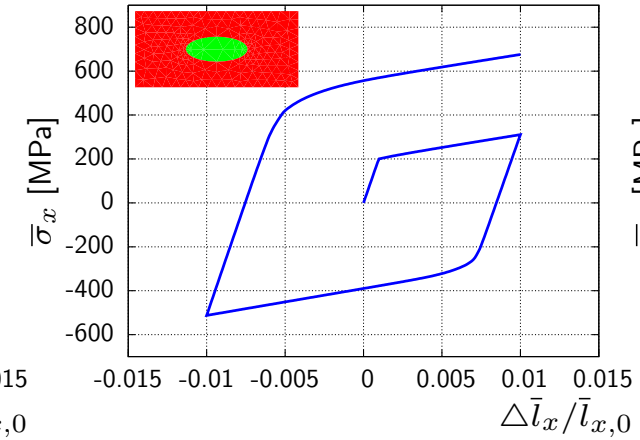


$$f_B = \frac{510-420}{510} = 0.18$$

volume fraction $25\%$

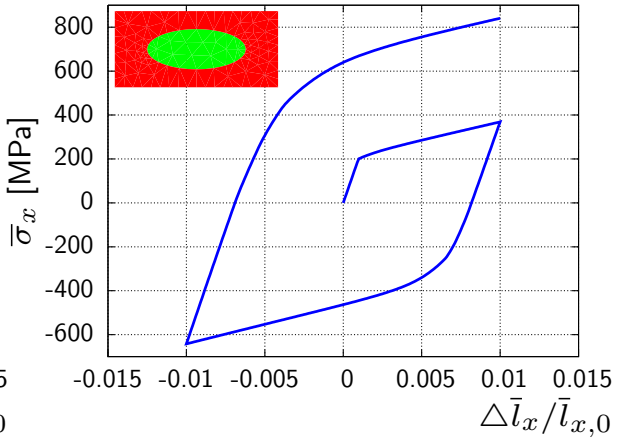


$$f_B = \frac{640-440}{640} = 0.31$$

Bauschinger factor

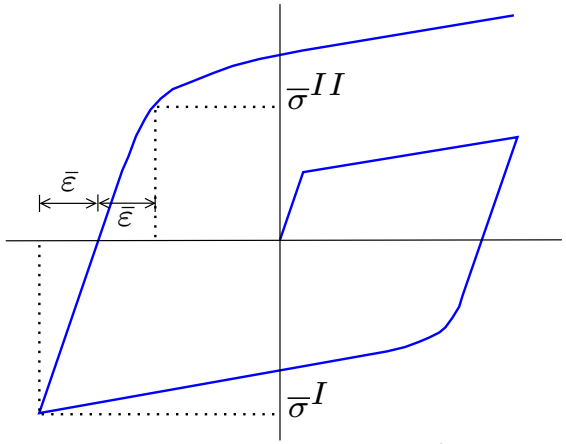


$$f_B = \left(|\overline{\sigma}^I| - \overline{\sigma}^{II}\right) \Big/ |\overline{\sigma}^I|$$

unloaded situation 1 $(\overline{\sigma}_{11} = 0\,,\ \overline{\varepsilon} > 0)$

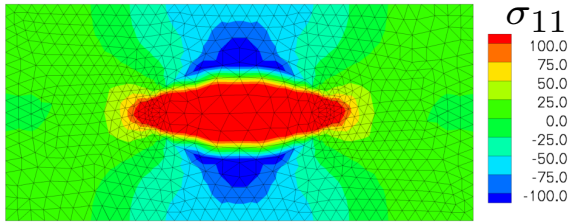


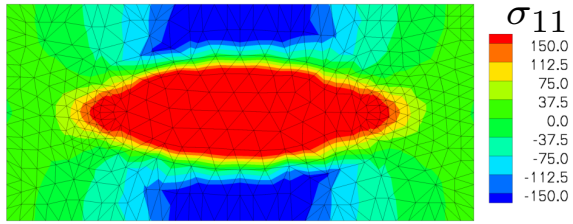


unloaded situation 2 $(\overline{\sigma}_{11} = 0\,,\ \overline{\varepsilon} < 0)$

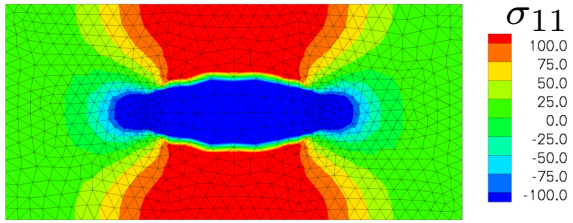


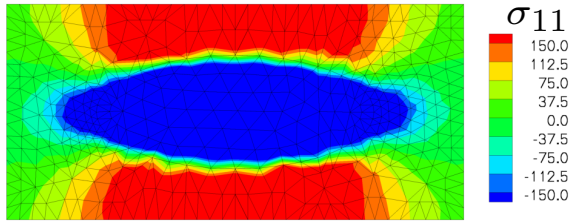




# Discretization of Microscopic Problems

**Unstruct. mesh** **Struct. mesh** **Gauss-point Method**

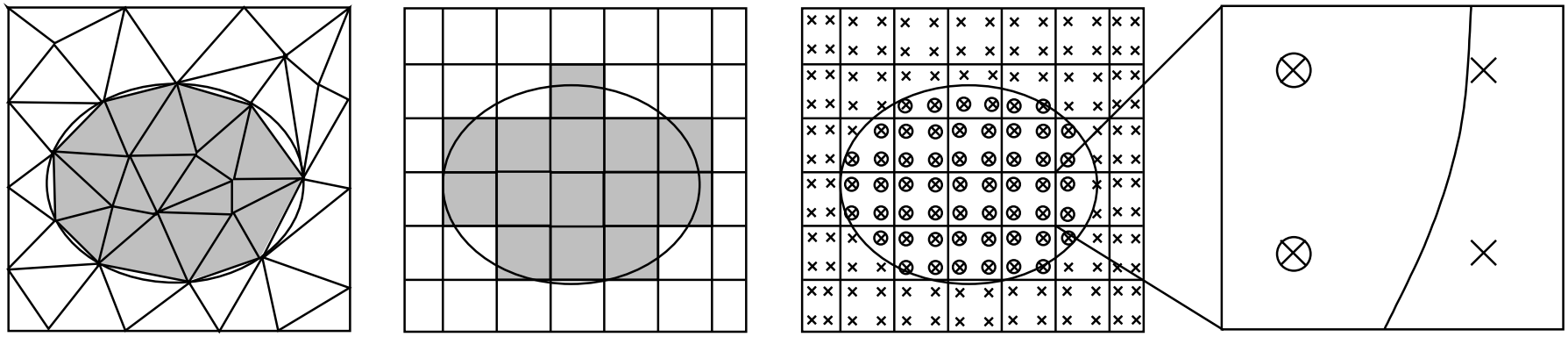

- Unstructured meshes:
  - ⋆ High approximation accuracy of geometry, lower number of elements
  - ⋆ Difficult automated mesh generation, partially distorted meshes
- Structured meshes:
  - ⋆ Direct mesh generation from micrograph images possible
  - ⋆ Poor approximation accuracy, high number of elements required
- Gauss-point Method:
  - ⋆ Direct mesh generation from micrograph images possible, improved approximation accuracy for geometry and internal fields
- X-FEM: implementation demanding, but high approximation accuracy



# Gauss-Point Method: Convergence of Microscopic Fields

**Gauss-Point Method** | **Standard Method**

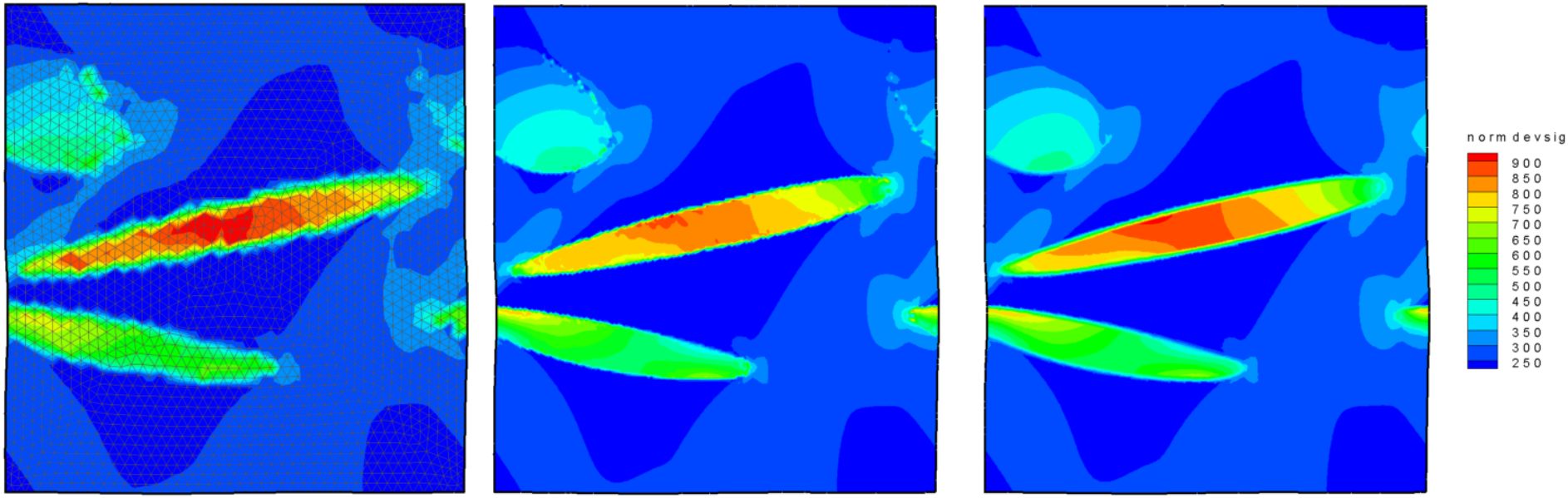


$n_{ele} = 1086$ $n_{ele} = 14632$ $n_{ele} = 12308$

**Considered Numerical Example:**
Macroscopic Uniaxial Tension Test with periodic boundary conditions and triangular elements with quadratic ansatz functions at microscale

$\Rightarrow$ Approximation accuracy of microscopic fields is comparable for fine meshes

$\Rightarrow$ Possible improvements for Gauss-point method by local mesh refinement



# Gauss-Point Method: Convergence of Macroscopic Response

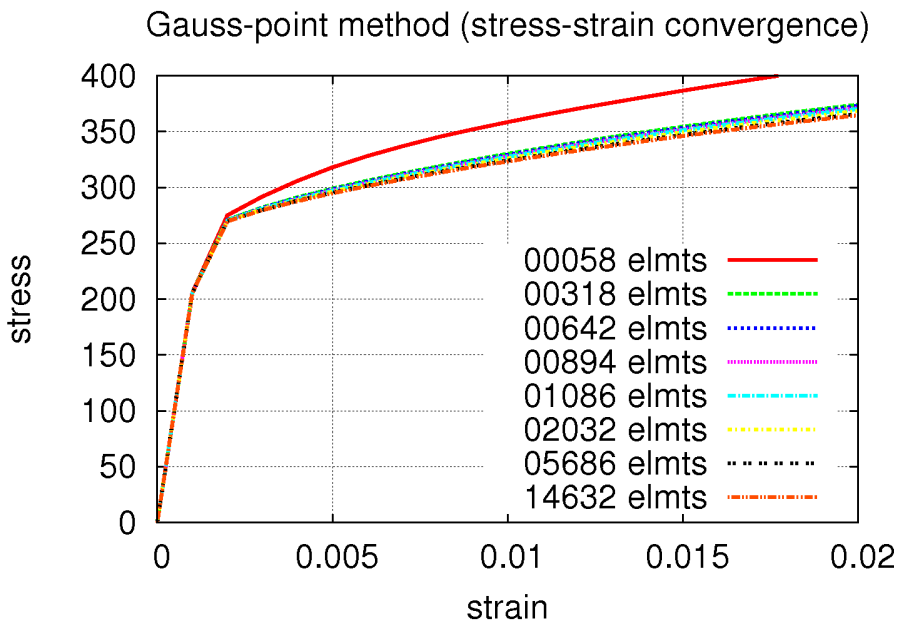


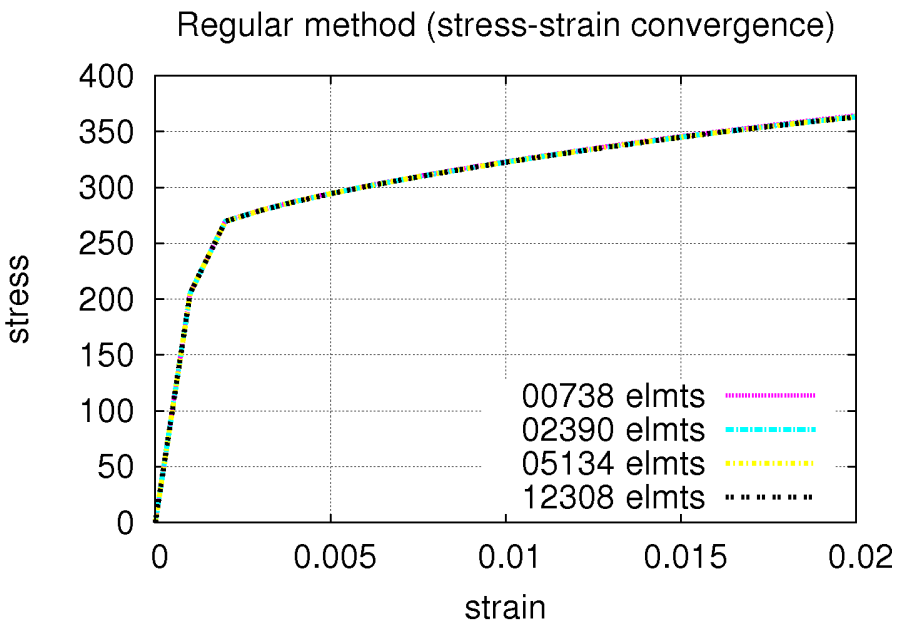


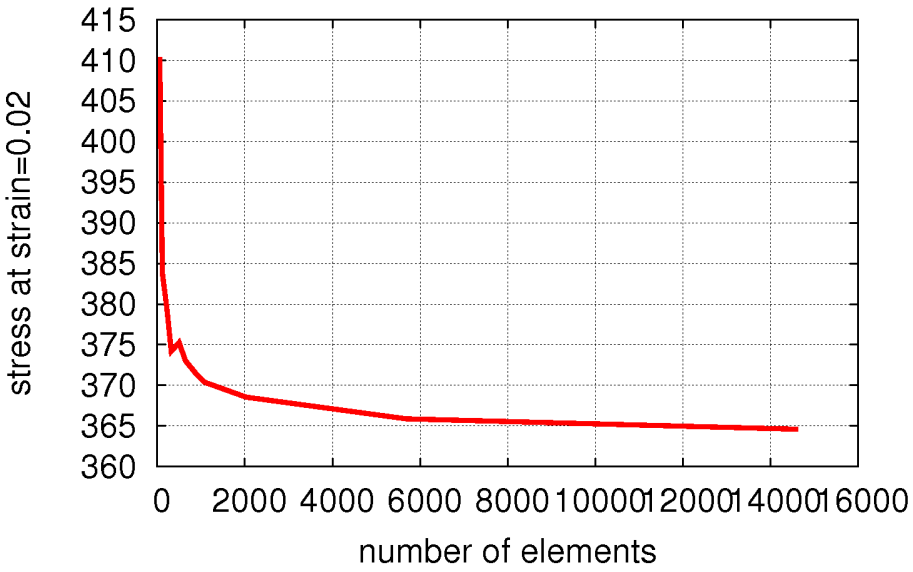


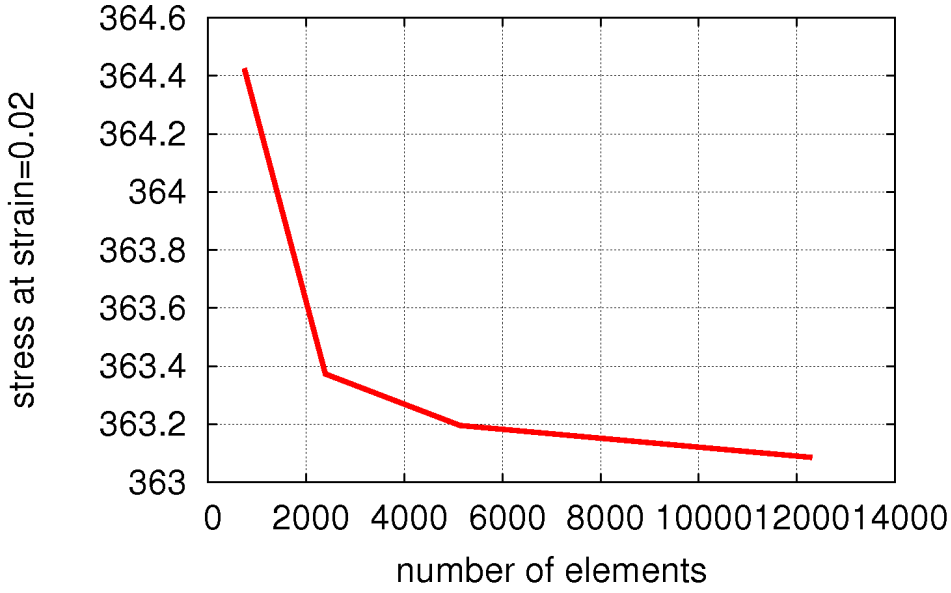


⇒ Better convergence behavior for standard method if local refinement is used



# Example: Deep-Drawing of a Hat Profile

## Setup:

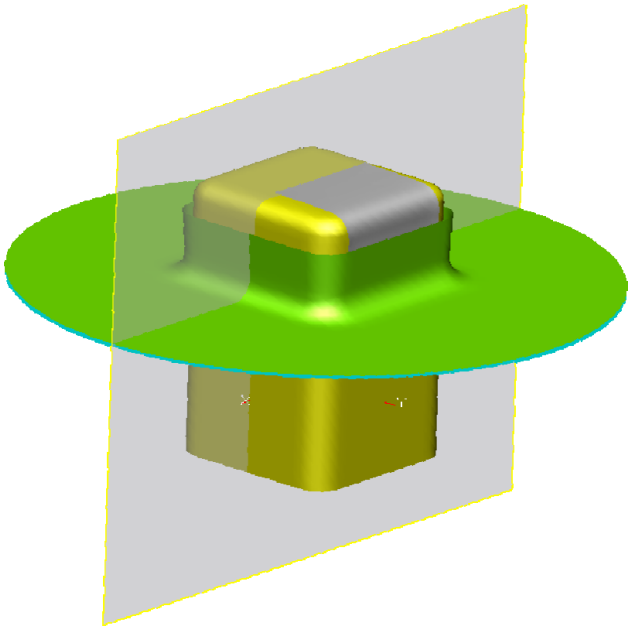

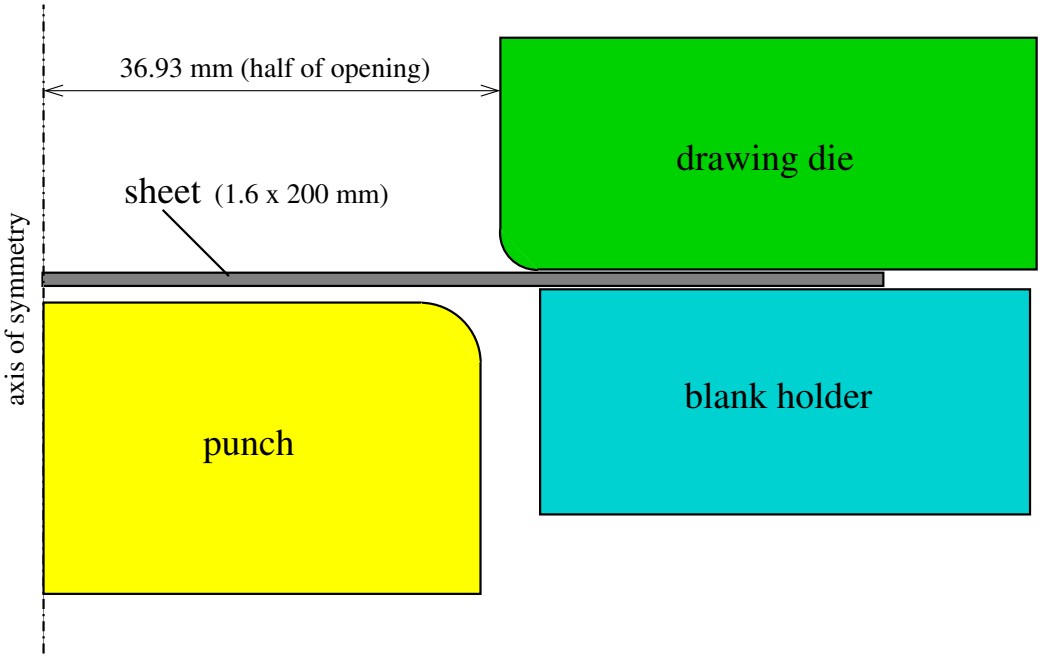


## Process steps:

1. Deep-drawing

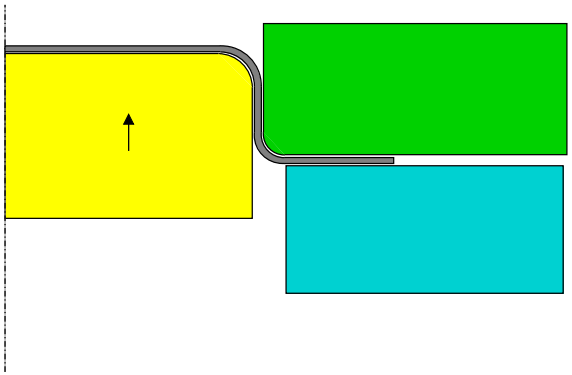

2. Unloading process

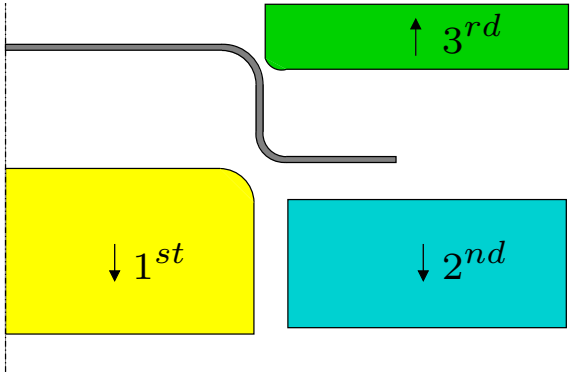




# Example: FE-Discretization of Macro- and Micro-BVP

## Macro-FE-Mesh:

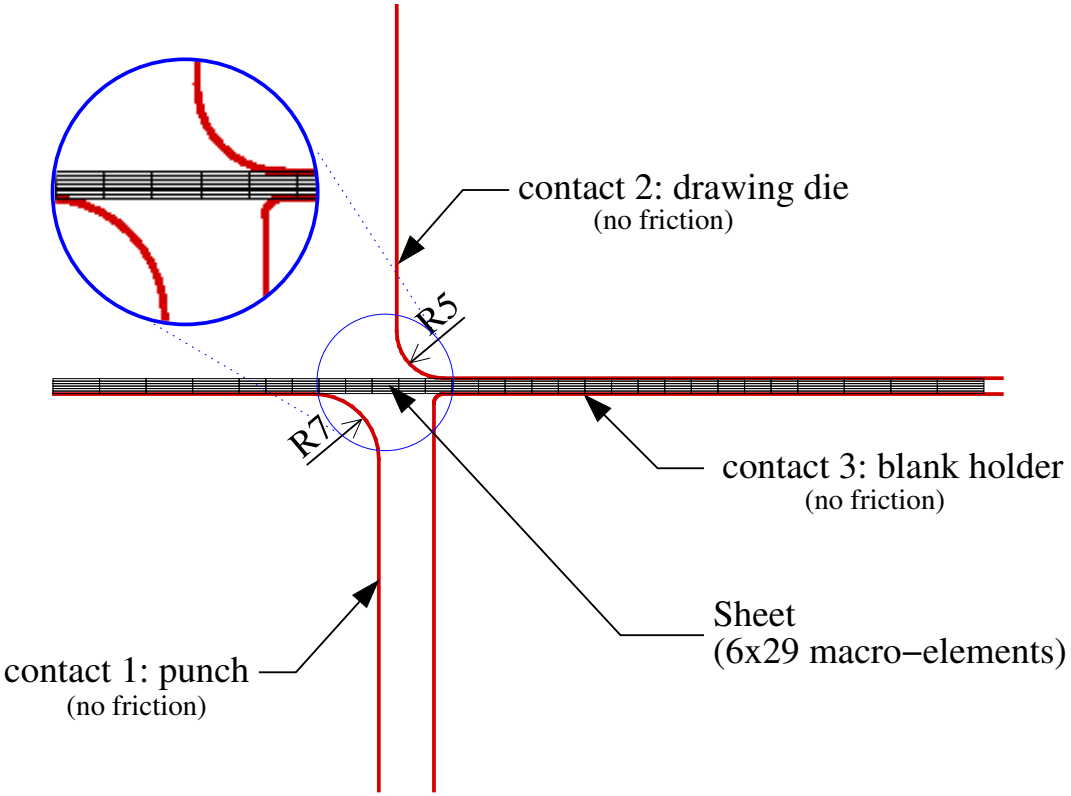


- 174 linear quadrilateral elements
- 288 nodes
- plain strain
- penalty contact formulation
- dynamic (Newmark method: $\beta_1 = 1$, $\beta_2 = 3/2$)

## Micro-FE-Mesh:

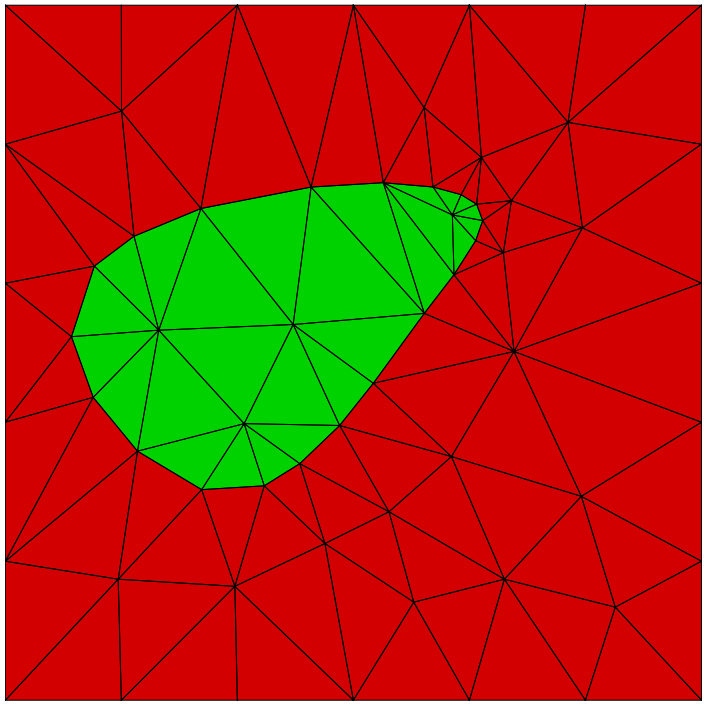

- 102 quadratic triangle elements (plain strain)
- 227 nodes
- periodic boundary conditions



# Example: FE$^2$-Simulation of Deep-Drawing and Unloading

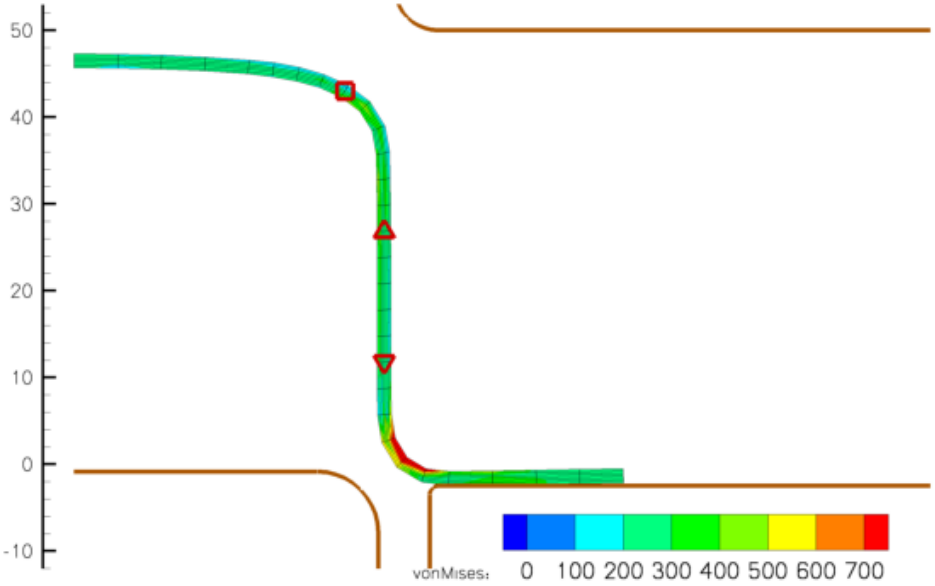


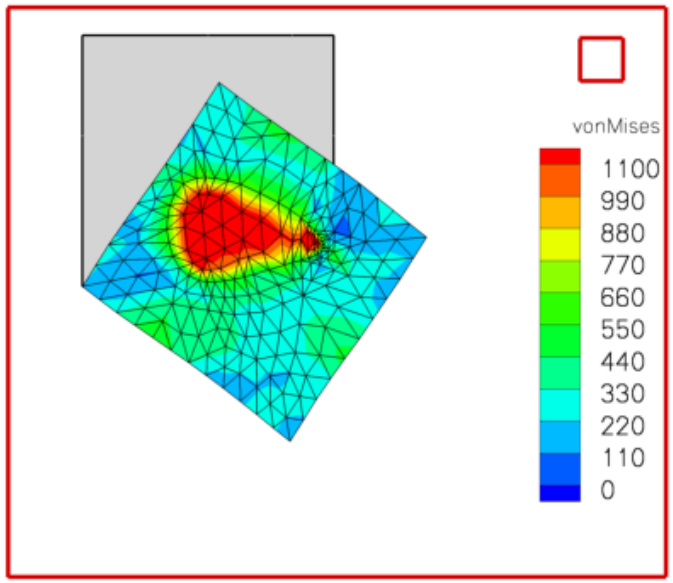


movie

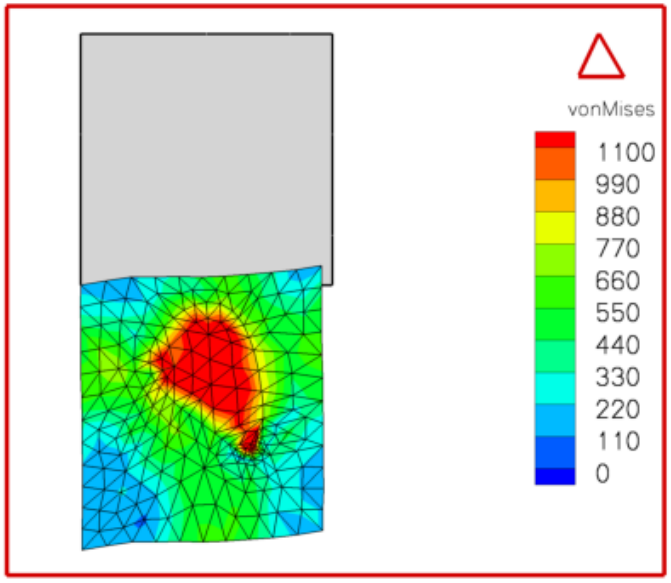


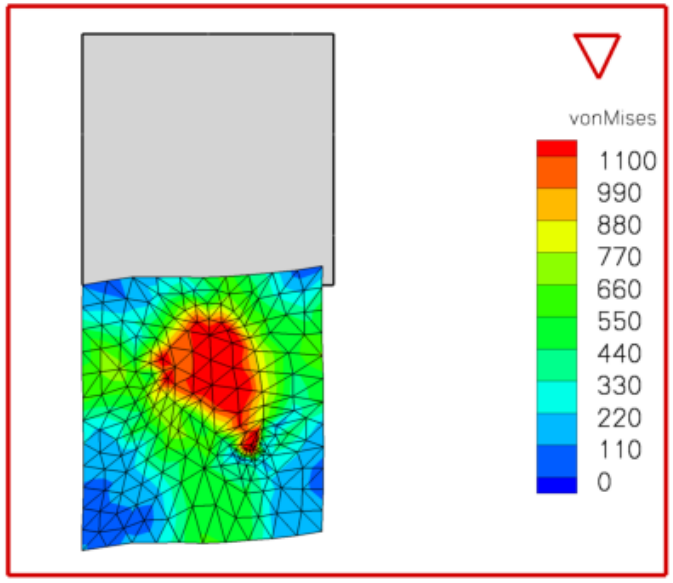




# Definitions of an RVE

- **Hill (1963):** Overall moduli have to be independent of the surface value of traction and displacement, so long as these values are "macroscopically uniform"

- **Hashin (1983):** RVE should be large enough to contain sufficient microstructural information, but much smaller than macroscopic body

- **Drugan and Willis (1996):** RVE is smallest volume element for which the overall modulus macroscopic representation is sufficiently accurate to represent the mean constitutive response

- **Ostoja-Starzewski (2001):** RVE is i) unit cell of periodic microstructure, ii) volume possessing statistically homogeneous and ergodic properties

- **Stroeven, Askes, and Sluis (2002):** Determination of RVE size is not straightforward! It depends on material under consideration and on the structure sensitivity of the physical quantity that is measured

For a more detailed discussion see ZEMAN [2003]



# Non-Uniqueness of RVEs

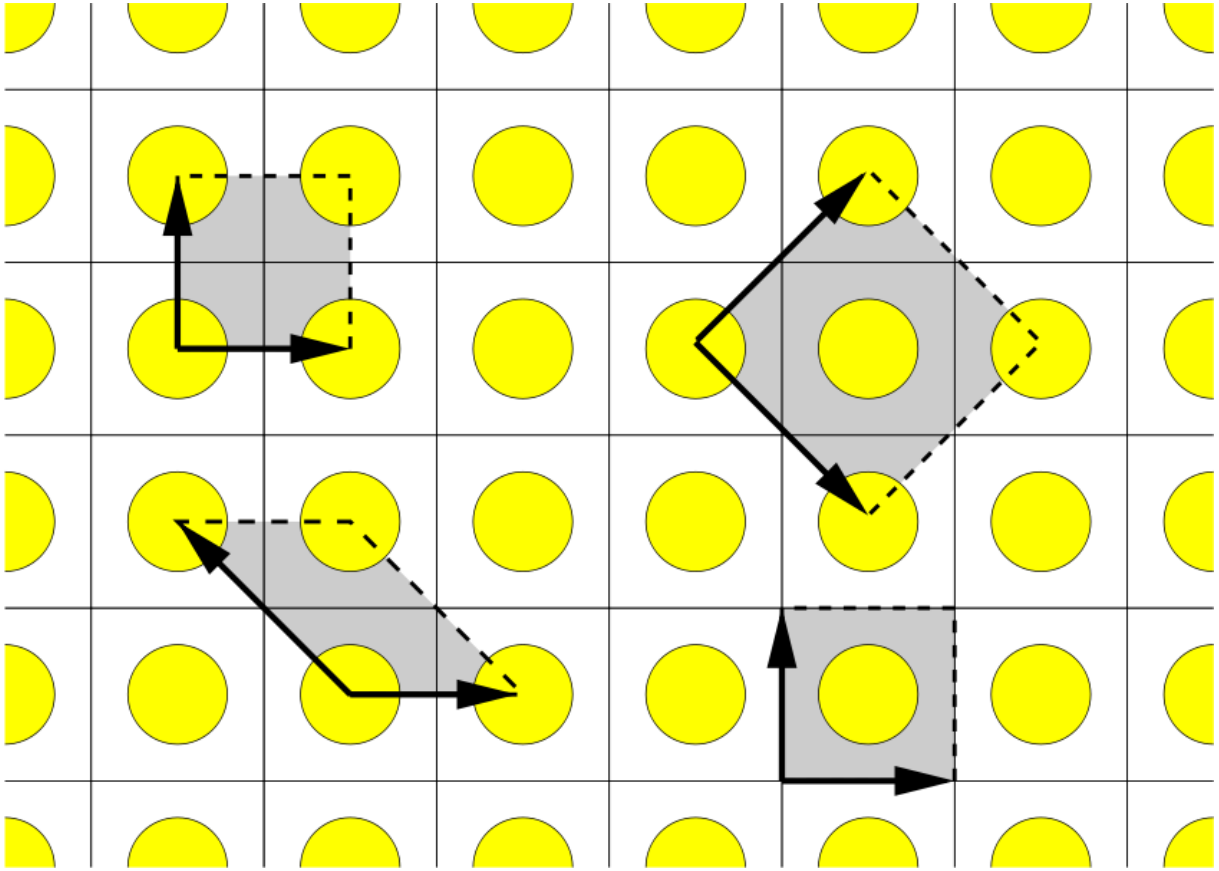

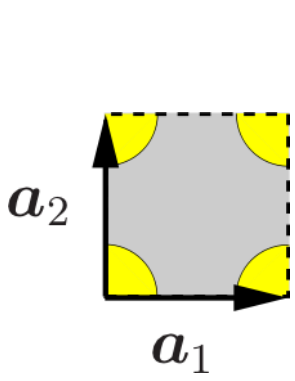


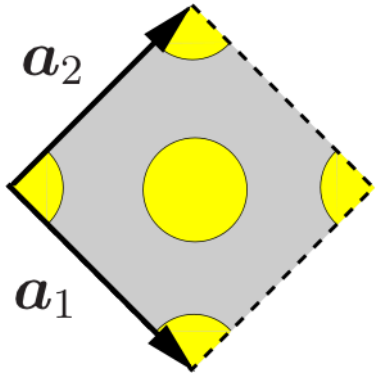


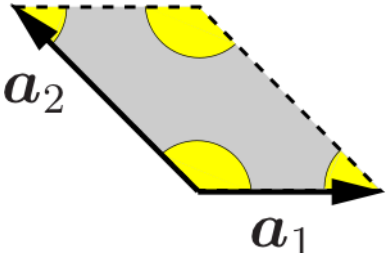


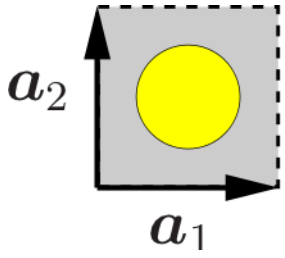




# Simplified Microstructures by Substructuring

Digital image of real microstructure

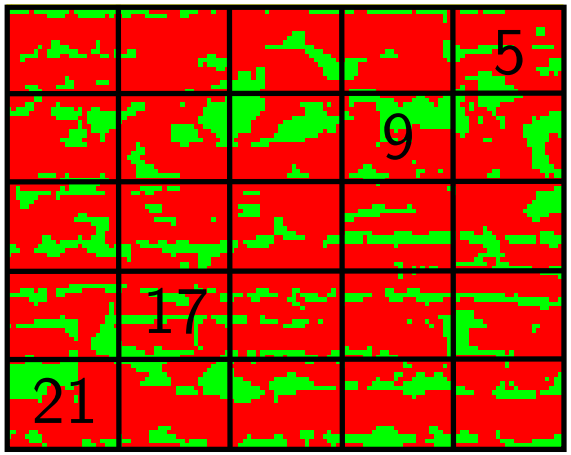


Covariogram

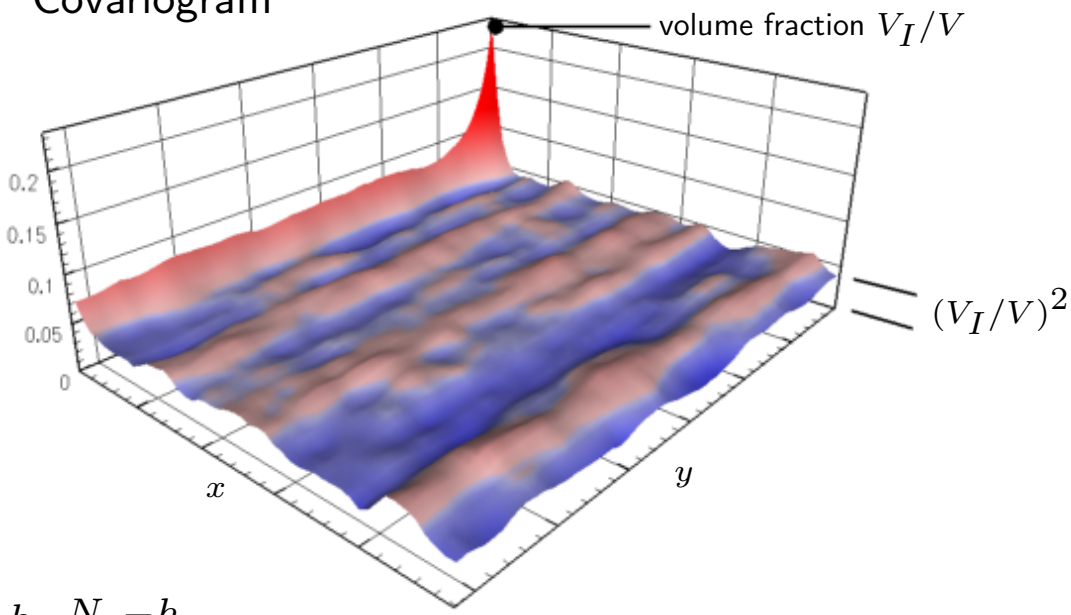


Inclusion phase covariogram

$$K = \frac{1}{(N_x - h_x)(N_y - h_y)} \sum_{k_x=1}^{N_x-h_x} \sum_{k_y=1}^{N_y-h_y} \chi(k_x, k_y)\chi(k_x + h_x, k_y + h_y)$$

sample 5

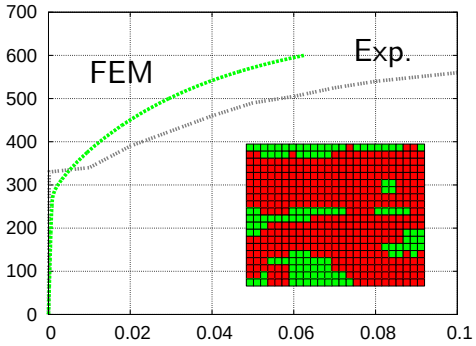


sample 9

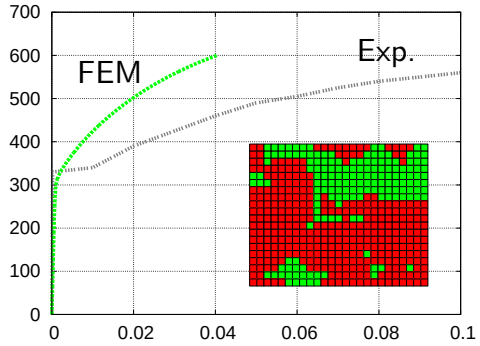


sample 17

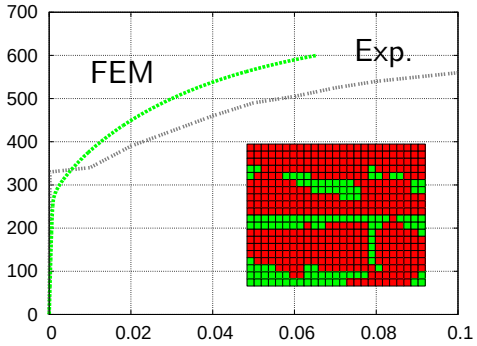


sample 21

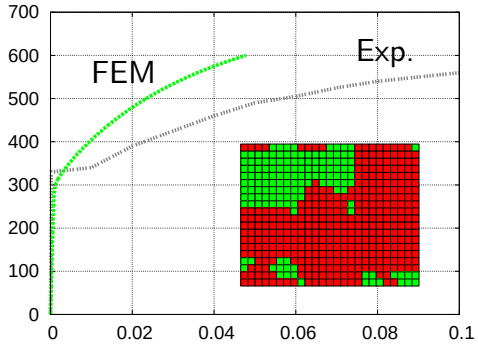




# Characterization of Microstructural Morphology

**4 Basic parameters for the description of each phase:**

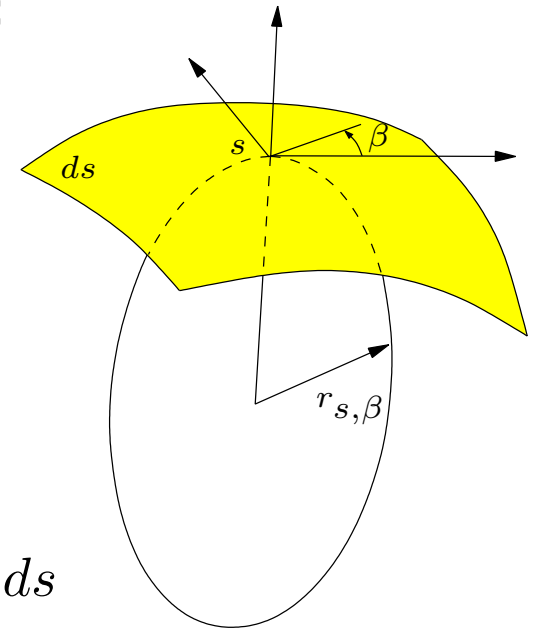


- $\mathcal{P}_V$ - Volume density $[-]$
- $\mathcal{P}_S$ - Surface density $[m^{-1}]$
- $\mathcal{P}_M$ - Density of the integral of mean curvature $[m^{-2}]$

$$\mathcal{P}_M = \frac{1}{2V} \int \{\min_\beta[\kappa] + \max_\beta[\kappa]\} ds$$

with curvature $\kappa(s,\beta) = \frac{1}{r_{s,\beta}}$ and volume of microstructure $V$

- $\mathcal{P}_K$ - Density of the integral of total curvature $[m^{-3}]$

$$\mathcal{P}_K = \frac{1}{V} \int \min_\beta[\kappa] \max_\beta[\kappa] ds$$

Ohser & Mücklich [2000],



# Matricity as a Characterization Measure

Compute the skeletal lines of each phase in a given microstructure by shrinking the phases to one-pixel lines, then one obtains the graphical illustrations

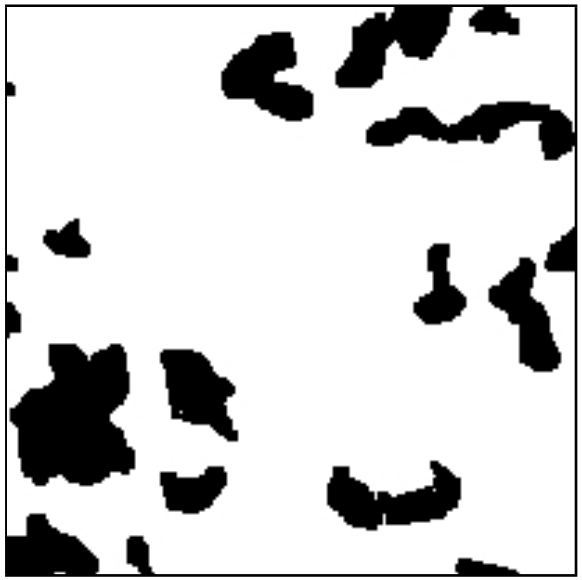

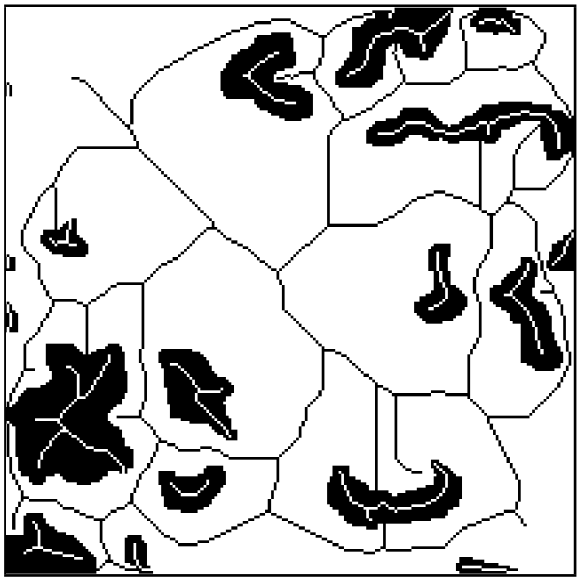

By calculating the skeletal line lengths of the inclusion and matrix phase $S_I$ and $S_M$ we get the matricity by

$$M_I := \frac{S_I}{S_I + S_M}, \quad M_M := \frac{S_M}{S_I + S_M} \quad \text{with} \quad M_I + M_M = 1$$

For the above microstructure the matricities are $M_I = 0.252$ and $M_M = 0.748$.

Acknowledgement: Professor Schmauder, IMWF Stuttgart



# $n$-Point Probability Functions

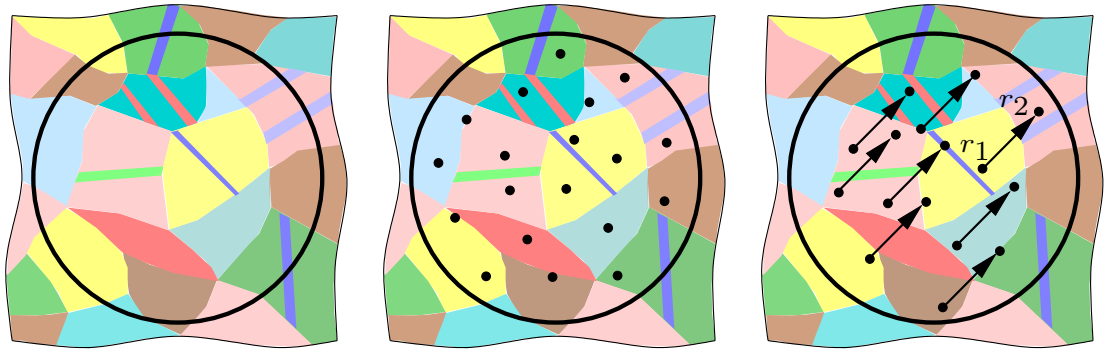


Let $D_r(\alpha)$ denote the domain occupied by the $r$-th phase in the particular sample $\alpha$, then the indicator function reads

$$\chi_r(\boldsymbol{x}, \alpha) = \begin{cases} 1, & \text{if } \boldsymbol{x} \in D_r(\alpha) \\ 0, & \text{otherwise} \end{cases}$$

The $n$-point probability function is then defined by the ensemble average

$$S_{r_1,\ldots r_n}(\boldsymbol{x}_1, \ldots \boldsymbol{x}_n) = \overline{\chi_{r_1}(\boldsymbol{x}_1, \alpha) \cdots \chi_{r_n}(\boldsymbol{x}_n, \alpha)}$$

and represents the probability that $n$ points $\boldsymbol{x}_1, \ldots \boldsymbol{x}_n$ are located in phase $r$.

First order: $S_r(\boldsymbol{x}) = \overline{\chi_r(\boldsymbol{x}, \alpha)}$, Second order: $S_{rs}(\boldsymbol{x}_1, \boldsymbol{x}_2) = \overline{\chi_r(\boldsymbol{x}_1, \alpha)\chi_s(\boldsymbol{x}_2, \alpha)}$



# $n$-Point Probability Functions

Consider binary image of ergodic microstructure with $N_x \times N_y$ pixels, then the functions of first and second order are computed by

$$S_r = \frac{1}{N_x N_y} \sum_{i=0}^{N_x-1} \sum_{j=0}^{N_y-1} \chi_r(i,j)$$

$$S_{rs}(m,n) = \frac{1}{(i_M - i_m)(j_N - j_n)} \sum_{i=i_m}^{i_M-1} \sum_{j=j_n}^{j_N-1} \chi_r(i,j)\chi_s(i+m, j+n)$$

with $i_m = \max[0, -m]$, $i_M = \min[N_x, N_x - m]$ and $j_m$, $j_M$ analogous.

For periodic ergodic microstructures, the second-order function is computed by

$$S_{rs}(m,n) = \frac{1}{N_x N_y} \sum_{i=0}^{N_x-1} \sum_{j=0}^{N_y-1} \chi_r(i,j)\chi_s((i+m)\%N_x, (j+n)\%N_y)$$

and the number of operations reduces when using the Discrete Fourier transformation (DFT)

$$S_{rs}(m,n) = \frac{1}{N_x N_y} \mathcal{F}^{-1}[\mathcal{F}[\chi_r(m,n)]\overline{\mathcal{F}[\chi_s(m,n)]}]$$



# Detection of Periodic Information in Microstructure

Discrete Fourier Transformation (DFT) of microstructure

$$\mathcal{F}(n_x, n_y) = \sum_{k_x=1}^{N_x} \sum_{k_y=1}^{N_y} \exp\left(2\,\pi\,i\,\frac{n_x\,k_x}{N_x}\right) \exp\left(2\,\pi\,i\,\frac{n_y\,k_y}{N_y}\right) \chi(k_x, k_y)$$

for $n_x = 1, .., N_x$ and $n_y = 1, .., N_y$ and indicator function

$$\chi := \begin{cases} 1, & \text{if } (k_x, k_y) \text{ is in inclusion phase,} \\ 0, & \text{else.} \end{cases}$$

$\mathcal{F}$ is correlated to 2-point correlation function, see Parzen [92].

**FFTW ("Fastest Fourier Transform in the West")**
by Frigo & Johnson [1997]:
First a "plan" is generated by testing several algorithms and computing fastest one for the given hardware system, then FFT's are computed by using "plan"

Spectral Density (SD)

$$\mathcal{P}_{SD}(n_x, n_y) = \frac{1}{2\pi\,N_x\,N_y} |\mathcal{F}(n_x, n_y)|^2$$


# Detection of Periodic Information in Microstructure

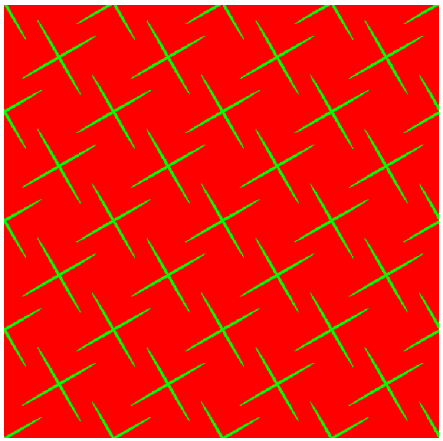
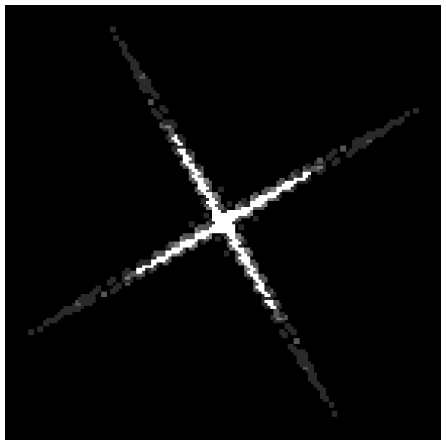
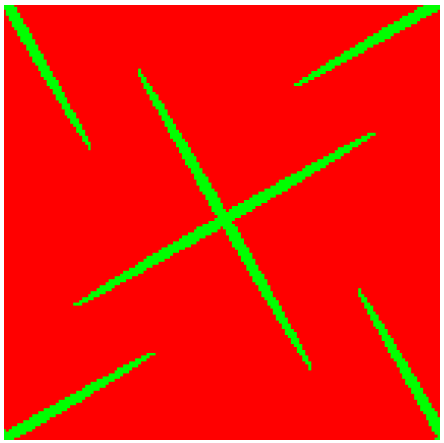
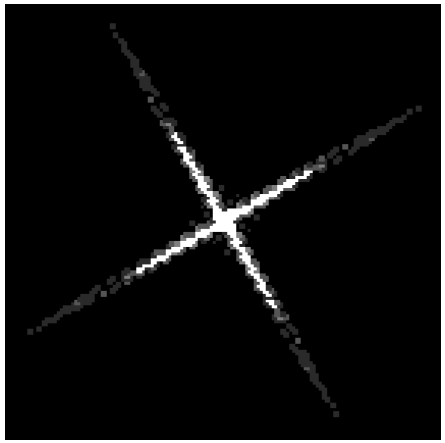

- SD of periodic microstructure and periodic unit cell are identical
- Spectral density (SD) shows characteristic anisotropy directions

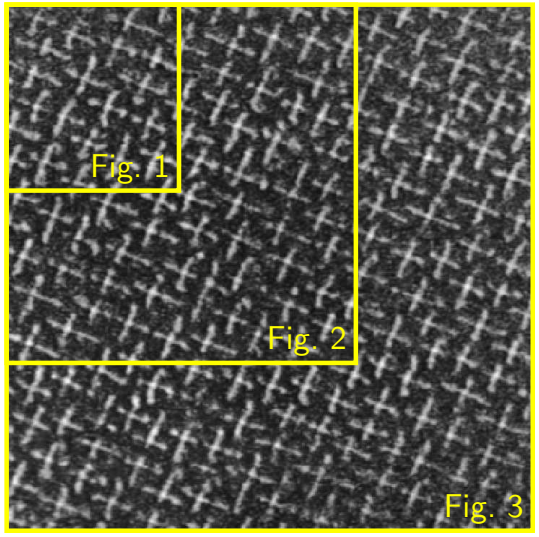


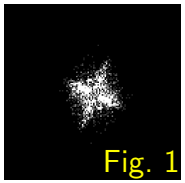


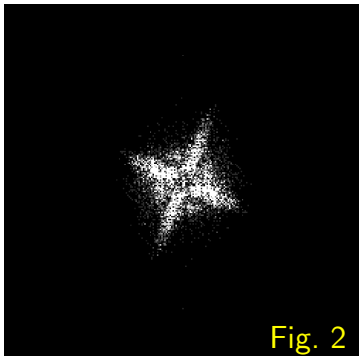


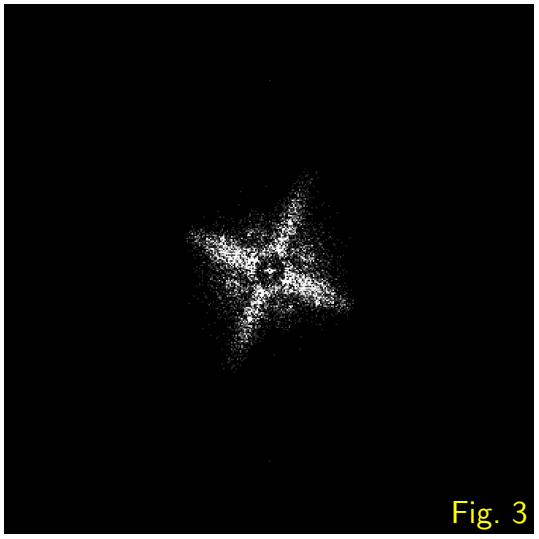




# Lineal-Path Functions

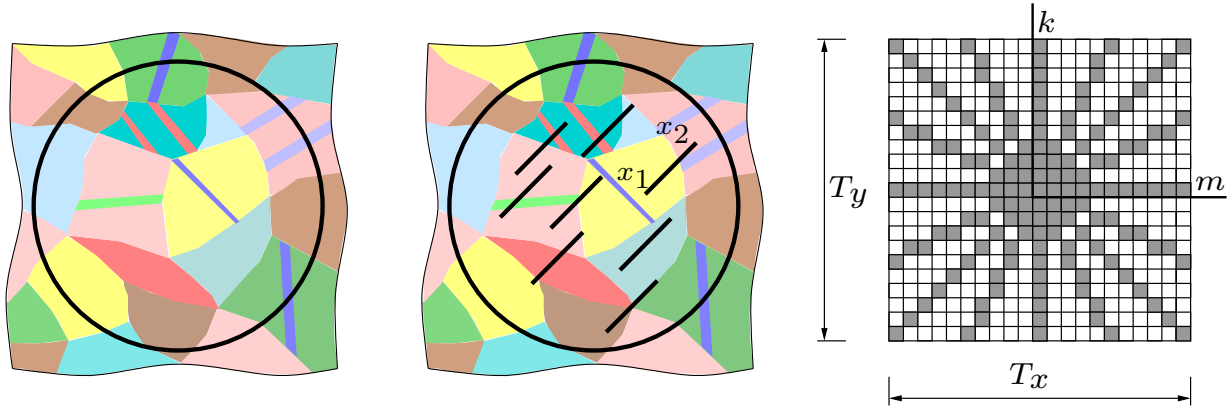


Let $D_r(\alpha)$ denote the domain occupied by the $r$-th phase in particular sample $\alpha$, then we introduce the indicator function

$$\lambda_r(\overrightarrow{\boldsymbol{x}_1\boldsymbol{x}_2}, \alpha) = \begin{cases} 1, & \text{if } \overrightarrow{\boldsymbol{x}_1\boldsymbol{x}_2} \subset D_r(\alpha) \\ 0, & \text{otherwise} \end{cases}$$

and obtain the lineal-path function by the ensemble average

$$\mathcal{P}^r_{LP}(\overrightarrow{\boldsymbol{x}_1\boldsymbol{x}_2}) = \overline{\lambda_r(\overrightarrow{\boldsymbol{x}_1\boldsymbol{x}_2}, \alpha)}\,,$$

which represents the probability that the $\overrightarrow{\boldsymbol{x}_1\boldsymbol{x}_2}$ segment lies in phase $r$.
For periodic ergodic microstructures the lineal-path function is computed by

$$\mathcal{P}^r_{LP}(m,k) = \frac{1}{N_x N_y} \sum_{p=1}^{N_x} \sum_{q=1}^{N_y} \lambda_r(p+m, q+k)$$



# Examples for Different Statistical Measures

target structure

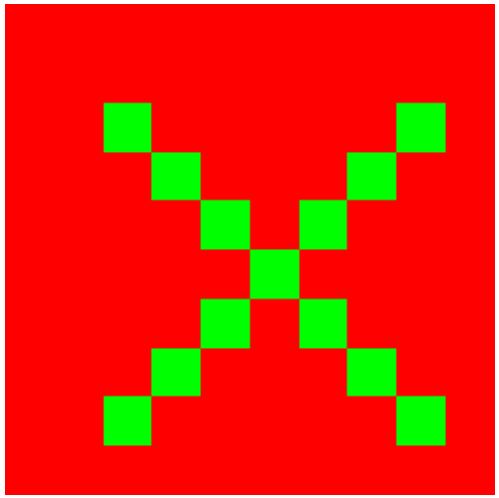

two-point probability function

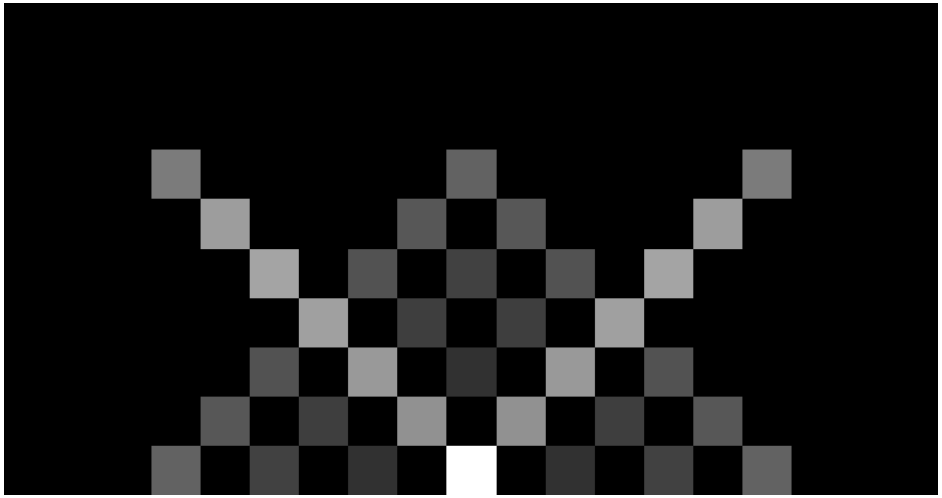


spectral density

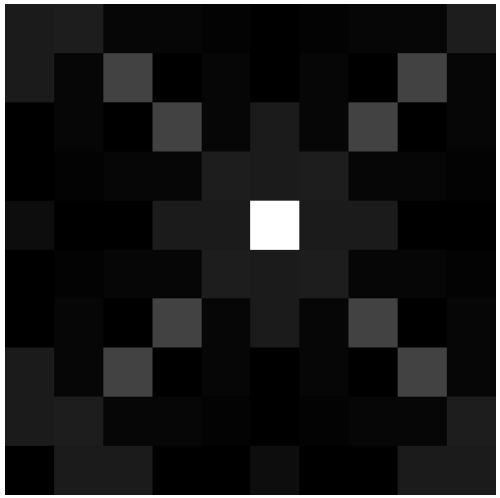


lineal-path function

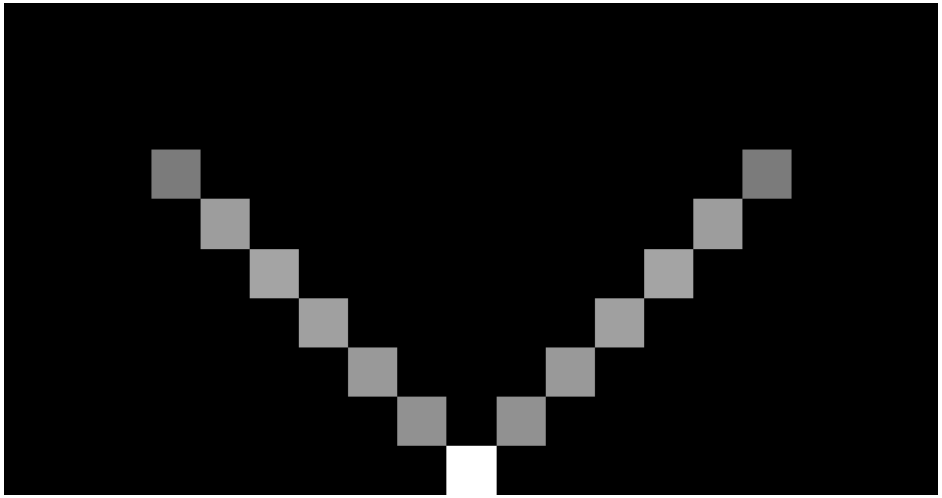




# Construction of Statistically Similar RVEs (SSRVEs)

Real Microstructure  Statistically Similar RVE (SSRVE)

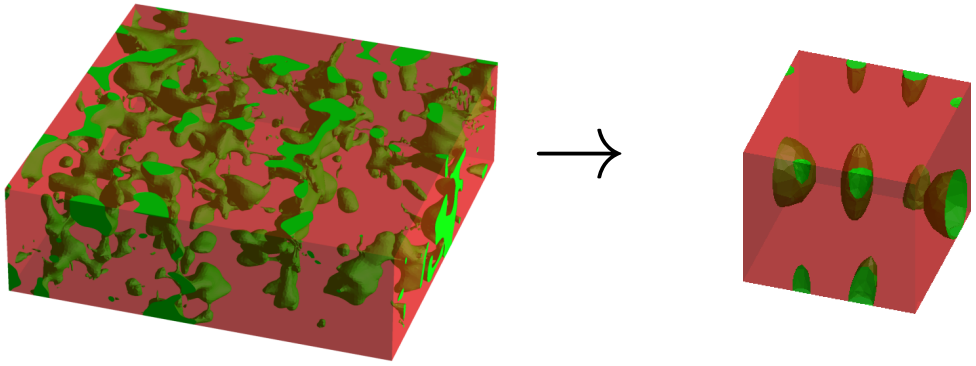

Macroscopic mechanical response is mainly governed by the morphology of the microstructure.

Motivated by Povirk [1995] we consider a general least-square functional

$$\mathcal{L}(\boldsymbol{\gamma}) = \sum_{L=1}^{n_{sm}} \omega_{(L)} \left( \mathcal{P}_{(L)}^{real} - \mathcal{P}_{(L)}^{SSRVE}(\boldsymbol{\gamma}) \right)^2 \quad \rightarrow \quad \min_{\boldsymbol{\gamma}}$$

where $n_{sm}$ represents the number of statistical measures taken into account.

$$\mathcal{L}(\boldsymbol{\gamma}) = \omega_V \left( 1 - \frac{\mathcal{P}_V^{SSRVE}(\boldsymbol{\gamma})}{\mathcal{P}_V^{real}} \right)^2 + \omega_{SD} \frac{1}{N_x N_y} \sum_{m=1}^{N_x} \sum_{k=1}^{N_y} \left( \mathcal{P}_{SD}^{real}(m,k) - \mathcal{P}_{SD}^{SSRVE}(m,k,\boldsymbol{\gamma}) \right)^2$$
$$+ \omega_{LP} \frac{1}{N_x N_y} \sum_{m=1}^{N_x} \sum_{k=1}^{N_y} \left( \mathcal{P}_{LP}^{real}(m,k) - \mathcal{P}_{LP}^{SSRVE}(m,k,\boldsymbol{\gamma}) \right)^2$$



# Simple Example: Visualization of Objective Function (2 Dofs)

Target structure

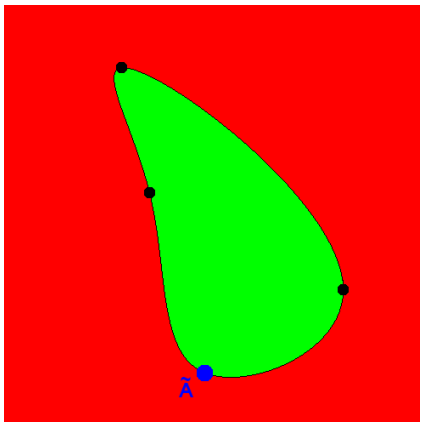


dimensions: 30x30 $\mu m$

SD of target structure

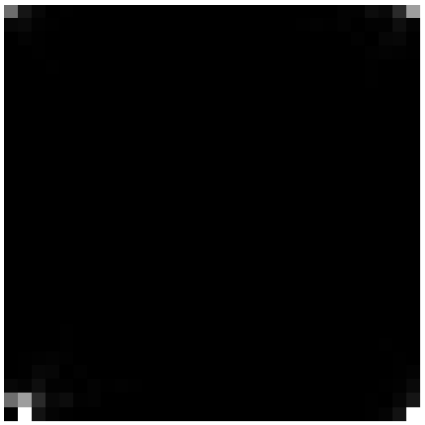

resolution: 30x30 pixels

Unitcell

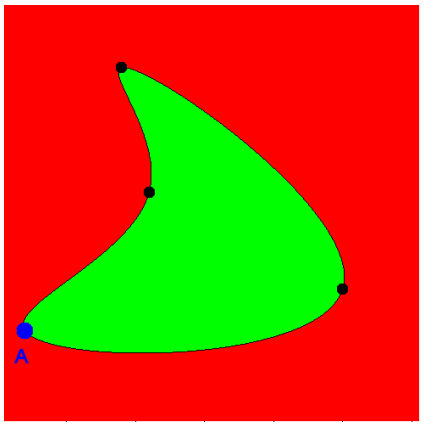


dimensions: 30x30 $\mu m$

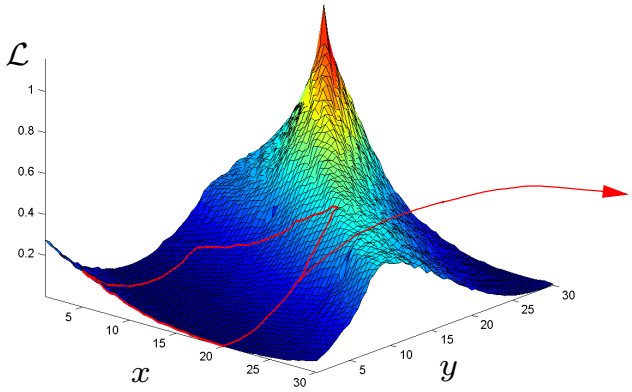


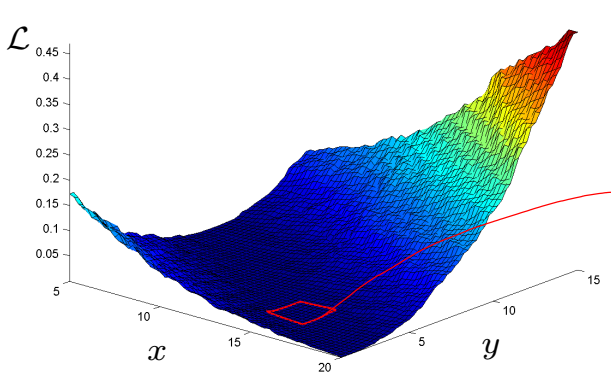


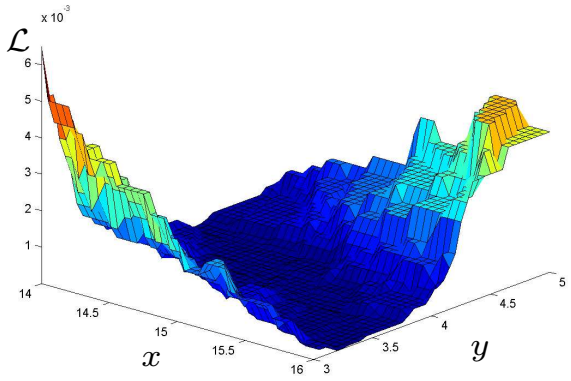


$\rightarrow$ Surface of objective function is far from being smooth

$\rightarrow$ Many local minima exist if more degrees of freedom are considered



# Optimization by Moving-Frame Algorithm

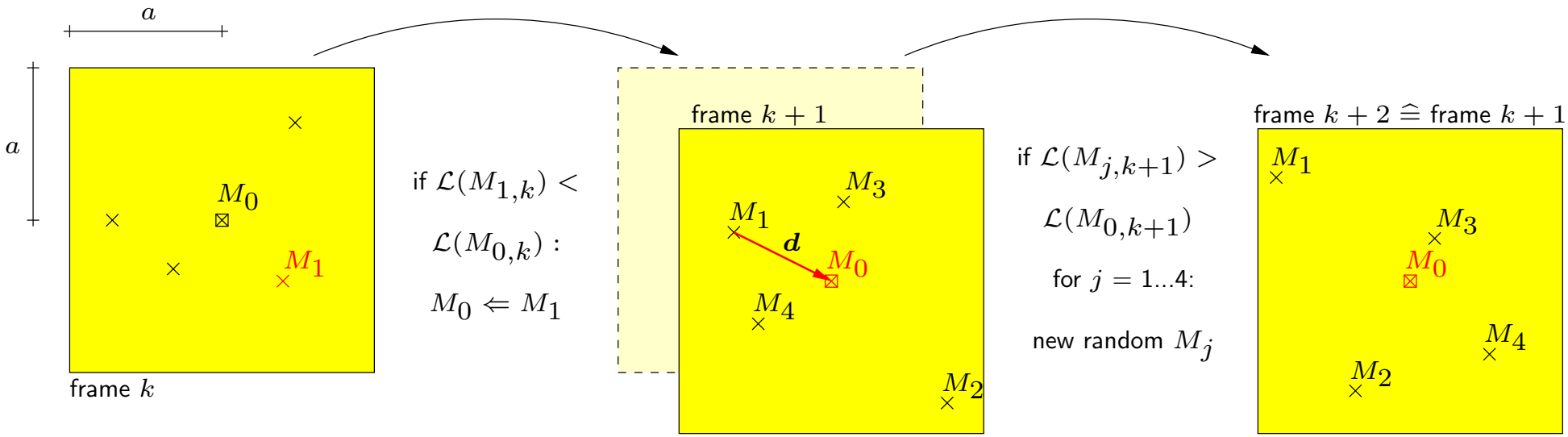


- Set starting point $M_{0,k}$ and generate $n$ random points in a frame of size $(2a)$x$(2a)$
- Evaluate objective function $\mathcal{L}$ at these points and $M_{0,k}$
- Set the frame center to point of the lowest value of $\mathcal{L} \rightarrow M_{0,k+1}$
- If frame center does not change (e.g. $M_{0,k+1} = M_{0,k+2}$), set $l_{iter} = l_{iter} + 1$ else initialize $l_{iter} = 0$; stop optimization if $l_{iter} = l_{itermax}$

**Improved results:** • Modified frame size $a$ depending on difference $|\boldsymbol{d}|$ and $l_{iter}$

• Combination of method with line-search algorithm



# Simple Example: Optimization Process


movie

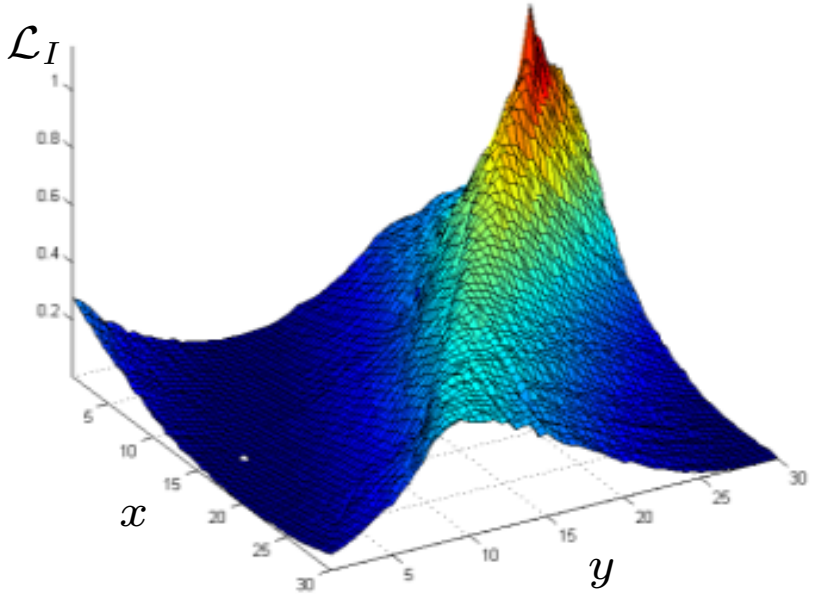


- Target structure: generated by 4 random sampling points defining B-Spline
- Unitcell (to be found): keep 3 points and vary only one sampling point, dimensions of unitcell: 30x30 $\mu m$
- Optimization procedure parameters:

| | | |
|---|---|---|
| size of frame | $a$ | $= 5\ \mu m$ |
| number of "simplex"-points | $n$ | $= 4$ |
| max. number of iterations | $l_{itermax}$ | $= 50$ |



# Study: Real Micrograph of a DP Steel as Target Structure Leading to Macroscopic Kinematic Hardening

## Micrograph

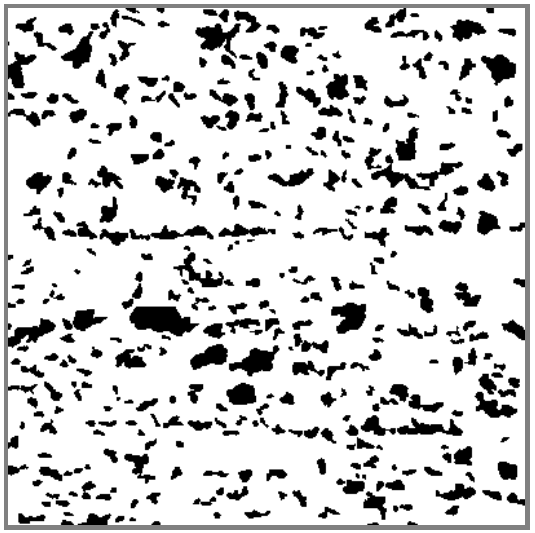

## FE-discretization

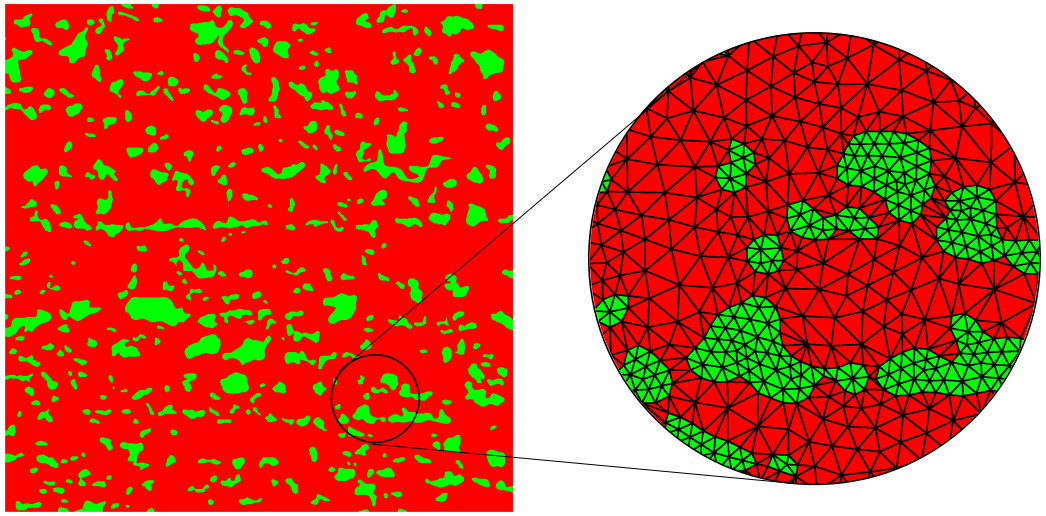

- white/red phase: ferrite (matrix)
- black/green phase: martensite (inclusion)

- 77,641 nodes $\hat{=}$ 155,282 degrees of freedom
- 38,594 six-node triangular elements

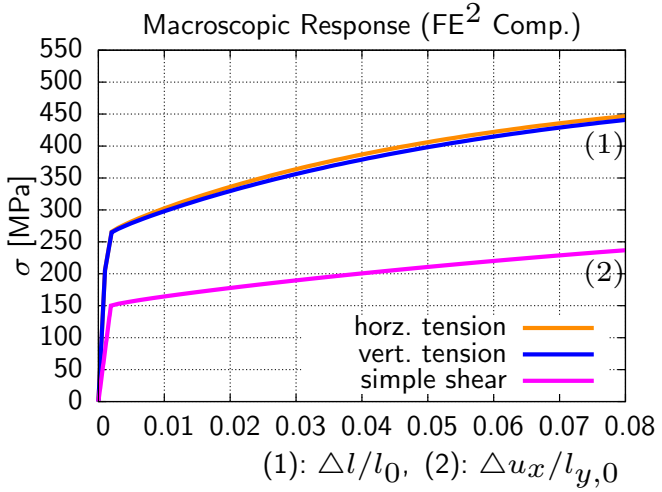




# Evaluation of the Mechanical Response

Consider a relative error $r$ computed as the deviation of the macroscopic SSRVE stress response from the target structure response at each evaluation point $i$

$$r_x^{(i)} = \frac{\overline{\sigma}_{x,i}^{\text{real}} - \overline{\sigma}_{x,i}^{\text{SSRVE}}}{\overline{\sigma}_{x,i}^{\text{real}}}, \quad r_y^{(i)} = \frac{\overline{\sigma}_{y,i}^{\text{real}} - \overline{\sigma}_{y,i}^{\text{SSRVE}}}{\overline{\sigma}_{y,i}^{\text{real}}}, \quad r_{xy}^{(i)} = \frac{\overline{\sigma}_{xy,i}^{\text{real}} - \overline{\sigma}_{xy,i}^{\text{SSRVE}}}{\overline{\sigma}_{xy,i}^{\text{real}}}.$$

for the macroscopic virtual experiments:

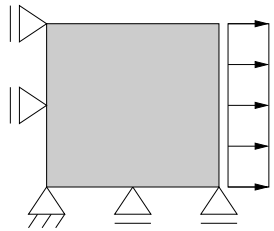

horizontal tension

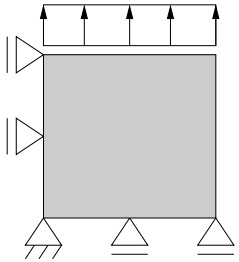

vertical tension

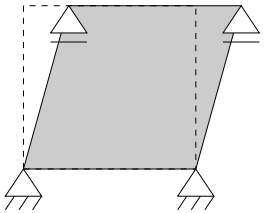

simple shear

Then the average error for each virtual experiment is computed by

$$\widetilde{r}_j = \sqrt{\frac{1}{n}\sum_{i=1}^{n}[r_j^{(i)}]^2} \quad \text{with} \quad r_j^{(i)} := r_j\left(\tfrac{i}{n}\triangle l_{\max}/l_0\right) \text{ and } j = x, y, xy.$$

As a comparative measure we define the overall average error

$$\widetilde{r} = \sqrt{\frac{1}{3}\left(\widetilde{r}_x^2 + \widetilde{r}_y^2 + \widetilde{r}_{xy}^2\right)}.$$



# Considered Types of SSRVE Construction

## Type I

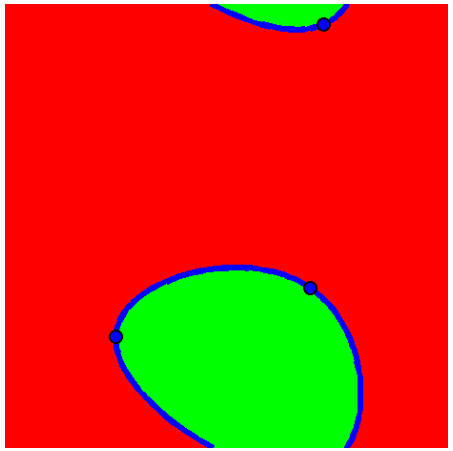

1 inclusion
$n_{sp} = 3$

## Type II

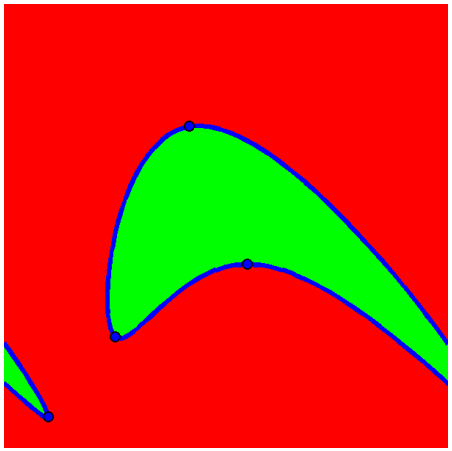

1 inclusion
$n_{sp} = 4$

## Type III

2 inclusions
$n_{sp} = 6$

## Type IV

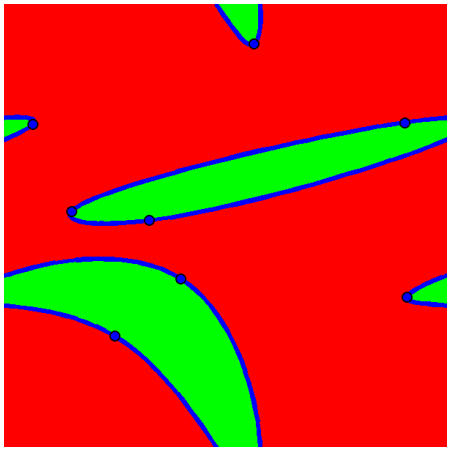

2 inclusions
$n_{sp} = 8$

## Type V

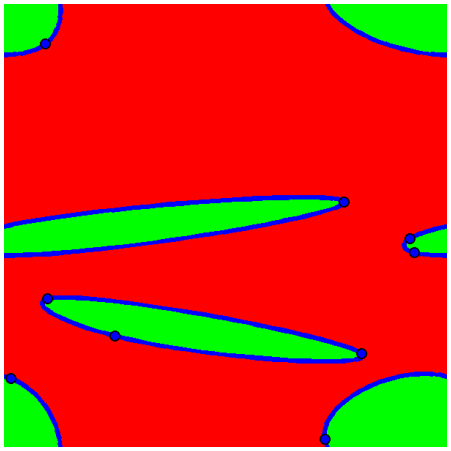

3 inclusions
$n_{sp} = 9$



# Construction of SSRVEs based on $\mathcal{L}_V$, $\mathcal{L}_{SD}$ and $\mathcal{L}_{LP}$

Objective function for $n_{sm} = 3$ with $\omega_V = \omega_{SD} = 1$ and $\omega_{LP} = 10$ :

$$\mathcal{L}(\boldsymbol{\gamma}) = \omega_V \mathcal{L}_V + \omega_{SD} \underbrace{\frac{1}{N_x\, N_y} \sum_{m=1}^{N_x} \sum_{k=1}^{N_y} \left( \mathcal{P}_{SD}^{real}(m,k) - \mathcal{P}_{SD}^{SSRVE}(m,k,\boldsymbol{\gamma}) \right)^2}_{\mathcal{L}_{SD}}$$

$$+ \omega_{LP} \underbrace{\frac{1}{N_x\, N_y} \sum_{m=1}^{N_x} \sum_{k=1}^{N_y} \left( \mathcal{P}_{LP}^{real}(m,k) - \mathcal{P}_{LP}^{SSRVE}(m,k,\boldsymbol{\gamma}) \right)^2}_{\mathcal{L}_{LP}}$$

SSRVEs from the optimization:

Target (155,282 dofs)

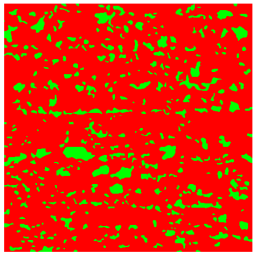

Type I (2754 dofs)

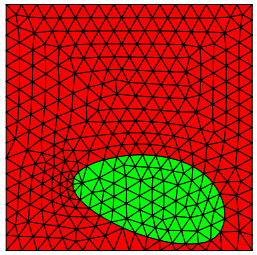

Type II (2462 dofs)

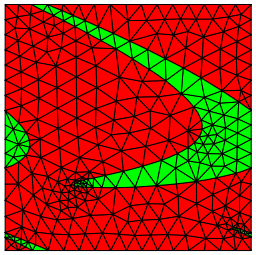

Type III (2814 dofs)

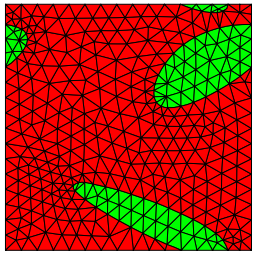

Type IV (2962 dofs)

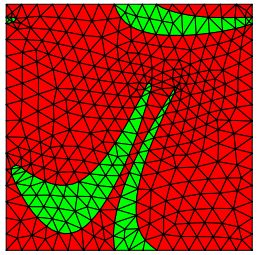

Type V (3534 dofs)

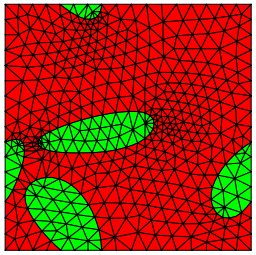



# Comparison of Mechanical Response ($\mathcal{L}_V$, $\mathcal{L}_{SD}$, $\mathcal{L}_{LP}$)

Errors of the virtual experiments:

| SSRVE | $\mathcal{L}$ $[10^{-3}]$ | $\mathcal{L}_V$ $[10^{-5}]$ | $\mathcal{L}_{SD}$ $[10^{-4}]$ | $\mathcal{L}_{LP}$ $[10^{-5}]$ | $n_{\text{ele}}$ | $\widetilde{r}_x$ [%] | $\widetilde{r}_y$ [%] | $\widetilde{r}_{xy}$ [%] | $\widetilde{r}$ [%] |
|---|---|---|---|---|---|---|---|---|---|
| I | 39.41 | 238.05 | 230.96 | 139.38 | 656 | 1.16 $\pm$ 0.29 | 1.58 $\pm$ 0.39 | 3.34 $\pm$ 0.91 | 2.24 |
| III | 8.66 | 8.82 | 62.87 | 22.81 | 670 | 0.26 $\pm$ 0.20 | 2.24 $\pm$ 0.52 | 0.41 $\pm$ 0.22 | 1.32 |
| V | 4.22 | 1.42 | 36.62 | 5.41 | 850 | 1.12 $\pm$ 0.35 | 0.92 $\pm$ 0.26 | 1.10 $\pm$ 0.23 | 1.05 |
| II | 9.29 | 14.90 | 71.31 | 20.08 | 582 | 8.24 $\pm$ 2.10 | 2.10 $\pm$ 0.31 | 7.45 $\pm$ 2.87 | 6.53 |
| IV | 3.70 | 4.33 | 33.88 | 2.73 | 708 | 2.22 $\pm$ 0.80 | 4.89 $\pm$ 1.24 | 2.43 $\pm$ 1.22 | 3.40 |

Mechanical response and errors

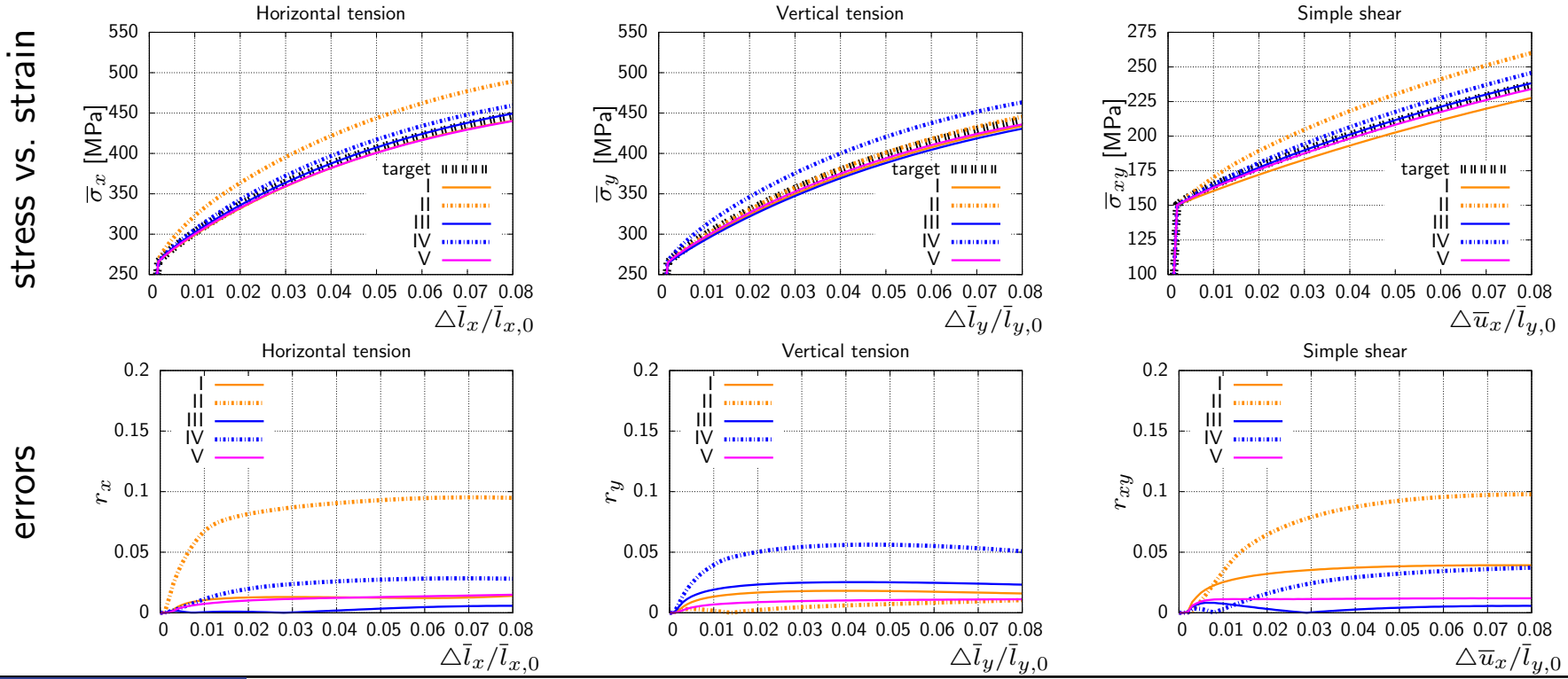




# Bauschinger Effect: Real Structure vs. SSRVE Type V

## Bauschinger factor

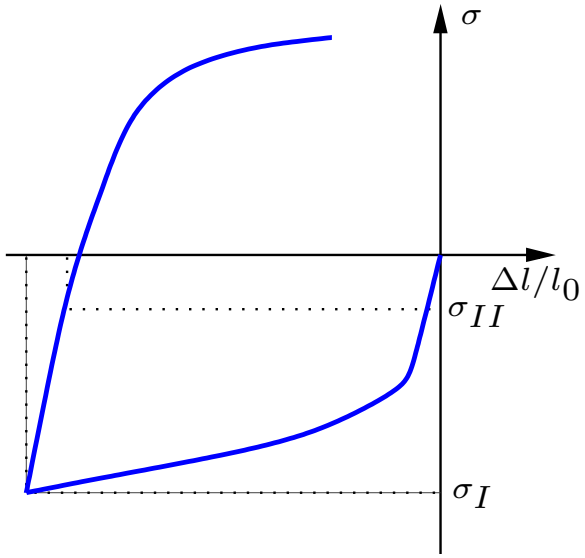


$$f_B := \frac{\sigma_I - \sigma_{II}}{\sigma_I}$$

with

$$\sigma_I = \sigma_{11}(-0.05)$$

$$\sigma_{II} = \sigma_{11}(-0.05 + 0.002)$$

## Numerical Computations

### Real Structure

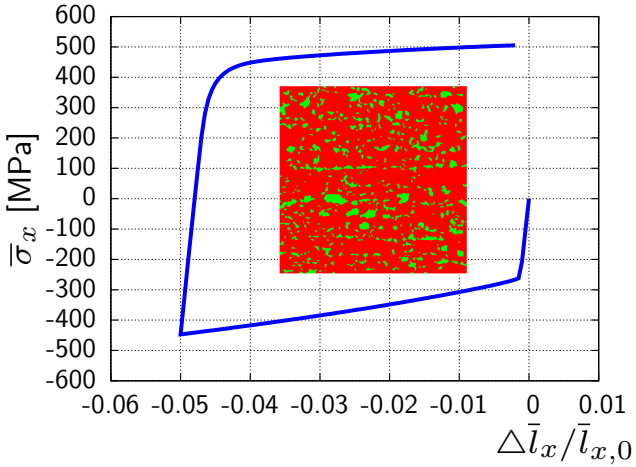


$$f_B = \frac{-447+3}{-447} = 0.99$$

### SSRVE Type V

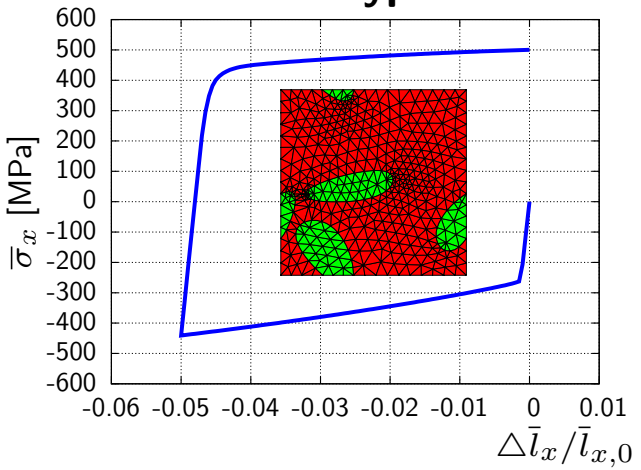


$$f_B = \frac{-440-3}{-440} = 1.01$$

Stress distribution at maximum compression

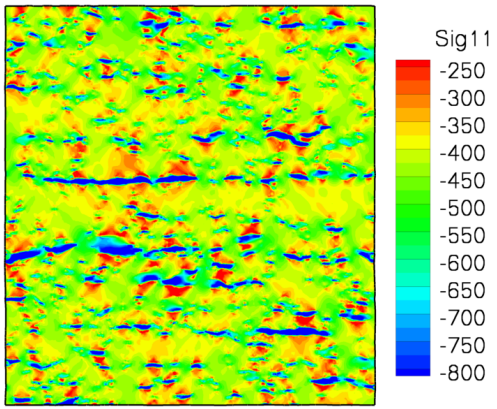


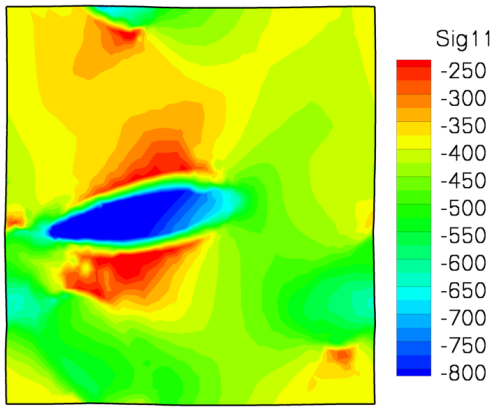




# Simulation of a Radially Loaded Circular Disc with a Hole

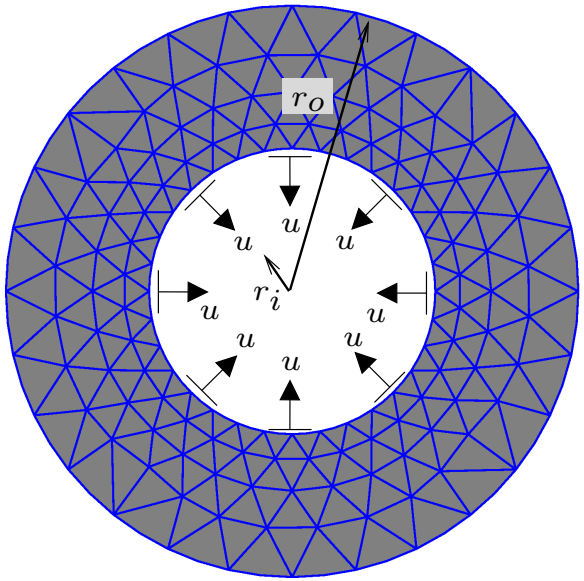


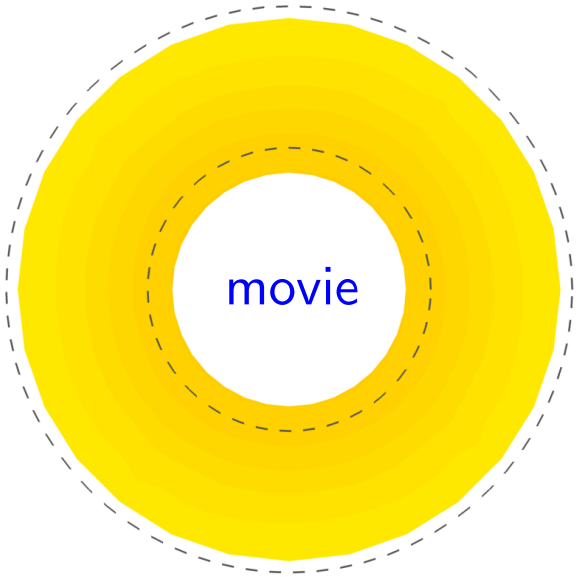


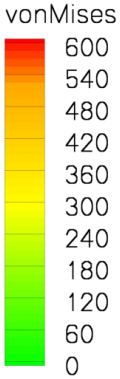


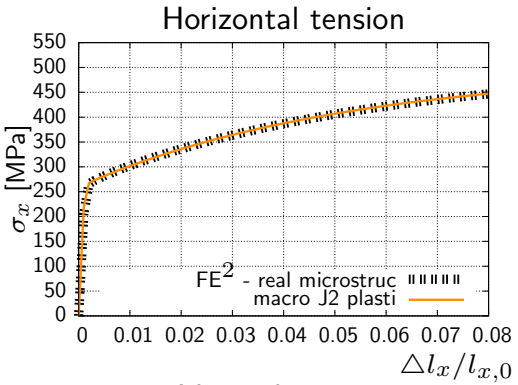


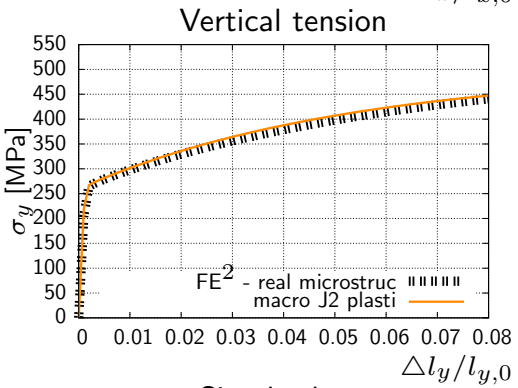


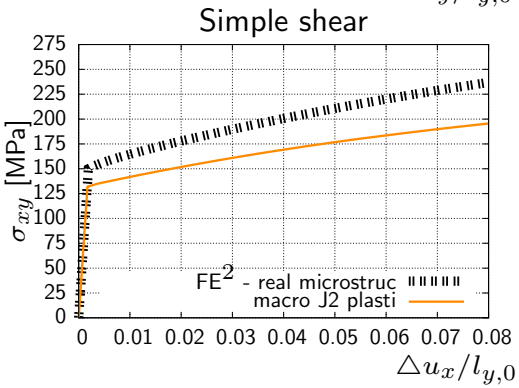


## Macroscopic BVP

- $r_i = 2\,\mathrm{cm}$, $r_o = 4\,\mathrm{cm}$
- 252 quadratic triangular elements (3 gp's)
- 564 nodal points
- plain strain simulation

## Macroscopic Comp.

Finite J2 plasticity:

$$
\begin{aligned}
E &= 200{,}000.0\,\mathrm{MPa} \\
\nu &= 0.3 \\
y_0 &= 230.0\,\mathrm{MPa} \\
y_\infty &= 436.0\,\mathrm{MPa} \\
\eta &= 16.7 \\
h &= 7.0\,\mathrm{MPa}
\end{aligned}
$$

Adjustment of "simple" constitutive model to experiments is not satisfying
$\rightarrow$ Incorporation of microstructural information seems to be necessary



# FE$^2$-Simulation of a Radially Loaded Circular Disc with a Hole

(SSRVE Type V)

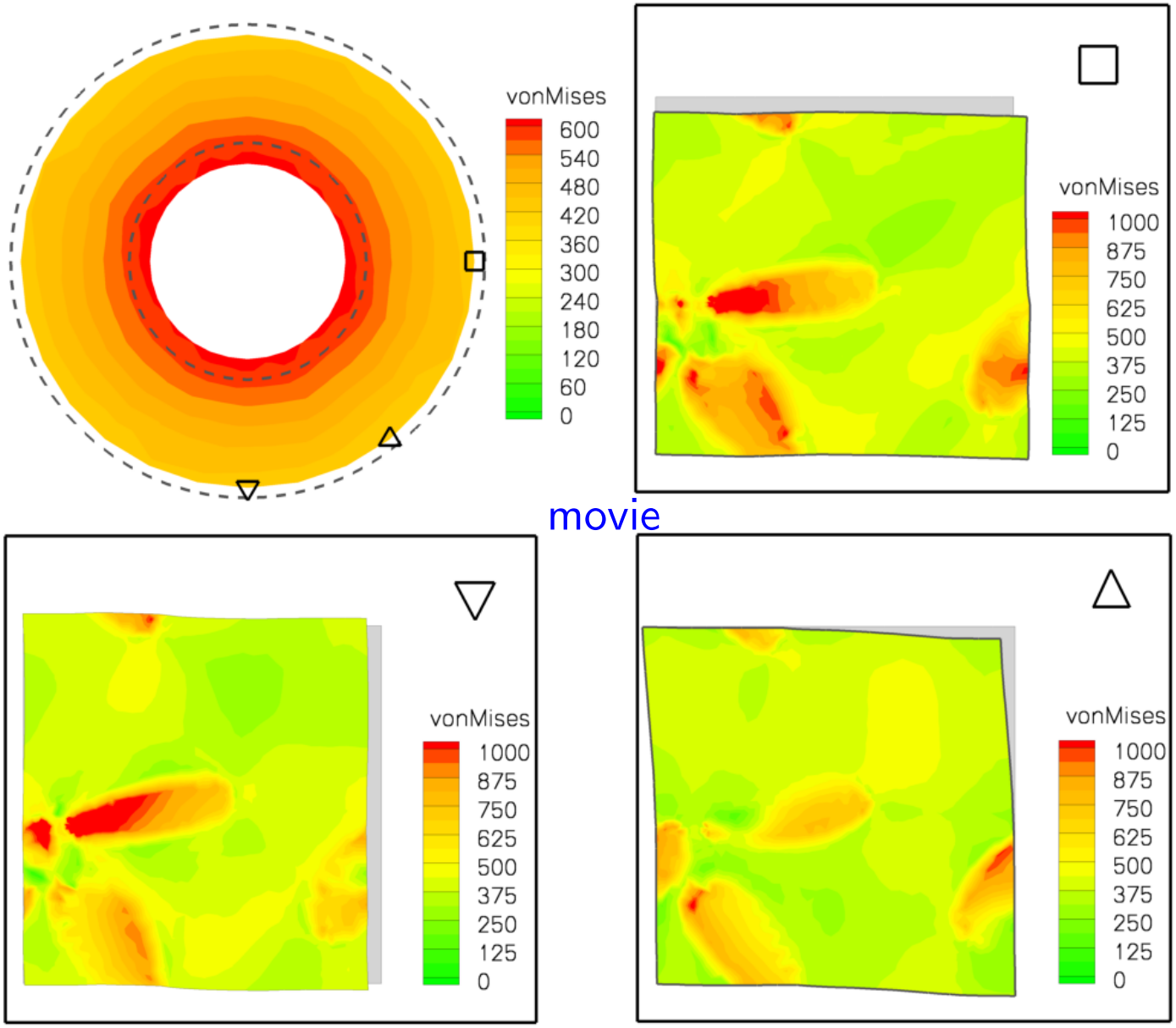

# FE$^2$-Simulation of a Radially Loaded Circular Disc with a Hole

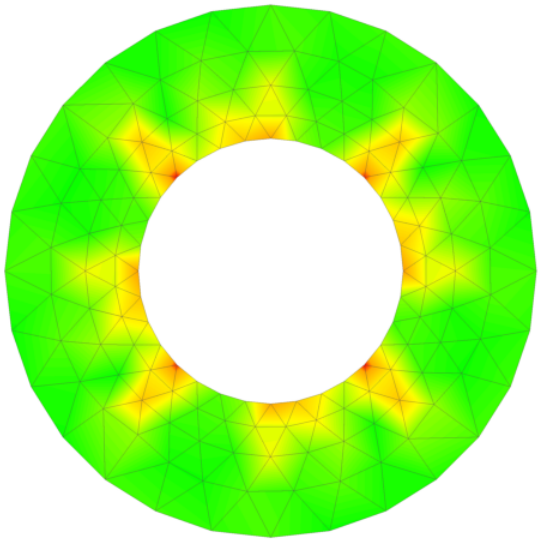


- reduced radial displacement: $u = 0.0112\,\mathrm{cm}$
- parallel computation (ParFEAP, 8 cores)
- $r_{\sigma_{vM}}(\overline{\boldsymbol{x}}) = \left| \dfrac{\overline{\sigma}_{vM}^{target}(\overline{\boldsymbol{x}}) - \overline{\sigma}_{vM}^{SSRVE}(\overline{\boldsymbol{x}})}{\max\limits_{\overline{\boldsymbol{x}}} \left[ \overline{\sigma}_{vM}^{target}(\overline{\boldsymbol{x}}) \right]} \right|$ with $i = 1 \ldots 3$

$\rightarrow$ Stresses obtained from the target structure and the SSRVE are similar

**Target structure:**

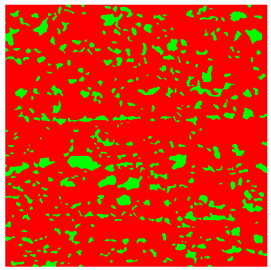

- 38,594 quadratic triangular elements
- 155,282 dof's
- periodic bc's

**SSRVE (Type V):**

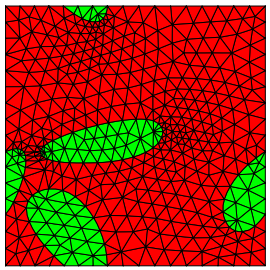

- 850 quadratic triangular elements
- 3,534 dof's
- periodic bc's

**Factor of computation period :** $\dfrac{t_{\textbf{target}}}{t_{\textbf{SSRVE}}} \approx 200$



# Acquisition of EBSD-FIB Data

(Cooperation with Prof. Dr. Dierk Raabe, Max-Planck-Institut für Eisenforschung, Düsseldorf)

## Crystal orientations

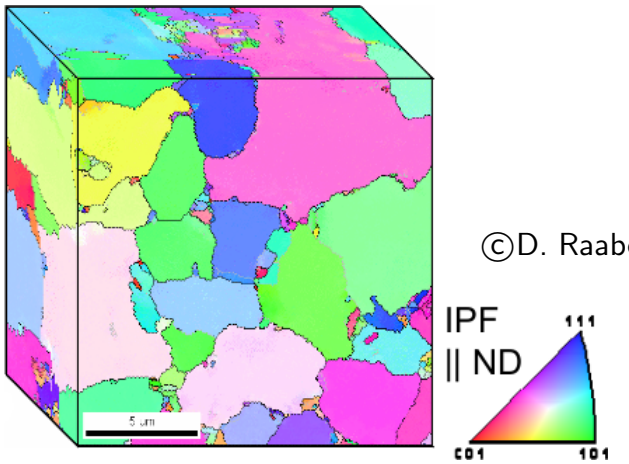


©D. Raabe, MPIE

## Image quality

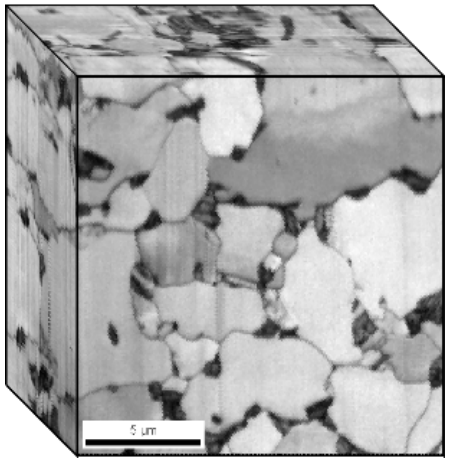


## 2D phase reconstruction

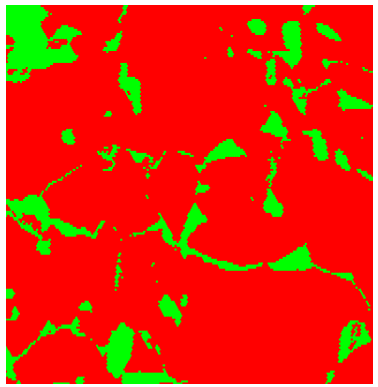

## Discretization (8.5 mio. dofs)

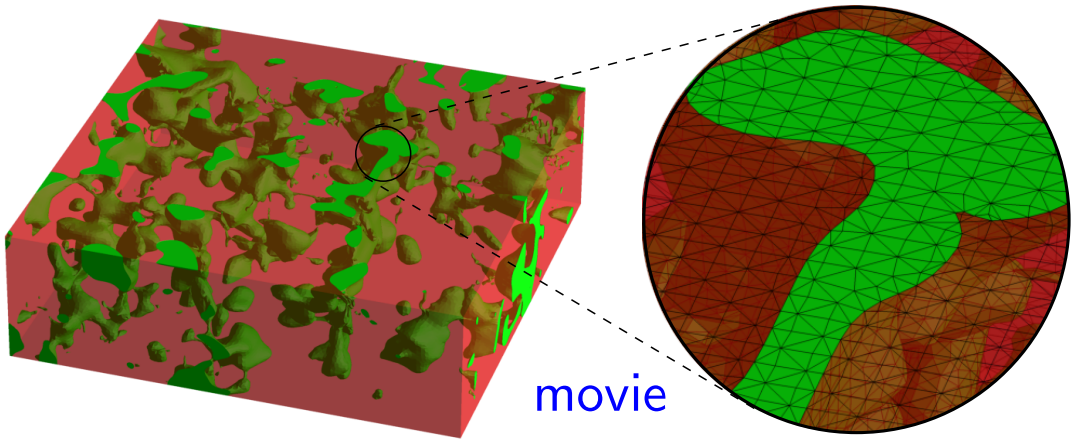


## Tension test (3D vs. 2D)

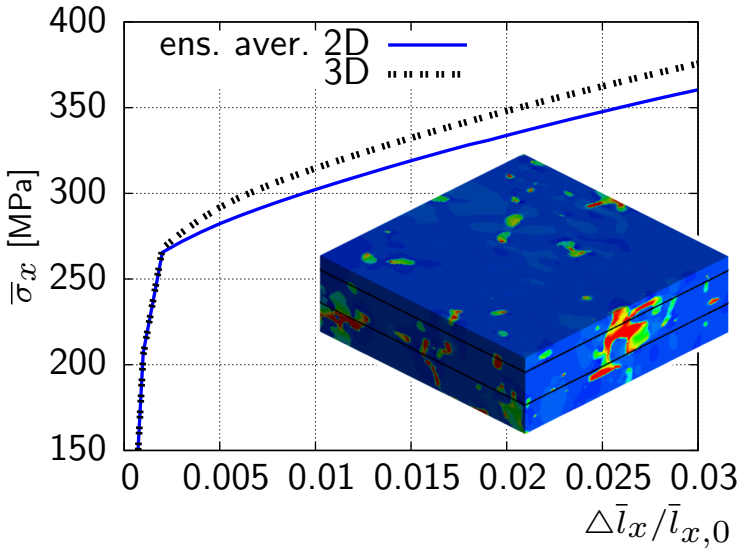




# 3D SSRVEs based on Generalized Ellipsoids

3D SSRVEs are generated with ellipsoidal inclusion based on Superellipsoids

$$\sum_{i=1}^{d} \left( \frac{|\mathbf{v}_i \cdot (\mathbf{x} - \mathbf{x}_c)|}{r_i} \right)^{p_i} = 1$$

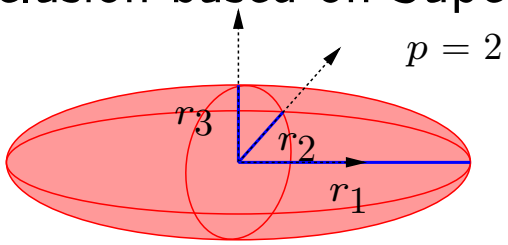


Restrictions:

$\Rightarrow$ exponent $p = 2$ for convex and smooth ellipsoids

$\Rightarrow$ equal semiaxis $r_2$ and $r_3$

## Parametrization of Ellipsoids

| Center coordinates | Rotation by | Ellipsoid with semiaxis |
|---|---|---|
| $\gamma = [x_c, y_c, z_c,$ | $\theta, \varphi,$ | $r_0, a]$ |

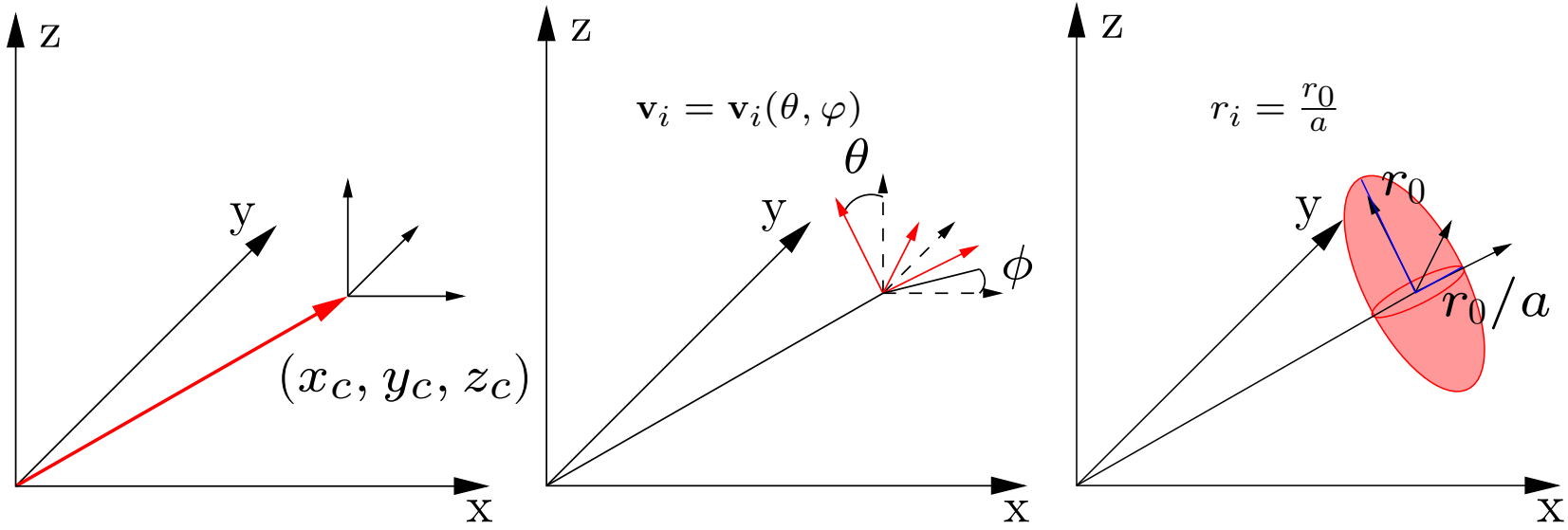




# Results for SSRVE with 2 Inclusions

## Target structure

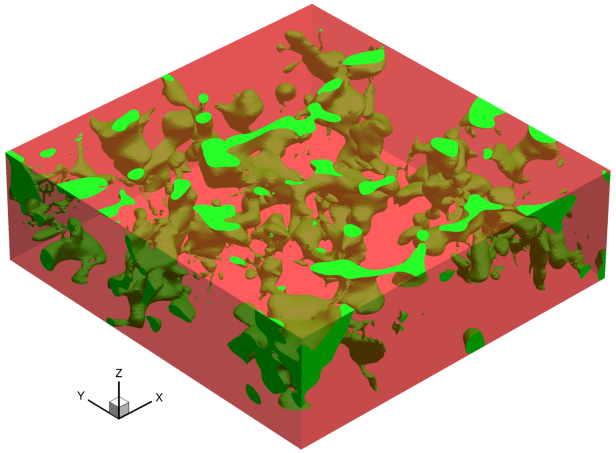

Rel. error: Spect. Dens.

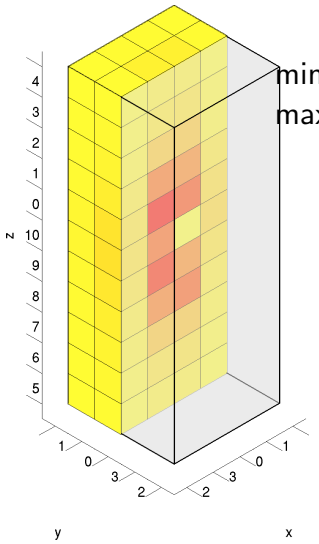


Lineal Path

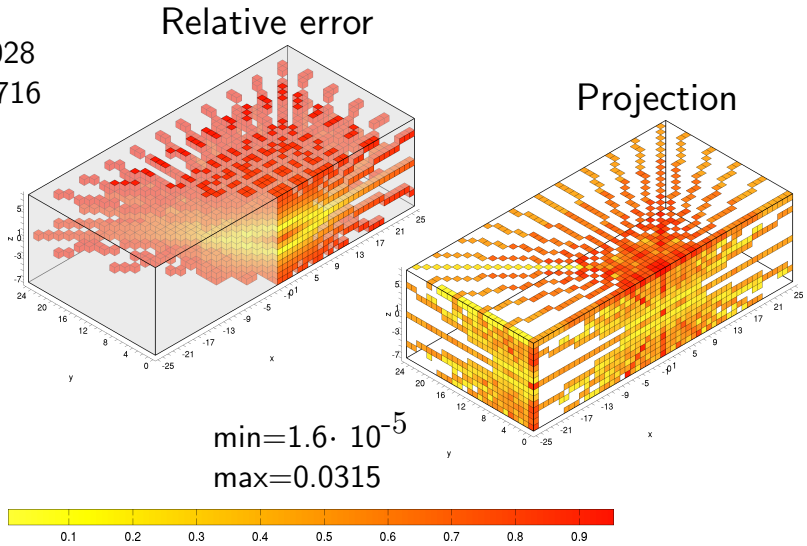


## SSRVE: 2 Ellipsoids

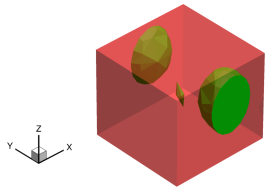

| SSRVE | $\mathcal{L}$ $[10^{-2}]$ | $\mathcal{L}_V$ $[10^{-4}]$ | $\mathcal{L}_{SD}$ $[10^{-3}]$ | $\mathcal{L}_{LP}$ $[10^{-4}]$ | $n_{\text{ele}}$ |
|---|---|---|---|---|---|
| 2 Ellipsoids | 6.484 | 448.5 | 12.84 | 0.714 | 1889 |

Parametrization: $\gamma = [x_c, y_c, z_c, \theta, \varphi, r_0, a]$

## Relative error of Mechanical Response

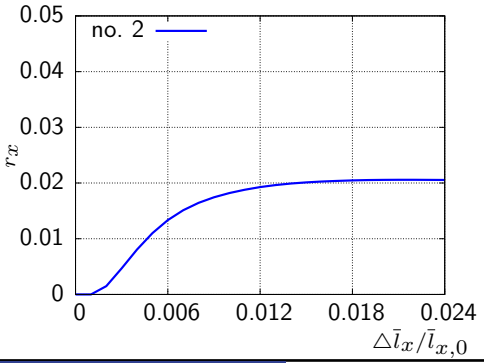


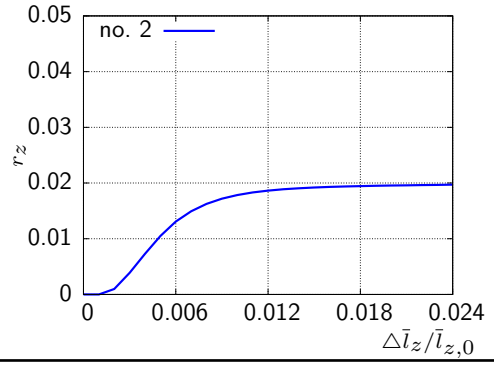


relative error at each evaluation point $i$:

$$r_x^{(i)} = \frac{\left| \overline{\sigma}_{x,i}^{\text{real}} - \overline{\sigma}_{x,i}^{\text{SSRVE}} \right|}{\overline{\sigma}_{x,i}^{\text{real}}}$$

$$\tilde{r}_x = 0.0163 \pm 0.0066$$
$$\tilde{r}_z = 0.0147 \pm 0.0068$$



# Results for SSRVE with 3 Inclusions

## Target structure

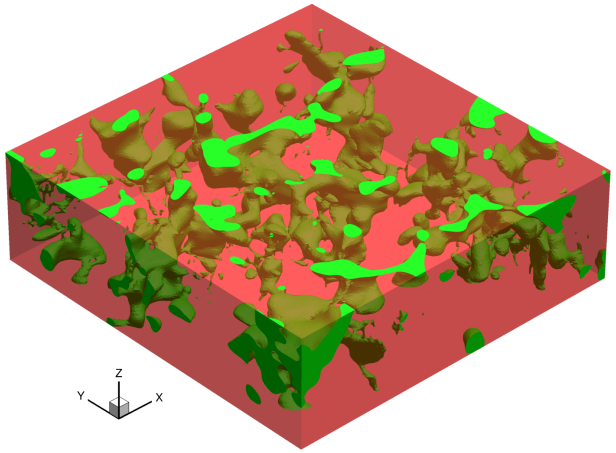

Rel. error: Spect. Dens.

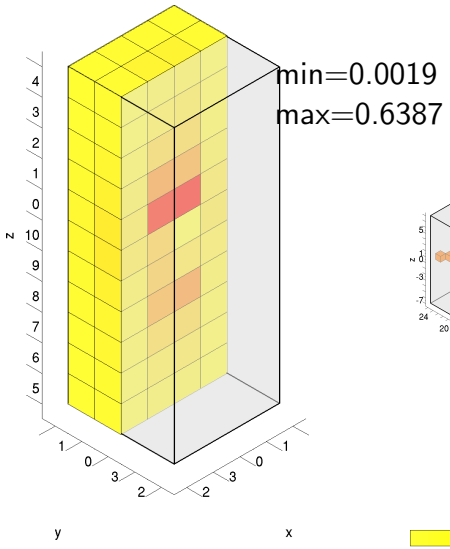


Lineal Path

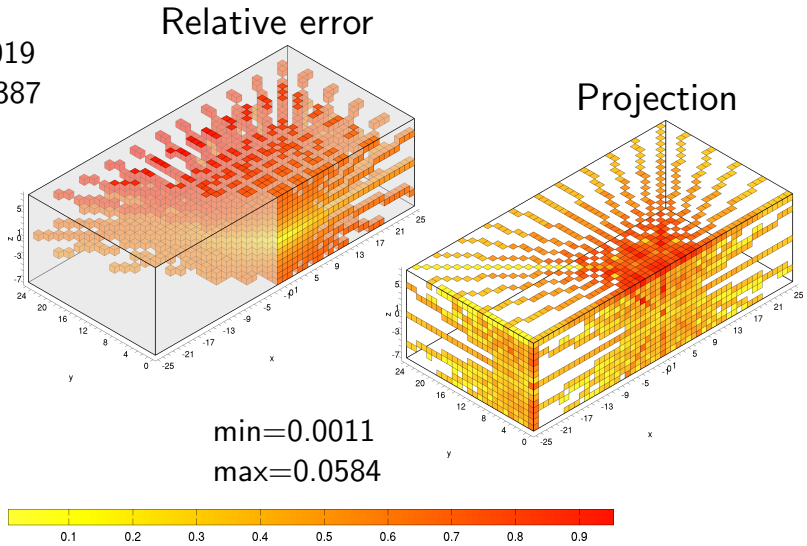


## SSRVE: 3 Ellipsoids

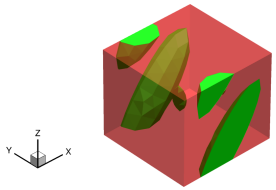

| SSRVE | $\mathcal{L}$ $[10^{-2}]$ | $\mathcal{L}_V$ $[10^{-4}]$ | $\mathcal{L}_{SD}$ $[10^{-3}]$ | $\mathcal{L}_{LP}$ $[10^{-4}]$ | $n_{\text{ele}}$ |
|---|---|---|---|---|---|
| 3 Ellipsoids | 11.686 | 1.113 | 14.454 | 10.229 | 3176 |

Parametrization: $\gamma = [x_c, y_c, z_c, \theta, \varphi, r_0, a]$

## Relative error of Mechanical Response

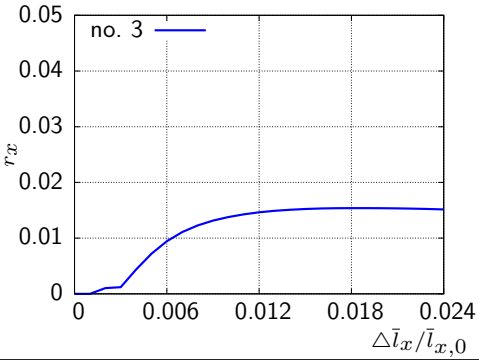


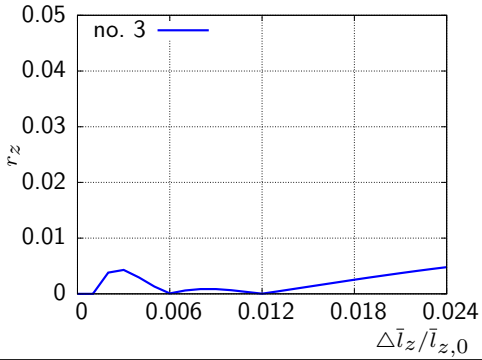


relative error at each evaluation point $i$:

$$r_x^{(i)} = \frac{\left| \overline{\sigma}_{x,i}^{\text{real}} - \overline{\sigma}_{x,i}^{\text{SSRVE}} \right|}{\overline{\sigma}_{x,i}^{\text{real}}}$$

$$\tilde{r}_x = 0.0113 \pm 0.0055$$
$$\tilde{r}_z = 0.0018 \pm 0.0015$$



# Results for SSRVE with 5 Inclusions

## Target structure

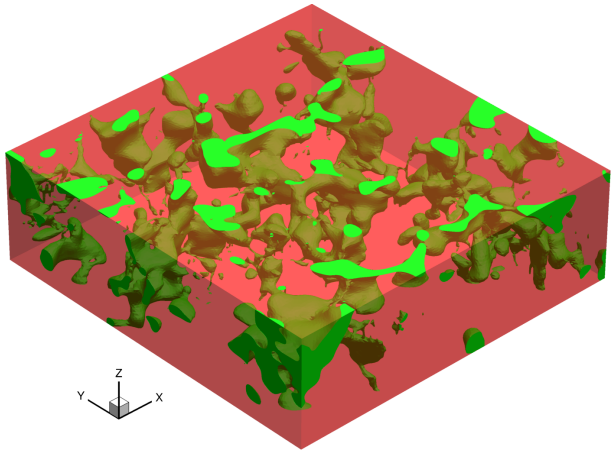

Rel. error: Spect. Dens.

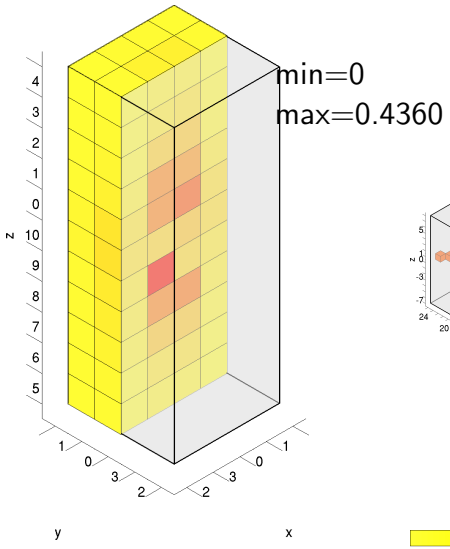


Lineal Path

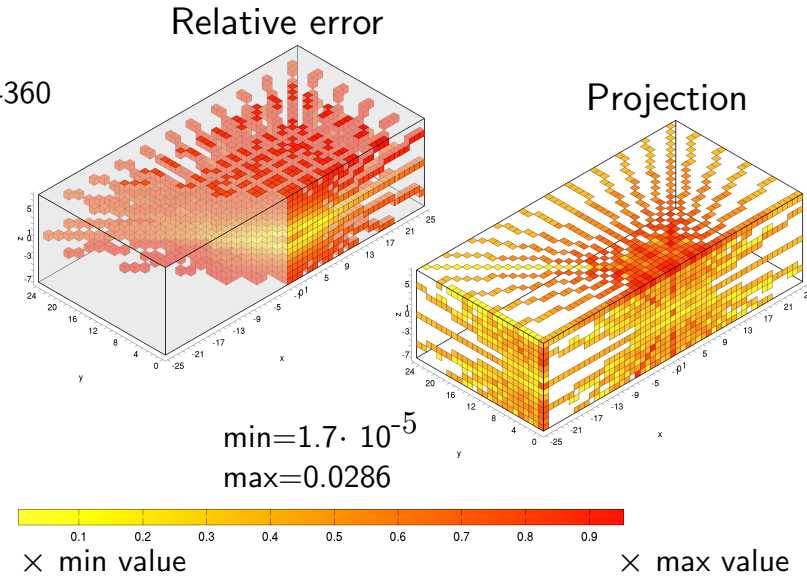


## SSRVE: 5 Ellipsoids

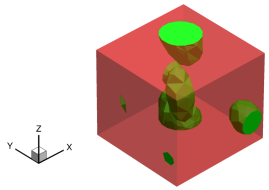

| SSRVE | $\mathcal{L}$ $[10^{-2}]$ | $\mathcal{L}_V$ $[10^{-4}]$ | $\mathcal{L}_{SD}$ $[10^{-3}]$ | $\mathcal{L}_{LP}$ $[10^{-4}]$ | $n_{\text{ele}}$ |
|---|---|---|---|---|---|
| 5 Ellipsoids | 3.072 | 172.4 | 12.84 | 0.5586 | 5709 |

Parametrization: $\gamma = [x_c, y_c, z_c, \theta, \varphi, r_0, a]$

## Relative error of Mechanical Response

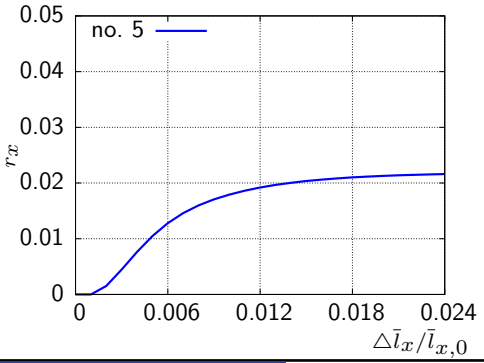


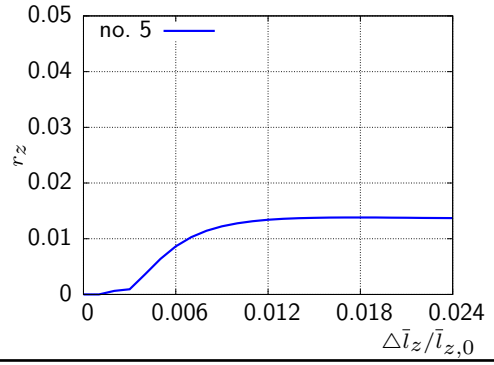


relative error at each evaluation point $i$:

$$r_x^{(i)} = \frac{\left|\overline{\sigma}_{x,i}^{\text{real}} - \overline{\sigma}_{x,i}^{\text{SSRVE}}\right|}{\overline{\sigma}_{x,i}^{\text{real}}}$$

$$\tilde{r}_x = 0.0154 \pm 0.0072$$
$$\tilde{r}_z = 0.0102 \pm 0.0051$$



# Comparison of Mechanical Results: Target vs. SSRVE

| SSRVE | $\mathcal{L}$ $[10^{-2}]$ | $\mathcal{L}_V$ $[10^{-2}]$ | $\mathcal{L}_{SD}$ $[10^{-3}]$ | $\mathcal{L}_{LP}$ $[10^{-5}]$ | $n_{\text{ele}}$ | $\tilde{r}_x$ [%] | $\tilde{r}_z$ [%] | $\tilde{r}$ [%] |
|---|---|---|---|---|---|---|---|---|
| 2 Ellipsoids | 6.484 | 4.485 | 12.84 | 7.139 | 1889 | 5.03 $\pm$ 2.08 | 1.49 $\pm$ 0.67 | 3.71 |
| 3 Ellipsoids | 11.686 | 0.011 | 14.454 | 102.29 | 3176 | 4.63 $\pm$ 1.95 | 0.19 $\pm$ 0.16 | 3.28 |
| 5 Ellipsoids | 3.072 | 1.724 | 7.622 | 5.856 | 5709 | 5.04 $\pm$ 2.1 | 1.03 $\pm$ 0.50 | 3.64 |

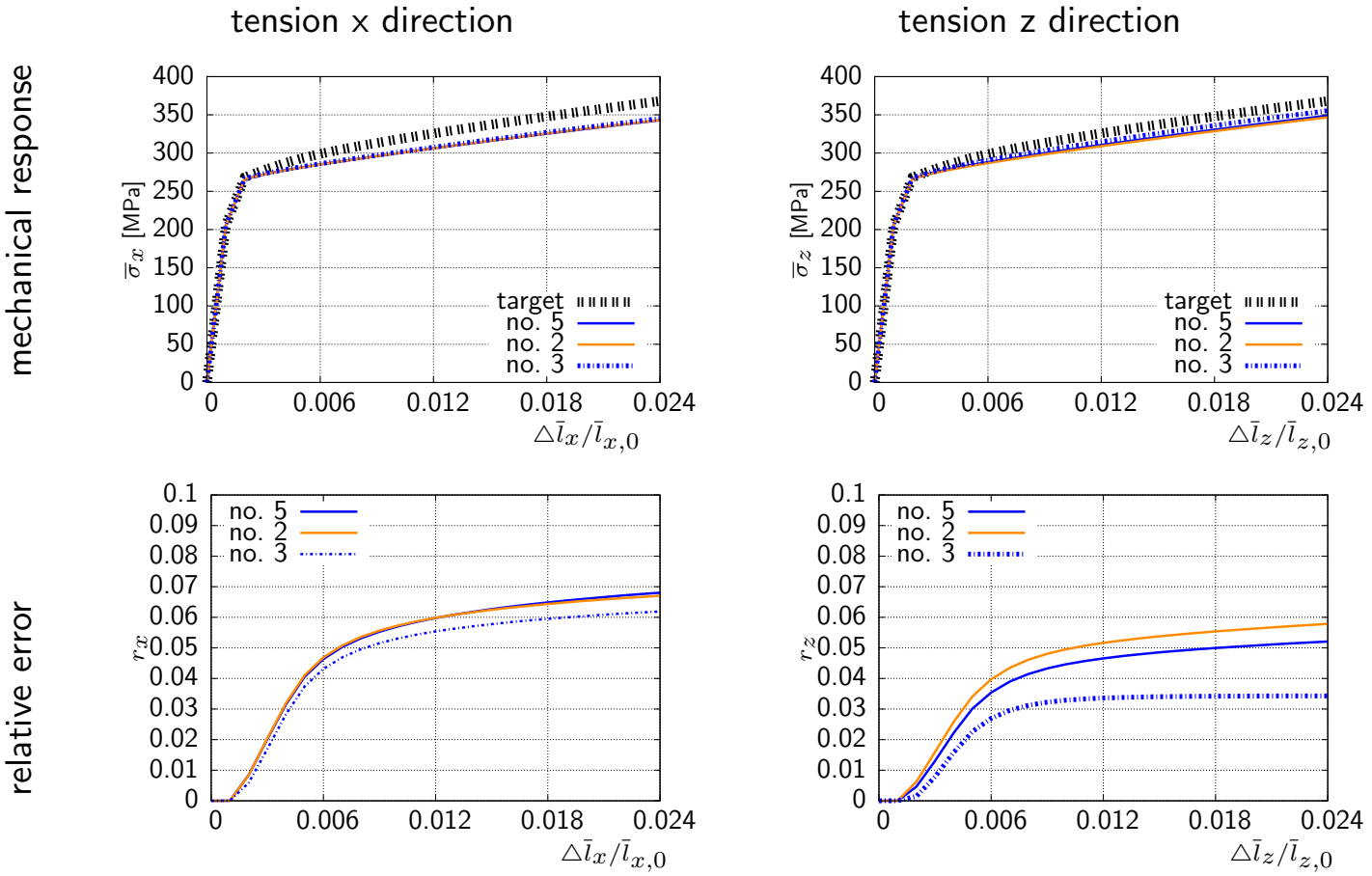


relative error at each evaluation point $i$: $r_x^{(i)} = \dfrac{\left|\overline{\sigma}_{x,i}^{\text{real}} - \overline{\sigma}_{x,i}^{\text{SSRVE}}\right|}{\overline{\sigma}_{x,i}^{\text{real}}}$,



# Example: Simulation of the Nakajima Test

## Specimen geometry

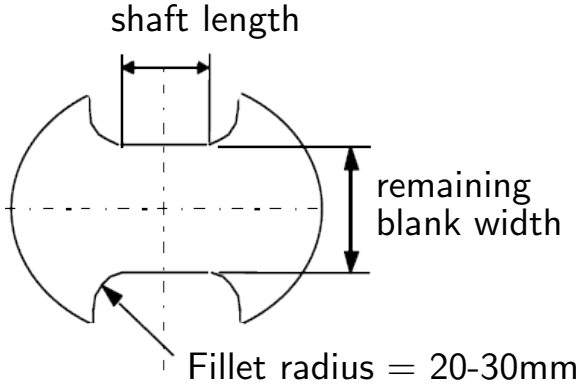


each test piece leads
to one point on FLC

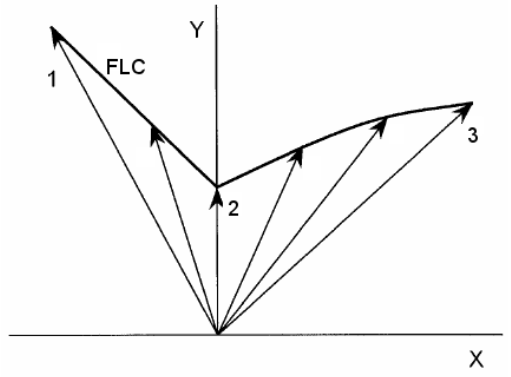


x = minor true strain
y = major true strain
1 = uniaxial tension
2 = plane strain
3 = biaxial tension

## Nakajima forming method

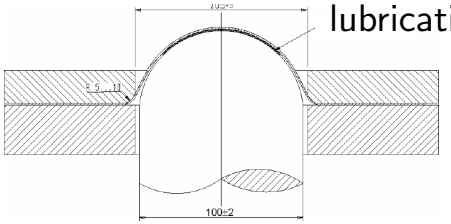


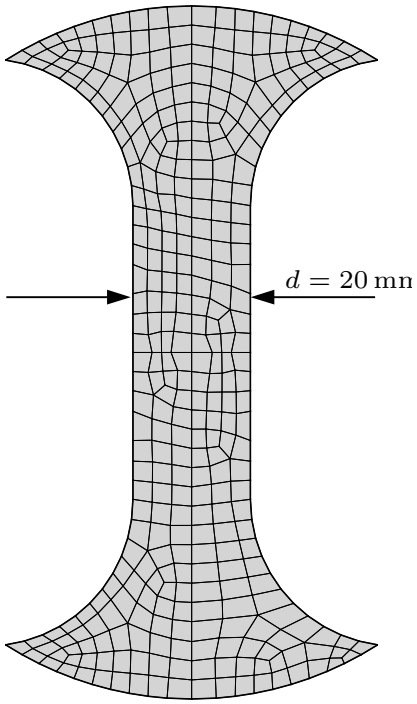


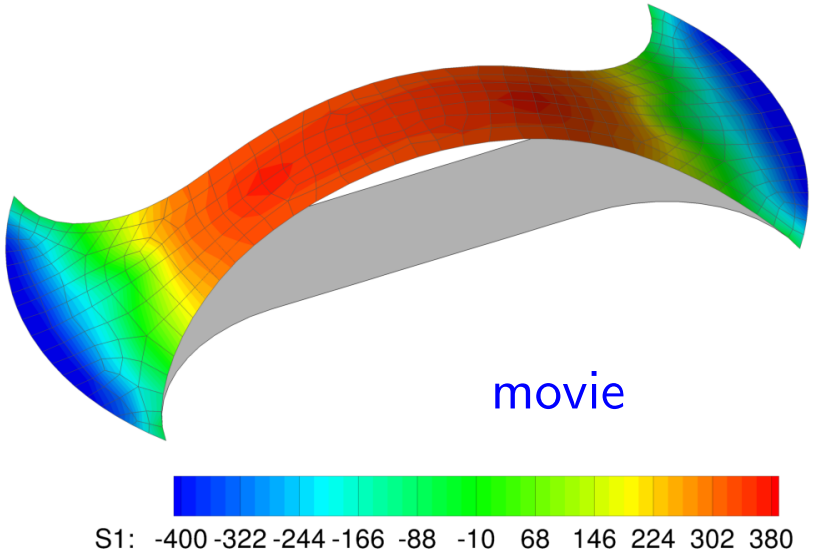


## Boundary Value Problem

- 340 quadrilateral shell elements
- 397 nodal points
- disp. bc's at both ends
- penalty contact for punch
- $J_2$ Plasticity model

(Drawings taken from ISO/DIS 12004-2)

Details on the shell formulation see
Wagner & Gruttmann, IJNME(64), (2005)



# FE$^2$-Simulation of the Nakajima (on-going work)

## Specimen geometry

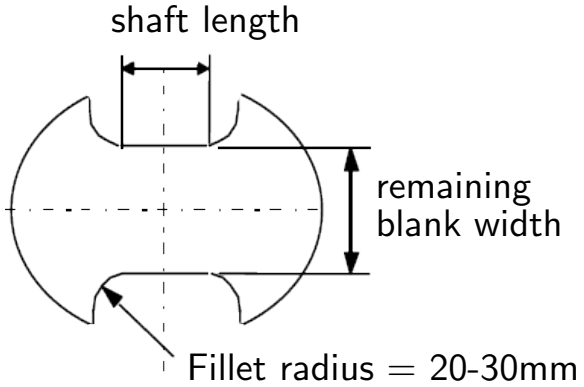


## Forming Limit Curve

each test piece leads
to one point on FLC

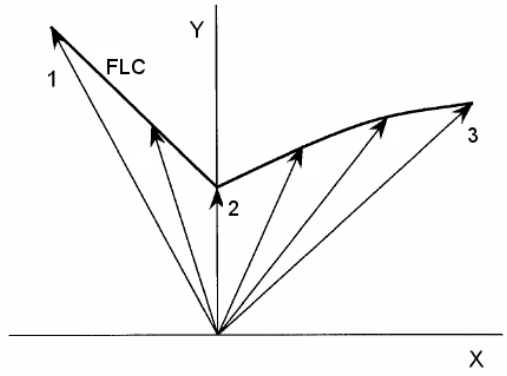


x = minor true strain
y = major true strain
1 = uniaxial tension
2 = plane strain
3 = biaxial tension

## Nakajima forming method

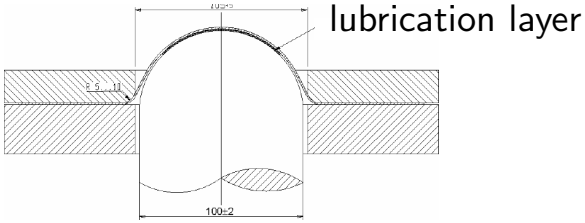


## Macroscopic BVP

- $\frac{1}{4}$ is computed to use symmetry conditions at the macroscale
- 4 $\times$ 2111 10-noded tetrahedral elements
- 5 evalulation points per element

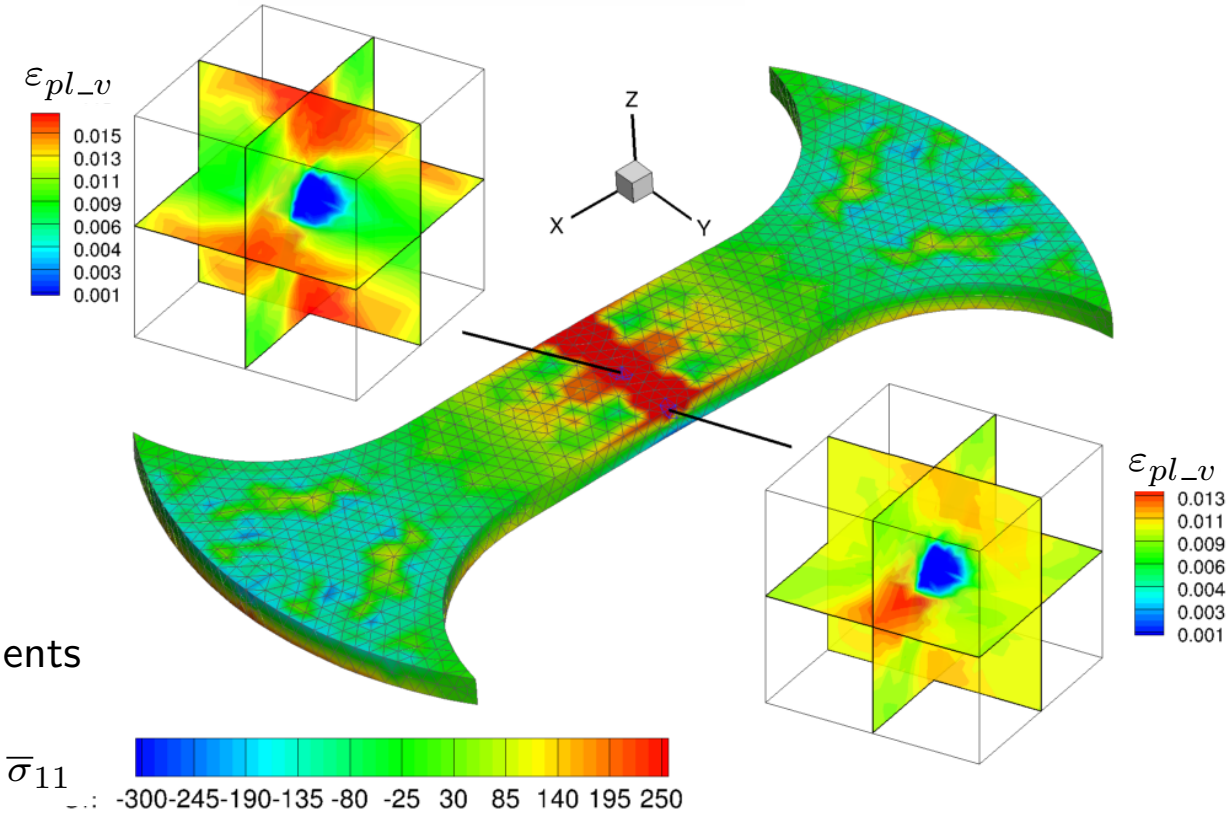


(Drawings taken from ISO/DIS 12004-2)



# Computational Homogenization based on Statistically Similar Representative Volume Elements

## Conclusions

- Advantages of direct micro-macro transition approaches ($FE^2$):
  - $\rightarrow$ no complex macroscopic material law required
  - $\rightarrow$ incorporation of microscopic field fluctuations
  - $\rightarrow$ indicators for failure initialization provided
  - $\rightarrow$ incorporation of further microscopic mechanical phenomena is rather accessible

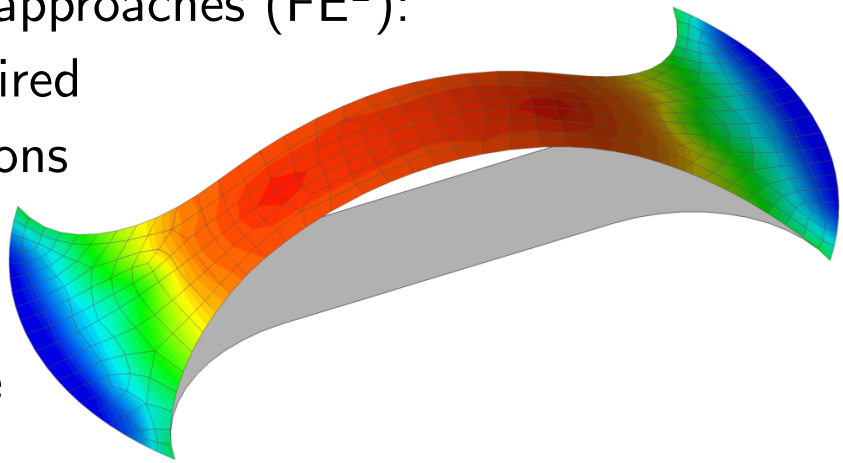

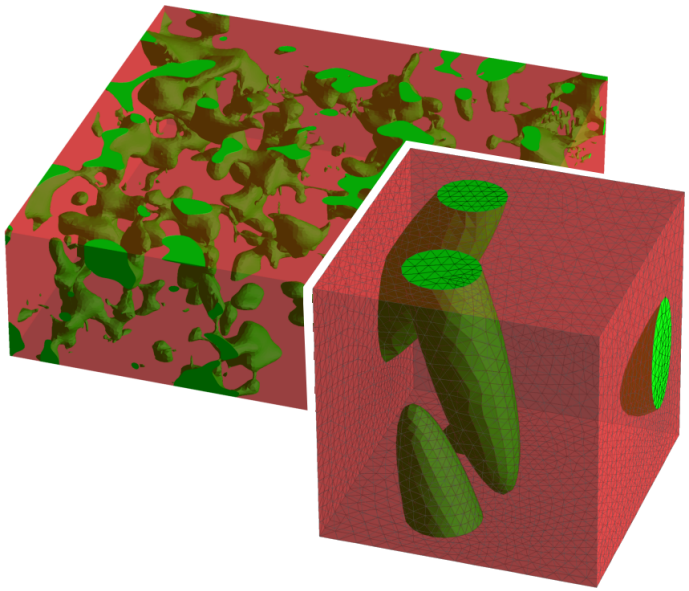

- But: method is computationally expensive
- Construction of SSRVEs leads to calculations of significantly improved efficiency
- Three-dimensional SSRVEs for dual-phase steels are enabled based on 3D EBSD/FIB